学位論文

Potential Importance of Midlatitude Oceanic Frontal Zones for the Annular Variability in the Tropospheric Westerlies and Its Coupling with the Stratospheric Variability

(対流圏東西風の環状モード変動とその成層圏変動との結合に対する中緯度海洋前線帯の潜在的重要性)

平成 26 年 7 月博士(理学)申請

東京大学大学院理学系研究科
地球惑星科学専攻

小川 史明

Doctoral dissertation

Potential Importance of Midlatitude Oceanic Frontal Zones for the Annular Variability in the Tropospheric Westerlies and Its Coupling with the Stratospheric Variability

Fumiaki OGAWA

Department of Earth and Planetary Science,
Graduate School of Science, The University of Tokyo

July 2014

Abstract

A midlatitude oceanic frontal zone is a confluent region of warm and cool ocean currents, characterized by strong meridional gradient in both sea-surface temperature (SST) and surface-air temperature (SAT). Though narrow in its meridional width, the potential of the frontal zone has been recently recognized to exert thermodynamic impacts actively on the tropospheric general circulation, which essentially differs from the passive nature of other portions of the midlatitude ocean basins. Recent observational and modeling studies indicate that a "stormtrack", where migratory cyclones and anticyclones recurrently develop, and a midlatitude westerly (polar front) jet (PFJ) in the climatological-mean state form along a midlatitude frontal zone, where tight SAT gradient energizes weather disturbances. Nevertheless, potential impacts of an oceanic frontal zone on the "annular mode", the dominant low-frequency variability in the extratropical troposphere manifested as the latitudinal displacement of PFJ, has been overlooked except that elimination of frontal SST gradient in an atmospheric general circulation model (AGCM) can weaken the wintertime annular mode variability by distorting its meridional structure.

As a response to the springtime formation of the "ozone hole" and associated stratospheric cooling over Antarctica due to anthropogenic ozone depletion in the late 20th century, a statistically significant trend in the tropospheric circulation has been observed extensively over the summertime extratropical Southern Hemisphere (SH). The trend is characterized by the intensification of the westerlies whose distribution is congruent with the Southern Annular Mode (SAM). Nevertheless, potential impacts of the midlatitude oceanic frontal zone in the Southern Ocean on the tropospheric SAM and the troposphere-stratosphere dynamical coupling via SAM have been overlooked and thus few studies have been conducted comprehensively.

The purpose of the present study is to explore the possible impacts of midlatitude oceanic frontal zones as mentioned above on the formation and variability of the extratropical tropospheric general circulation. To mimic the SH, sets of idealized "aqua-planet" experiments have been conducted with zonally symmetric distributions of SST prescribed globally at the lower boundary of

a given AGCM. By systematically changing the latitude and intensity of the frontal gradient in the SST profile, the aqua-planet experiments have been conducted with the aim of clarifying various impacts that a midlatitude oceanic frontal zone can actively exert on tropospheric wave disturbances and thereby on dynamical properties of the tropospheric annual mode and its vertical connectivity with the stratospheric variability.

The first part of this dissertation investigates how firmly the latitude of oceanic frontal zone can define the dynamical characteristics of the wintertime tropospheric annular mode. The investigation is through a set of aqua-planet experiments conducted under the perpetual wintertime condition. As a zonally symmetric SST field assigned to an AGCM for the control experiment, the meridional SST profile observed in the southwestern Indian Ocean is used, which is characterized by a prominent SST front at 45°S. Several different SST profiles have been constructed for sensitivity experiments by shifting the frontal latitude artificially with 5° intervals or eliminating the frontal gradient by raising SST artificially poleward of 40°S.

The experiments reveal that the model-simulated meridional profile of the variance of zonally symmetric low-frequency variability of PFJ exhibits strong sensitivity to the position of the SST front, if situated at midlatitude or subpolar latitude. The sensitivity of the variance distribution reflects the characteristics of the wintertime annular mode, which has been extracted statistically through an empirical orthogonal function (EOF) analysis as the pattern of zonal-mean zonal wind anomalies that can account for the largest fraction of their spatially integrated variance. In the positive phase of the annular mode, the PFJ axis exhibits strong sensitivity to the latitude of the SST front with an obvious tendency to be situated slightly poleward of the front systematically. The PFJ accompanies a stormtrack in the vicinity of the oceanic front, where migratory high-frequency wave disturbances are particularly active and their poleward eddy flux of westerly momentum converges to maintain the PFJ. Insensitively to the latitude of the SST front, by contrast, the PFJ axis in the negative phase of the annular mode is located consistently around 38°S, as is realized without frontal SST gradient. The sensitivity of the low-level stormtrack latitude is also weaker substantially than in the positive phase. It is thus suggested that in the negative phase of the annular mode the

latitudes of the stormtrack and eddy-driven PFJ tend to be determined mainly by atmospheric internal dynamics under the negligible influence of the frontal SST gradient.

It follows that, at least for the experiments with a midlatitude or subpolar SST front, the wintertime annular mode may be interpreted a manifestation of wobble of the extratropical tropospheric circulation between two "dynamical regimes" – one under the strong influence of SST gradient as the lower-boundary condition, and the other under the strong control by atmospheric internal dynamics unrelated to the lower-boundary condition. In fact, meridional gradient of a surface turbulent flux of sensible heat across the oceanic front is stronger in the positive phase than in the negative phase. This tendency is consistent with the notion that the differential supply of sensible heat from the ocean across the front is important for the recurrent baroclinic development of transient eddies to form a stormtrack and thereby to drive the PFJ. This interpretation of the wintertime annular mode revealed in the aqua-planet experiments has no conflict with an interpretation of the annular mode given in the previous studies as a transition between the double- and single-jet regimes – one with dual distinct axes of PFJ and the subtropical jet (STJ) and the other with the dominant STJ under the diminished PFJ. Rather, the present study has clarified that those regimes correspond to the two "regimes" that are realized under stronger and weaker influence of an oceanic front on the tropospheric circulation.

In the aqua-planet experiments, the transition from one "regime" to another associated with the annular mode variability is triggered by low-frequency wave anomalies, which is consistent with transition events of the observed wintertime SAM. Typical transitional events are found to be triggered by local westerly forcing associated with the emanation of a quasi-stationary Rossby wave packet rather than a zonally uniform westerly forcing. Migratory high-frequency disturbances act to maintain anomalous westerlies but not act to trigger the polarity change of the annular mode.

Furthermore, the interpretation obtained in this study is found insightful about the observed inter-basin differences in the wintertime SAM signature that are embedded in the zonally symmetric anomalies. The latitudes of the lower-tropospheric westerly PFJ axis averaged separately over the individual SH ocean basins tend to be observed consistently around 42°S in the negative phase of

the SAM. In its positive phase, by contrast, the PFJ axis in the South Pacific tends to be located 10° poleward of those in the South Indian Ocean and South Atlantic, correspondingly to the differences in the frontal latitudes. These characteristics of the SAM are in good correspondence to those of the annular mode simulated in the aqua-planet experiments, and they are also suggestive of the possibility to re-interpret the climatological-mean state observed in the wintertime SH as the superposition of the two "dynamical regimes".

Contrastingly, regime-like behavior is virtually absent in the annular mode simulated with a subtropical SST front (at 30°S or 35°S), and the mode is manifested as wobble of the PFJ axis from its climatological mean. Though not actually observed in the SH, the annular mode in these experiments is similar to its counterpart simulated without frontal SST gradient. One of the possible factors that may be involved is hampering of baroclinic eddy growth along the subtropical SST front under the prevailing descent associated with the Hadley Cell.

The second part of the dissertation investigates the potential impacts of a midlatitude oceanic front on the stratosphere-troposphere connectivity of circulation variability through another set of aqua-planet experiments. Specifically, an assessment is made on how dependent the tropospheric circulation response to the anthropogenic ozone depletion as in the Antarctic stratosphere can be on the frontal SST gradient. The experiments with the springtime stratospheric ozone depletion as observed in the late 20th century demonstrate that the intensification of the tropospheric westerlies in summer is realistically reproduced only in the presence of the zonally symmetric oceanic front at 45°S as observed in the summertime SH. The tropospheric eddy activity responds significantly to the ozone depletion to drive the tropospheric zonal-wind anomalies as observed. In contrast, the tropospheric response is virtually absent if the frontal SST gradient is smoothed out. The processes through which the intensification of the stratospheric westerlies as a direct response to the ozone depletion is translated into the troposphere can be regarded as being essentially the same as their counterpart through which the self-excited stratospheric year-to-year variability in spring through summer is connected to the tropospheric annular variability. In fact, the meridional structure of the tropospheric annular variability simulated with the frontal SST gradient

is similar to that of the observed SAM. In contrast, the elimination of the frontal SST gradient causes the substantial weakening of both the tropospheric eddy activity and eddy-driven westerlies in midlatitude and subpolar regions, resulting in the distortion of the meridional structure of the annular mode and thereby the diminishing of its vertical coupling with the stratospheric variability. It is thus interpreted that the translation of the ozone-induced intensification of the stratospheric westerlies into the troposphere can be propped up by the midlatitude oceanic front through activating tropospheric eddies and thus the troposphere-stratosphere coupling through the annular mode. While acting to drive tropospheric westerlies in the same sense, the anomalous activity of tropospheric eddies as responses to the stratospheric ozone depletion and their anomalous activity associated with self-excited year-to-year annular variability is somewhat different, which urges further investigation. Nevertheless, this study is the first to reveal the critical importance of a midlatitude oceanic frontal zone for the ozone-induced tropospheric climate changes observed in the late 20th century, shedding light on the processes involved in the dynamical coupling between tropospheric and stratospheric variability via the annular mode, which are still under debate.

The present study contributes to fundamental advance in understanding the importance of midlatitude oceanic frontal zones for the extratropical atmospheric general circulation. While the importance of midlatitude frontal SST gradient has been indicated for the climatological-mean stormtrack and PFJ, the present study is the first comprehensive study to elucidate that the frontal SST gradient should be taken into account in understanding not only their climatological-mean state of the extratropical tropospheric westerlies but also their low-frequency variability, also known as annular mode, its vertical connectivity with the stratospheric variability and associated long-term trends. These new perspectives make significant contributions to deepening the understanding of the fundamental properties of the tropospheric general circulation. They also imply that realistic representation of midlatitude oceanic frontal zones in climate models may be required for the realistic representation of the tropospheric annular variability, the climatic-mean state and its reliable projection.

Abstract (in Japanese)

中緯度海洋前線帯は，中緯度における暖流と寒流の合流域であり，強い水温勾配および地表気温勾配を伴っている．南北幅は狭いものの，この海域は他の中緯度海域が示す大気変動に対する受動的な性質とは本質的に異なり，中高緯度対流圏大循環の形成に対して能動的に影響し得ることが近年の研究から明らかになりつつある．観測データや数値実験による先行研究では，移動性擾乱活動の活発域であるストームトラックとそれら擾乱により駆動される西風の極前線ジェットは，気候平均状態として中緯度海洋前線帯の近傍に形成され，そこでは強い地表気温勾配が擾乱活動を活発化させていることが示されている．一方，偏西風の長周期変動として中高緯度域の天候に深く関わる「環状モード変動」は極前線ジェットの南北変動として認識されてきたものの，海洋前線帯による影響に関心が払われたことはこれまで殆どなく，海洋前線帯の勾配を緩和させた場合に冬季の環状モード変動に変調が生じ得ることが数値実験による研究で指摘されているのみであった．

さらに，人為的影響により 20 世紀終盤に南極成層圏で生じたオゾン濃度の低下による「オゾンホール」の形成とそれに付随した低温化への応答として，南半球中高緯度の広い範囲で統計的に有意な対流圏西風の強化が観測されている．その水平構造は南半球環状モード(Southern Annular Mode, SAM)に類似していることが知られており，それに対して南大洋に存在する海洋前線帯が影響を与える可能性があるものの，環状モードを介した成層圏・対流圏結合変動における海洋前線帯の重要性については，これまで全く議論されてこなかった．

そこで本研究の目的は，中緯度の対流圏大循環の形成と変動において，従来看過されてきた中緯度海洋前線帯が与え得る影響について包括的に探求することである．現実の南半球を模して，大気大循環モデル(AGCM)の下方境界条件として東西一様な海面水温分布を与える「水惑星実験」にて，水温勾配の緯度や強度を系統的に変えることを通じて，対流圏環状モード変動の力学特性やその成層圏循環変動との結合に対し，中緯度海洋前線帯が対流圏波動擾乱を介して能動的に与え得る様々な影響の解明を目指す．

本論文の前半では，海洋前線帯の緯度が冬季対流圏環状モードの特徴をどれほど強く規定し得るかについて探求した．用いた水惑星実験においては，季節を冬季に固定し，中緯度の南西インド洋で観測される海面水温の南北分布を AGCM の境界条件として東西一様に与えた．この際，現実には南緯 45

度に位置する顕著な海洋前線帯を人為的に 5 度ずつ南北にずらして与えたり，南緯 40 度以南の水温を人為的に上げて前線帯に伴う水温勾配を消去したりして，数通りの異なる水温分布を与えた．

海洋前線帯が中高緯度に位置する場合，AGCM に現れた極前線ジェットの東西一様な長周期変動は海洋前線帯の緯度に強い依存性を示した．それは，東西平均東西風の変動のうち最大の分散を説明する偏差パターンとして統計的に抽出された冬季環状モードの性質にも反映されていた．環状モードの正の位相においては，極前線ジェットの軸が海洋前線帯の緯度に強く依存し，そのやや高緯度側に位置する傾向を示した．海洋前線帯近傍にはストームトラックを伴っており，活発な移動性擾乱活動に伴う西風運動量極向き輸送が極前線ジェットの西風を維持するよう働いていた．対照的に，環状モードの負の位相においては，海洋前線帯の緯度に依らず極前線ジェットは南緯 38 度付近に位置し，海洋前線帯がない場合の気候平均状態に良く対応していた．対流圏下層のストームトラックの緯度の海洋前線帯に対する依存性も，正の位相の場合に比べて著しく弱まった．すなわち，環状モードの負位相ではストームトラックと渦駆動の極前線ジェットの緯度は大気内部力学で決められており，大気下方の境界条件である水温勾配の影響が無視できるほど弱まることが示唆される．従って，少なくとも海洋前線帯が中高緯度に位置する場合の冬季環状モードは，中高緯度の対流圏大循環が下方境界条件としての水温前線の強い影響を受けるレジームと大気内部力学で主に規定されるレジームとの間をゆらぐことの現れとして解釈できる．実際，海洋から大気への乱流顕熱フラックスの海洋前線帯での南北勾配は，環状モードの正（負）の位相で強（弱）まった．これは，海洋前線帯を挟んだ顕熱供給の南北差が移動性擾乱の頻繁な発達を促し，極前線ジェットの駆動にとって重要なことと整合的である．水惑星実験から得られた冬季環状モードの解釈は，極前線ジェットが亜熱帯ジェットから分離される”ダブルジェット”レジームと，極前線ジェットが弱まり亜熱帯ジェットだけが明瞭な”シングルジェット”レジームの間の遷移として環状モードが現れるという先行研究の解釈とも矛盾しない．寧ろ，これらのレジームが海洋前線帯の対流圏循環に対する影響が強いレジームと弱いレジームに対応することが明らかとなった．

水惑星実験において環状モードの極性反転として表れた”レジーム”間の遷移は，観測される冬季 SAM と整合的に，長周期の波状擾乱によって引き起こされていた．遷移イベントは，東西一様な西風強制というよりも，寧ろ準停滞性ロスビー波束の射出に伴う局在化した西風強制で引き起こされていた．一方，短周期擾乱からのフィードバックは環状モードの極性を変えるのではなく，それを維持する役割をしていた．

さらに，本研究の解釈は，冬季 SAM における東西一様な偏差に重畳する海盆間での南北構造の差異を理解するために有用である．各海盆で東西平均した対流圏下層の西風軸は，SAM の負位相にはいずれも南緯 42 度付近に位置する一方，正位相では海洋前線帯の緯度の差異に対応し，西風軸は南太平洋では南大西洋・インド洋に比べ 10 度も高緯度側に位置する．これらの特徴は水惑星実験の結果と良く対応するだけでなく，冬季南半球の気候平均状態は両レジームの重ね合わせと再解釈することも可能である．

上記とは対照的に，水惑星実験において海洋前線帯が亜熱帯（緯度 30 度や 35 度）に位置する場合，環状モード変動はレジーム性を殆ど示さず，極前線ジェットの気候平均状態周りの南北揺動として現れる．これは現実の冬季南半球では観測されないが，海洋前線帯を除去した実験での環状モード変動の特徴に似る．その要因としては，ハドレー循環の下降運動によって亜熱帯海洋前線帯に沿った擾乱の傾圧的発達が抑制される傾向が考えられる．

論文の後半では，別の水惑星実験を用いて，大気循環の対流圏・成層圏鉛直結合に対する海洋前線帯の潜在的重要性を評価した．具体的には，人為起源の成層圏オゾン減少に対する対流圏循環の応答が海洋前線帯の存在にどの程度依存するのか調査した．その結果，20 世紀終盤に南極上空で観測されたようなオゾン減少が水惑星実験において与えられた場合，東西一様な海洋前線帯が中緯度にあれば対流圏の波活動が有意に応答して東西風偏差を形成し，実際に観測されたような夏季対流圏の西風強化が再現されるのに対し，その水温勾配を緩和するとこうした現実的な応答が現れないことが分かった．この際，オゾン減少への応答としての成層圏西風強化が対流圏にまで及ぶ過程は，自励的な変動としての成層圏東西風の年々変動が対流圏に及ぶ過程と本質的に同様と考えられる．実際，水惑星実験における対流圏の東西一様な年々変動としての環状モードは，海洋前線帯が存在する場合は観測される SAM と整合的な南北構造を示す．対照的に，前線帯の水温勾配を緩和すると対流圏の波活動が弱まり，中緯度・亜寒帯域の西風が弱化するのに伴い年々変動としての環状モードの南北構造は著しく歪められ，成層圏の変動との結合が著しく弱まったと解釈できる．従って，成層圏オゾンの減少で強制された東西風偏差の対流圏への下方伸展に対して，海洋前線帯が対流圏波活動の活発化と西風強化を介した対流圏・成層圏の環状モードの結合の強化を通じて下支えしていることが示唆される．ただし，成層圏の自然変動に伴う対流圏擾乱活動の変調は，オゾン減少に対する応答として現れるものと同様に西風を強制する一方で，それを引き起こす擾乱活動の変調自体はやや異なっており，その解釈は今後の重要な課題であると

考えられる．しかしながら本研究は，これまで活発に議論されながら十分な理解が為されてこなかった，成層圏オゾン減少に対する対流圏の気候応答のメカニズムにおいて，今まで完全に無視されてきた海洋前線帯が実は極めて重要であり得るということを初めて示したものである．

今回の研究は，中高緯度の大気大循環に対する中緯度海洋前線帯の重要性の把握において大きな進歩をもたらした．これまでの多くの研究で，中緯度海洋前線帯が中高緯度大気のストームトラックや極前線ジェットの気候平均状態に対して重要であることは示されていた．本研究ではさらに，対流圏中高緯度域に卓越する長周期変動としての東西一様な環状モード変動とそれを介した成層圏・対流圏結合変動，そして環状モードとして現れる長期変化に対しても，中緯度海洋前線帯の水温勾配の影響が考慮されなければならないことを初めて明らかにした．これらの新しい観点は，中高緯度対流圏大循環の根本的描像を理解する上で重要な貢献をなし得るものである．また，数値気候モデルにおいて海洋前線帯を適切に表現することが，環状モード変動の表現や，気候の再現性，信頼性の高い気候の将来予測に対しても重要であることが示唆される．

Contents

Chapter 1. General introduction

1.1. Tropospheric annular mode

The extratropical tropospheric circulation fluctuates with various temporal and spatial time scales. The fluctuations include subweekly weather disturbances associated with migratory synoptic-scale cyclones and anticyclones. More persistent climate variability tends to be associated with anomalies on greater horizontal scales. As a typical example, the dominant mode of the extratropical tropospheric circulation variability on intraseasonal through interannual scales is known to be in zonally symmetric structure, especially in the Southern Hemisphere (SH) (e.g. Kuroda and Kodera 1998; Thompson and Wallace 2000; hereafter referred to as TW2000). A number of studies have been performed to investigate the zonally symmetric variability, since the introduction of the notion of "zonal index cycle" by Rossby (1939). This study was preceded by a pioneering study by Exner (1913), who first identified a pattern of sea-level pressure (SLP) variability between the Arctic and midlatitude regions with fairly high degree of zonal symmetry. Today, this pattern is known as the Arctic Oscillation (AO) (Thompson and Wallace 1998; Wallace 2000) or the "Northern annular mode (NAM)", as indicated in Figure 1.1d.

Since the study by Kidson (1988), an empirical orthogonal function (EOF) analysis is often applied to extract a large-scale anomaly pattern that accounts for the largest fraction of the spatially integrated variance of low-frequency variability in pressure or geopotential height. Regression or composite analysis based on the principal component (PC) time series derived from the EOF analysis is useful for identifying a typical three-dimensional structure of the anomalies of pressure and other variables. In the extratropical troposphere, the dominant variability extracted in the first EOF represents the meridional fluctuations of the midlatitude westerlies with a high degree of zonal symmetry, with the exchange of atmospheric mass between the polar region and midlatitudes (TW2000, Figure1.1a, c). Virtually the same anomaly pattern can be extracted through EOF analyses applied to the anomalous westerlies, and the extracted pattern is often referred to as the

"annular mode" (Limpasuvan and Hartmann 1999; TW2000). TW 2000 pointed out that the dominant atmospheric variability in the extratropics is similar between the two hemispheres despite distinct inter-hemispheric differences in the zonal asymmetry in the lower boundary condition due to topography and land-sea thermal contrasts. Annular modes in the individual hemispheres are thus referred to as the "Southern annular mode (SAM)" (Fig1.1c) and NAM (Figure 1.1d) and their "positive (negative)" phase corresponds to the periods in which the midlatitude westerly jetstream shifts poleward (equatorward).

Statistically significant circulation anomalies are observed associated with SAM and NAM in largest magnitude in winter (Limpasuvan and Hartmann 2000). Owing to their hemispheric extent, NAM and SAM influence climatic conditions over extensive regions in the extratropics (Figure 1.2; TW2000; Gillett et al. 2006). Over extratropical regions, for example, anomalies in surface air temperature (SAT) tend to be positive in the midlatitudes and negative in the high latitudes associated with the positive phase associated with annular mode in both hemispheres, although with somewhat stronger zonal asymmetry in NAM due to the zonal asymmetry in the lower boundary condition (Limpasuvan and Hartmann 2000).

While the NAM anomaly is maintained by the feedback forcing from both anomalous activity of synoptic-scale eddies and planetary waves (Limpasuvan and Hartmann 1999, 2000; Kimoto et al. 2001; Lorenz and Hartmann 2003; Watanabe and Jin 2004), the SAM anomaly is maintained mainly through the anomalous activity of synoptic-scale eddies (Lorenz and Hartmann 2001). The anomalous convergence of eddy momentum flux near the tropopause associated with annular mode arises from the modulations in the latitude of the synoptic-wave propagation and their horizontal structure (Yu and Hartmann 1993; Hartmann and Lo 1998; Shiogama et al. 2004).[1]

The positive phase of wintertime SAM represents a double-jet structure with distinct separation between the two westerly jet axes, polar-front jet (PFJ) in midlatitudes and subtropical jet (STJ), while its negative phase represents a merged single jet structure with the dominant STJ in the upper troposphere (Yoden et al., 1987; Yu and Hartmann 1993; Hartmann and Lo; 1998). There

[1] The anomaly pattern that accounts for the second largest fraction of the variance as extracted in the second EOF tends to represent the variability of PFJ strength with little variation in its axial latitude.

exists an interpretation of wintertime SAM variability as a regime shift between two different quasi-equilibrium states of the tropospheric climate (Yoden et al. 1987; Itoh et al. 1999). Itoh et al. (1999) identified dual attractors in the phase space of PC time series as representative of regimes, in arguing their correspondence to the double and single jet structures. Nevertheless, the above arguments of the "regime-like" characteristic of the observed wintertime SAM are rather phenomenological, and in-depth investigation of the dynamics behind the regime-like behavior of annular modes is required. For example, while the characteristics of low-frequency NAM variability have been understood as modulations in planetary waves (e.g., Kimoto et al. 2001), the same interpretation may not necessarily be appreciable to the SAM variability because of the weakness of the climatological-mean planetary waves in SH. Rather, it has been pointed out that the phase transition of the wintertime SAM may be related to modulated activity in low-frequency wave anomalies (Shiogama et al. 2005).

The SAM and NAM often couple with the stratospheric variability of the polar vortex especially in the stratospheric "active" seasons of December-January-February in the NH and in the November in the SH (TW2000). In those seasons the stratospheric zonal wind is westerly, but not excessively strong for the upward propagation of planetary waves from the troposphere (Charney and Drain 1961). The stratospheric zonal wind anomalies represented as the anomalous polar-night jet (PNJ) with a high degree of zonal symmetry often propagate down to the surface (Figure 1.3), through the vertical coupling associated with the annular mode variability (Baldwin and Dunkerton 1999, 2001; Thompson et al. 2005).

Recent study has indicated that the meridional structure of the annular mode in the troposphere is sensitive to the climatological-mean background state (Eichelberger and Hartmann 2007). However, the mechanisms for the formation of the climatological-mean circulation, especially the eddy-driven PFJ, have not been fully understood yet, which is due to the overlooked influence by the midlatitude ocean, as specifically discussed in Section 1-3. Limpasuvan and Hartmann (2000) showed through their experiment with an atmospheric general circulation model (AGCM) that the annular mode can be reproduced even under such condition that sea-surface

temperature (SST) is fixed to the climatological seasonal march. Although they concluded that the annular mode arises from the internal dynamics of the atmosphere unrelated to the lower-boundary condition, their results do not necessary mean that the midlatitude ocean exerts no significant effect on the meridional structure or amplitude of the annular mode. This is because their experiment cannot rule out any influence of the midlatitude ocean on the annular mode by shaping the climatological-mean state of the PFJ, whose fluctuations are manifested as the annular mode variability. It has been pointed out by recent numerical studies (Nakamura et al. 2008; Sampe et al. 2013) that a midlatitude oceanic frontal zone is potentially important for the PFJ formation and thereby both the amplitude and meridional structure of annular mode. Nevertheless, impacts of a midlatitude oceanic frontal zone on the characteristics of the annular mode have not been studied in depth.

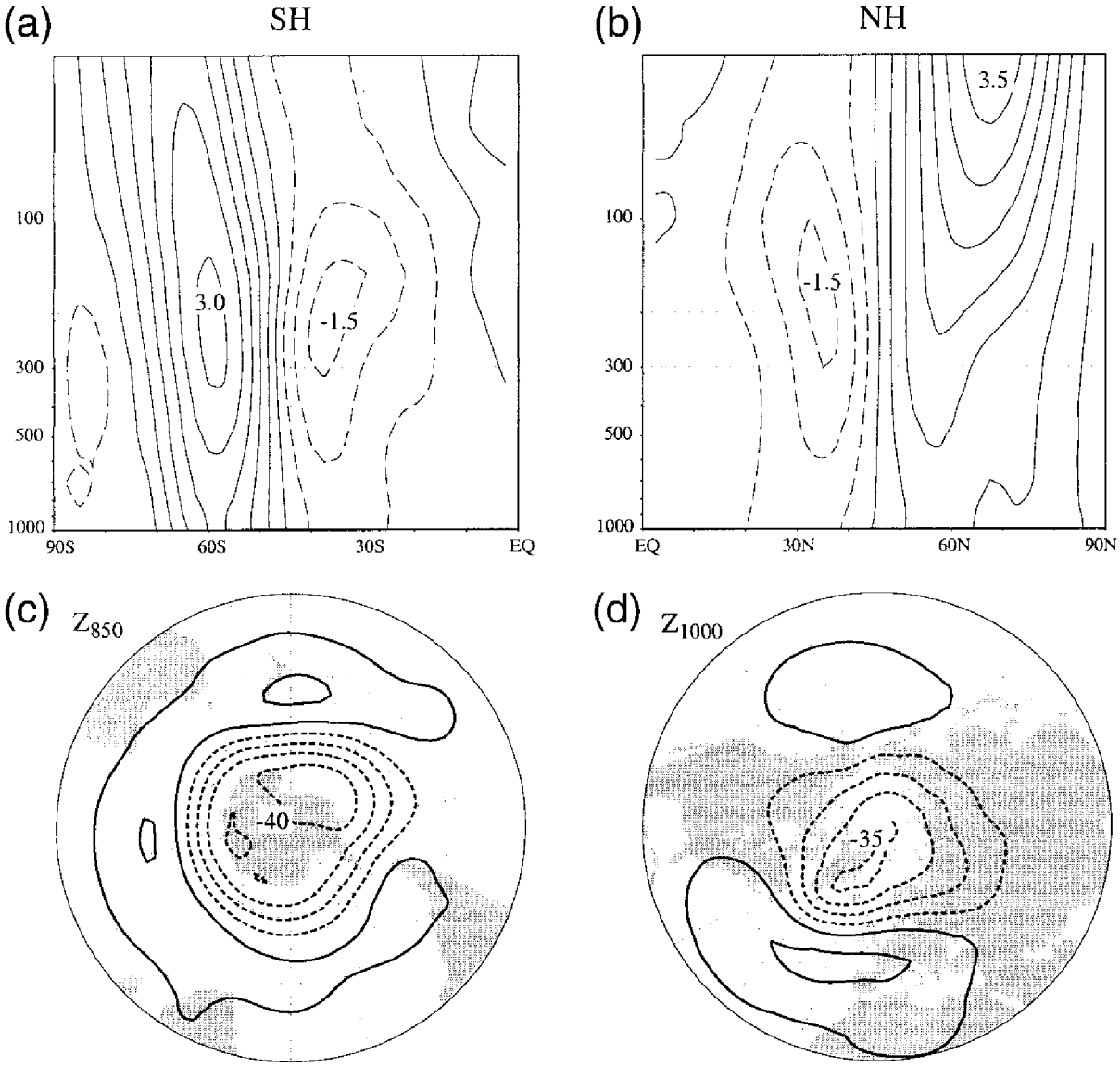

Figure1.1. (a,b) Latitude-height sections of Zonal-mean zonal wind anomalies [m/s] and (c,d) geopotential height anomalies in the lower troposphere [m] regressed on the standardized (a, c) SAM and (b, d) NAM indices based on the monthly-mean NCEP-NCAR reanalysis data from Jan 1958 to Dec 1997. Contour intervals are 0.5 for (a,b) and 10 for (c,d). Adapted from Thompson and Wallace (2000).

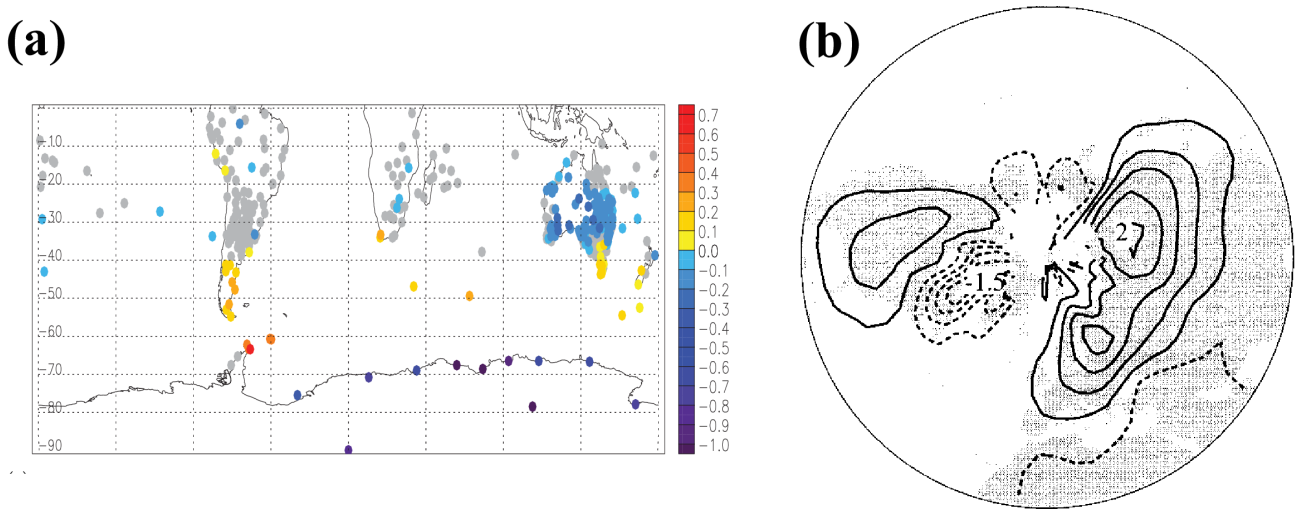

Figure 1.2. (a). Monthly mean station temperature anomalies [°C] regressed on the standardized SAM index. Only those anomalies statistically significant by 90% is colored. Adapted from Gillett et al. (2006). (b). Monthly-mean surface air temperature anomalies [°C] regressed upon the standardized NAM index for boreal wither (January–February-March). Positive (negative) anomaly is indicated by solid (dashed) line. Contour interval is 0.5. Adapted from Thompson and Wallace (2000).

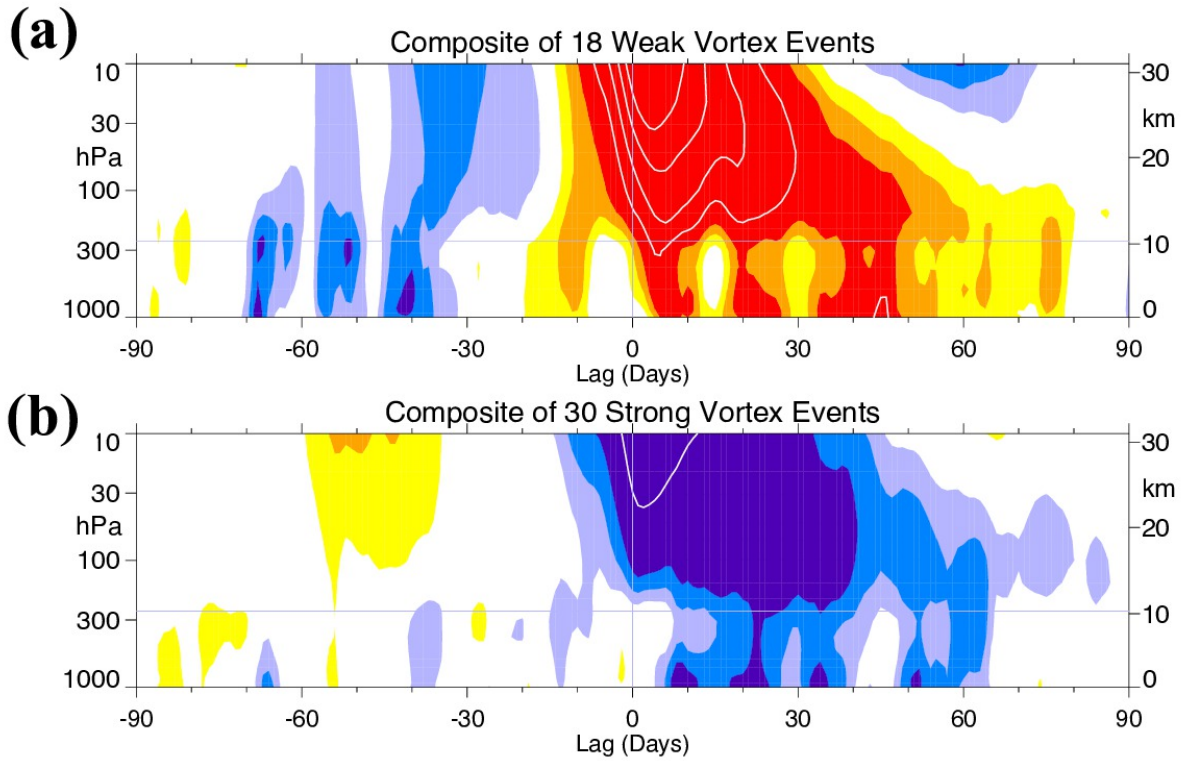

Figure 1.3. Time-height sections showing the NAM index composited for (a) 18 weak vortex events and (b) 30 strong vortex events. Day 0 for the weak (strong) vortex events are defined by the dates when the standardized NAM index at 10hPa crosses –3.0 (+1.5), respectively. The interval for the shading (contour) is 0.25 (0.5). Values between -0.25 and 0.25 are not shaded. The approximate boundary between the troposphere and the stratosphere is indicated by thin horizontal line. Adapted from Baldwin and Dunkerton (2001).

1.2. Observed climatic trends projected on the Southern Annular Mode

While the annular mode signature tends to be dominant in intraseasonal/interannual natural climate variability over the extratropics, previous studies have revealed that long-term changes observed in the tropospheric climate have congruent structure with the annular mode in both hemispheres (Thompson et al. 2000; Thompson et al. 2011). In a set of numerical experiments (Ring and Plumb 2007, 2008), annular mode is shown to be a preferred response to external forcing. In fact, the trends observed in the SH troposphere during the late 20th century were manifested as a strengthening of the surface westerlies on the poleward side of their climatological axis and their weakening on the equatorward side, corresponding to the phase shift of the SAM its positive polarity (Figure 1.4).

While the emission of greenhouse gas is considered to be the main driver of the trends in most of the seasons, recent observations and numerical studies have indicated that the poleward shift of the westerly jet axis in the summertime SH troposphere in the late 20th century was forced through the coupling with the stratospheric trend induced by ozone depletion ("ozone hole") (Thompson and Solomon 2002; Gillett and Thompson 2003; Thompson et al. 2011). The springtime ozone depletion induced by the emission of ozone-depleting substances cooled the polar stratosphere and thereby strengthened the polar vortex, followed by the phase shift of the summertime SAM in the troposphere to its positive polarity (Figure 1.5). It has been pointed out that the main driver of the summertime surface climate trends in the SH was the SAM trend induced by the stratospheric ozone depletion (Polvani et al. 2011). The climatic trends include surface cooling over Antarctica, and warming in the Antarctica Peninsula, southern Africa and most of the midlatitude/subtropical Southern Ocean, as well as increased precipitation in southeastern Australia (Thompson et al. 2011). Although the mechanisms and factors controlling the transmission of the high-latitude stratospheric signal into the troposphere still remain highly controversial (Haynes 2005; Garfinkel et al. 2013), there is an indication that downward influence through the SAM requires feedback forcing from tropospheric eddies, including migratory extratropical cyclones and anticyclones (Kushner and

Polvani 2004; Garfinkel et al. 2013). Deepening the understanding of the climate trend requires the sufficient understanding of in the factors that determines the meridional structure of SAM.

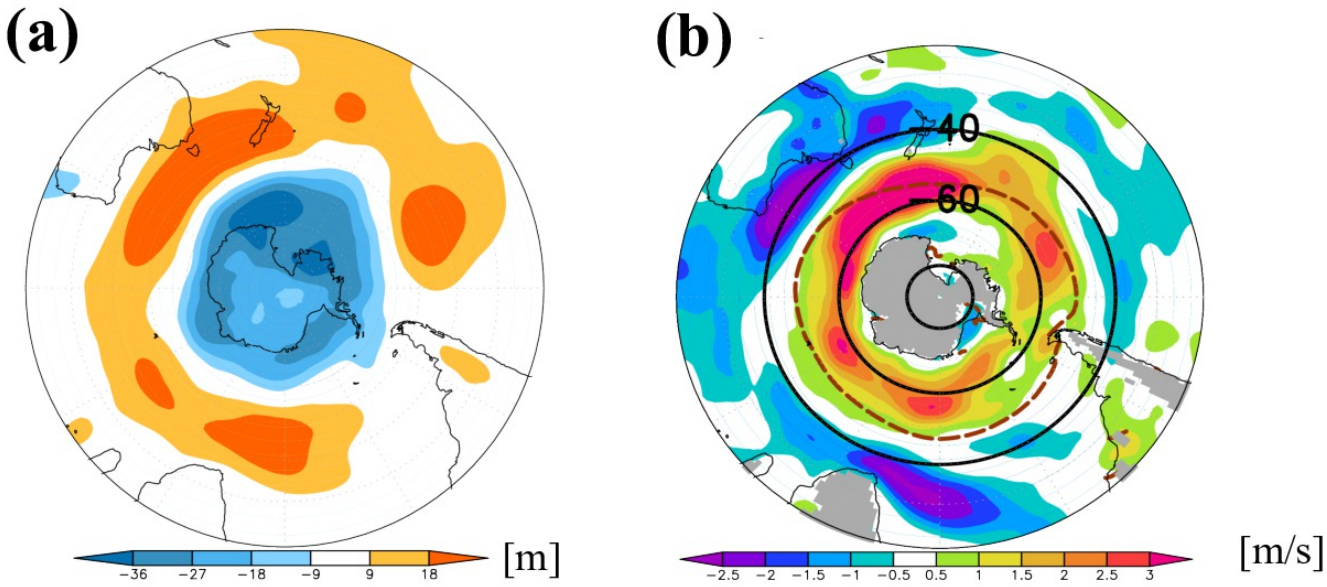

Figure 1.4. Trend in (a) geopotential height at 850 hPa and (b) zonal wind at 925hPa over the midlatitude SH observed during the last 21 years of the 20th century (1979/80-2000/01). The dashed line in (b) indicates the axial latitude of the climatological westerlies. Gray shades indicate the data-void regions.

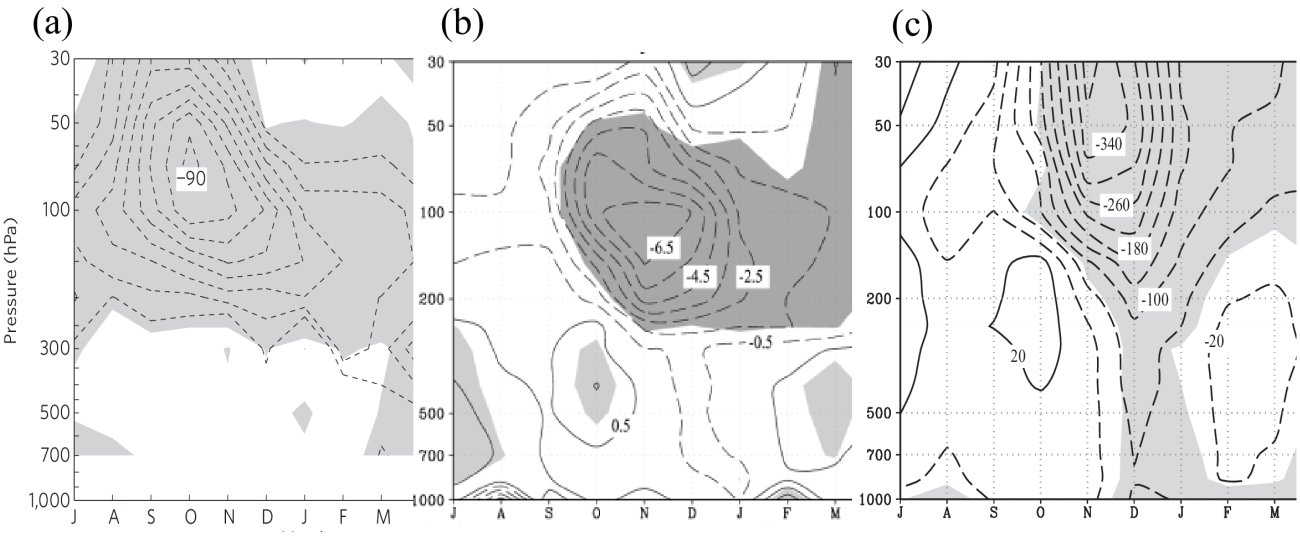

Figure 1.5. Seasonal march in (a) Ozone depletion ratio [%] of the 14yr-mean ozone concentration (1995-2009 except for 2002) from the other 14yr-mean (1966-1979) observed over Syowa station (69° S, 40° E). Adapted from Thompson et al. (2011). (b). Linear trends in station temperature (1969 –98) and (c) observed geopotential height. Trends exceeding a unit standard deviation of the natural variability in monthly mean data are shaded. Adapted from Thompson and Solomon (2002).

1.3. Advances in understanding of the climatological-mean stormtracks and zonal-mean circulation

a) Recent recognition of the importance of midlatitude oceanic frontal zones

As discussed in sections 1.1 and 1.2, the understanding of the annular mode is important for understanding not only the dominant natural climate variability but also anthropogenically induced the long-term climatic trends. Observations and modeling studies have shown that feedbacks between the westerlies and transient eddies are of critical importance for the maintenance of the SAM-associated deviations from the mean state (e.g., Lorenz and Hartmann 2001). Therefore, dynamical understanding of the annular mode cannot be separated from that of the climatological mean state. Nevertheless, the understanding of the mean state, including the latitude of a stormtrack – a region of recurrent development of migratory cyclones and anticyclones – and the associated eddy-driven PFJ was not necessary sufficient until recently, as the role of midlatitude ocean has been overlooked.

In the troposphere, two types of prominent westerly jets are observed, as evident in the SH zonal-mean circulation (Figure 1.6). One is STJ, whose distinct core is located at the tropopause level on the poleward flank of the Hadley Cell. Poleward motions along the upper branch of the Hadley Cell drive the STJ under the angular momentum conservation (Held and Hou 1980). Observed STJ is much stronger in the winter hemisphere than in the summer hemisphere. Equatorward motions in the lower branch of the Hadley Cell accompany the surface easterlies (Trades), into which the solid earth or the ocean supplies eastward angular momentum through friction. The STJ tends to be confined into the upper troposphere, and underneath at the surface the axis of the subtropical high-pressure belt tends to be situated in corresponding to downward motions of the Hadley Cell (Nakamura and Shimpo 2004).

The other westerly jet forms in midlatitudes, which is referred to as PFJ or subpolar jet. Unlike STJ, PFJ is driven and maintained by transient eddy heat and momentum fluxes (Palmén and Newton 1969). The formation of the upper-tropospheric PFJ core is through westerly momentum

transport mainly from STJ by synoptic-scale eddies whose activity propagates from midlatitudes into the subtropics. At the same time, poleward eddy heat flux acts to transport westerly momentum downward to form the surface westerlies for reducing the westerly shear under the constraint of the thermal wind balance (Lau and Holopainen 1984). The PFJ thus has deep structure, and the associated surface westerlies are giving up eastward angular momentum to the solid earth or the ocean through friction. An outstanding question is what determines the latitude of the eddy-driven PFJ. To answer this question, one thus needs to understand what determines the stormtrack latitude.

Transient eddies or synoptic-scale migratory cyclones and anticyclones, whose activity is organized into a stormtrack, can develop most efficiently along a region with high baroclinicity (e.g., Nakamura et al. 2004), consistent with the linear wave theory of baroclinic instability (Charney 1947; Eady 1949). The baroclinicity is proportional to the meridional temperature gradient, equivalent to the westerly wind vertical shear. Lee and Kim (2003) and Son and Lee (2005) have pointed out through their numerical experiments that the baroclinic zone under the STJ core is important for the formation of a stormtrack. However, the baroclinic eddy growth along the STJ is not often observed in the real atmosphere, the STJ core can acts as a well-defined waveguide for propagating eddies (Nakamura and Sampe 2002; Nakamura and Shimpo 2004). Meanwhile, Robinson (2006) showed through a set of two-layer numerical experiments that a stormtrack and PFJ in the model act to maintain themselves only when the equator-pole difference in a prescribed reference profile of radiative-equilibrium temperature toward which instantaneous temperatures are restored exceeds a certain threshold value. Their result suggests that a stormtrack and PFJ can be self-maintained without any influence of the lower boundary.

Nevertheless, the linear baroclinic instability theory (Charney 1947; Eady 1949) suggests the vital importance of an eastward-propagating surface “thermal Rossby wave” associated with background meridional SAT gradient for the development of a baroclinic disturbance. The particular importance in a more realistic situation of cyclogenesis was discussed further in Hoskins et al. (1985) (Figure. 1.7). Indeed, Sanders and Gyakum (1980) pointed out that the rapid growth baroclinic waves tend to be observed near oceanic fronts with sharp SST gradient in the NH ocean

basins. Likewise, Sinclair (1995) pointed out that surface cyclogenesis over the SH occurs most frequently near an oceanic frontal zone in the southwestern Indian Ocean. Previous numerical studies have nonetheless overlooked the significance of a surface baroclinic zone. For example, Lee and Kim (2003) described their model experiment without referring to the surface temperature profile prescribed as the lower-boundary condition. In addition, after reviewing a number of AGCM experiments, Kushnir et al. (2002) concluded that the atmospheric response to the observed large-scale midlatitude SST anomalies is not systematic, emphasizing passive characteristics of the midlatitude ocean to the atmospheric variability.

However, recent studies by Nakamura and Shimpo (2004) and Nakamura et al. (2004) pointed out the observed latitudinal correspondence of the lower-tropospheric stormtracks and the underlying oceanic frontal zones over the two hemispheres (Figures 1.8a-b). In each of the ocean basins, a surface baroclinic zone with sharp SAT gradient forms along an oceanic frontal zone. Driven by the eddy heat and momentum fluxes associated with transient eddies along a stormtrack, the observed PFJ tend to be situated slightly poleward of SST front (Nakamura et al. 2004). The observed association among a stormtrack, PFJ, and oceanic frontal zone is particularly evident in the South Indian Ocean (Figures 1.8a, c), where the cool Antarctic Circumpolar Current and the warm Agulhas Return Current are confluent to form the core region of the oceanic frontal zone in the SH (Sinclair 1995; Nakamura and Shimpo 2004). The cores of the SH stormtrack and PFJ are anchored by the sharp SST gradient and recurrent development of cyclones leads to the formation of a well-defined rainband (Figure 1.8d; Nakamura et al. 2008).

As an extension of the conventional models by Palmén and Newton (1969) and by Lee and Kim (2003), Nakamura et al. (2004) postulated a new conceptual model of the tropospheric general circulation (Figure 1.9), where they argue the necessity for taking a midlatitude oceanic frontal zone into account to understand the latitudes of a stormtrack and PFJ. The wind-stress curl exerted by the PFJ-associated surface westerlies acts in turn to drive the western boundary currents (Hoskins and Valdes 1990), whose thermal advections contribute to the maintenance of the frontal SST gradient (Nakamura et al. 2004).

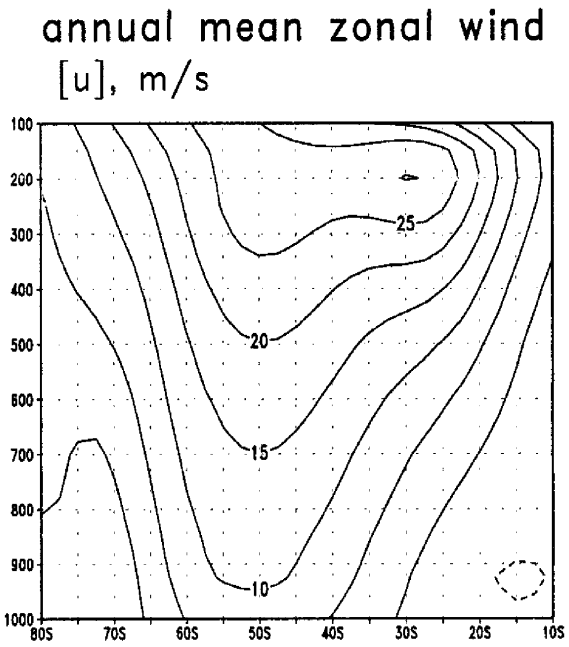

Figure 1.6. Latitude-height section showing the annual-mean zonal-mean zonal wind derived by NCEP-NCAR reanalysis data (1978-1997) in the Southern Hemisphere. Adapted from Lorenz and Hartmann (2001).

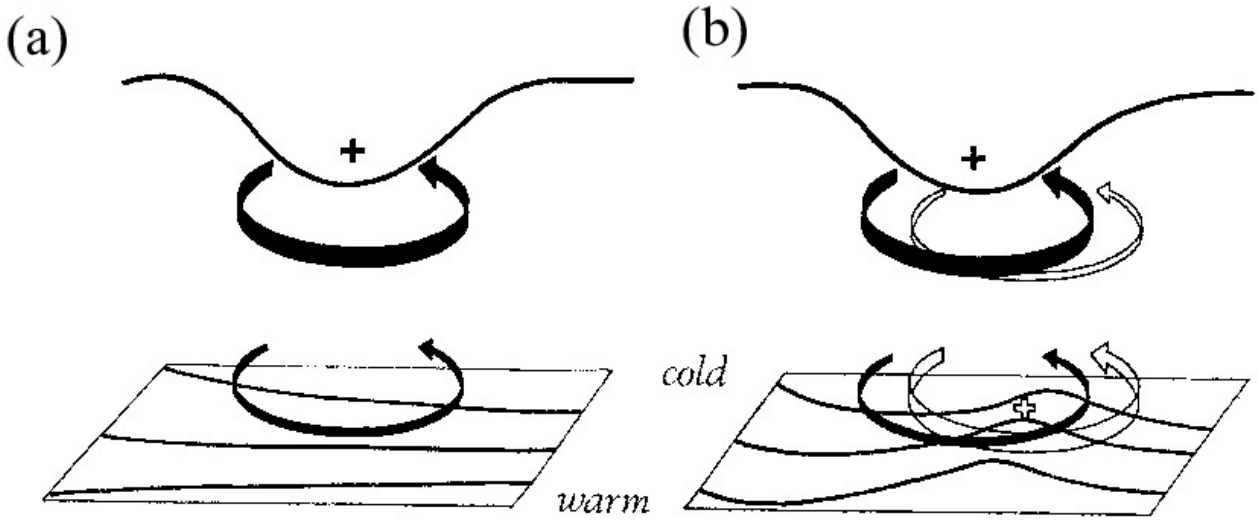

Figure 1.7. A schematic picture showing cyclogenesis through the coupling development between the anomalous potential volticity (PV) propagating near the tropopause and the anomalous temperature at the surface. Circulation anomaly induced by the upper-level PV (thin black arrows at the bottom of both figures) induces the thermal advection and thereby temperature anomaly (plus sign in (b)). It in turn induces anomalous circulation near the tropopause and thereby volticity advections near the tropopause (thin white arrow in (b)), which amplifies the upper level PV anomaly. Such a feedback process is important for the amplification of those anomalies. Adapted from Hoskins et al. (1985).

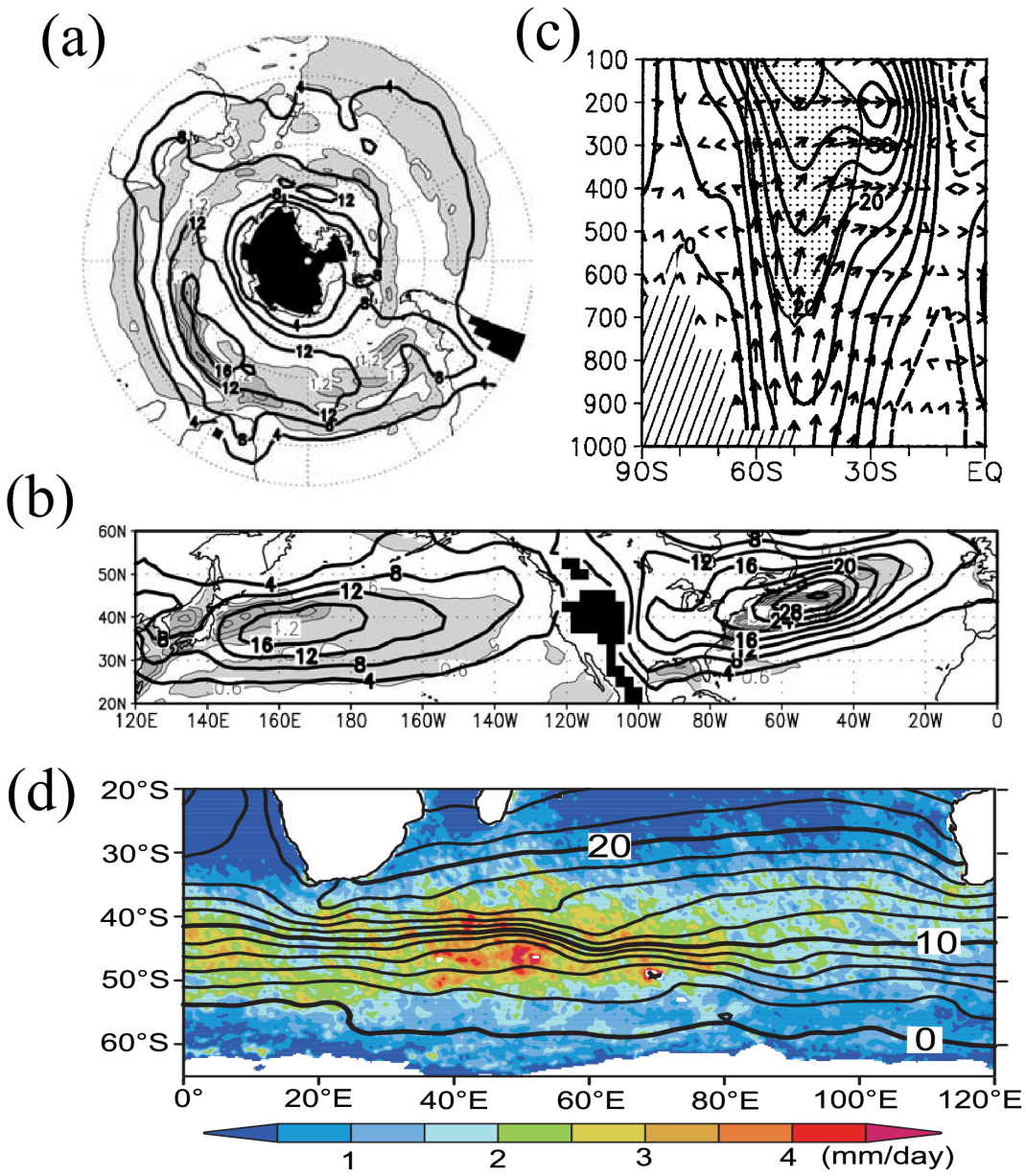

Figure 1.8. (a) The austral wintertime climatology (July–August) of 850-hPa poleward heat flux associated with subweekly disturbances in the SH (heavy lines for 4, 8, 12 and 16 K•m/s). Oceanic frontal zones are indicated by light and heavy stippling, where meridional SST gradient [°C/110 km] is 0.6~1.2 and above 1.2, respectively (with thin lines for every 0.6). (b) As in (a) but for the boreal winter (January-February) in the NH (heavy lines for every 4 K•m/s). Dark shading indicates data-void regions. (c) Climatological July section of meridional [m^2/s^2] and vertical [$Pa•m/s^2$] components of the extended E-P flux (Trenberth 1986), and zonal-mean zonal wind averaged for the South Indian Ocean (50°~90°E), based on the NCEP reanalysis. Adapted from Nakamura et al. 2004. (d). Climatology of the satellite-measured SST (OI-SST) [°C] and precipitation (AMSR-E) (mm/day; shade) over the South Indian Ocean for austral winter (June-August). Adapted from Nakamura et al. (2008).

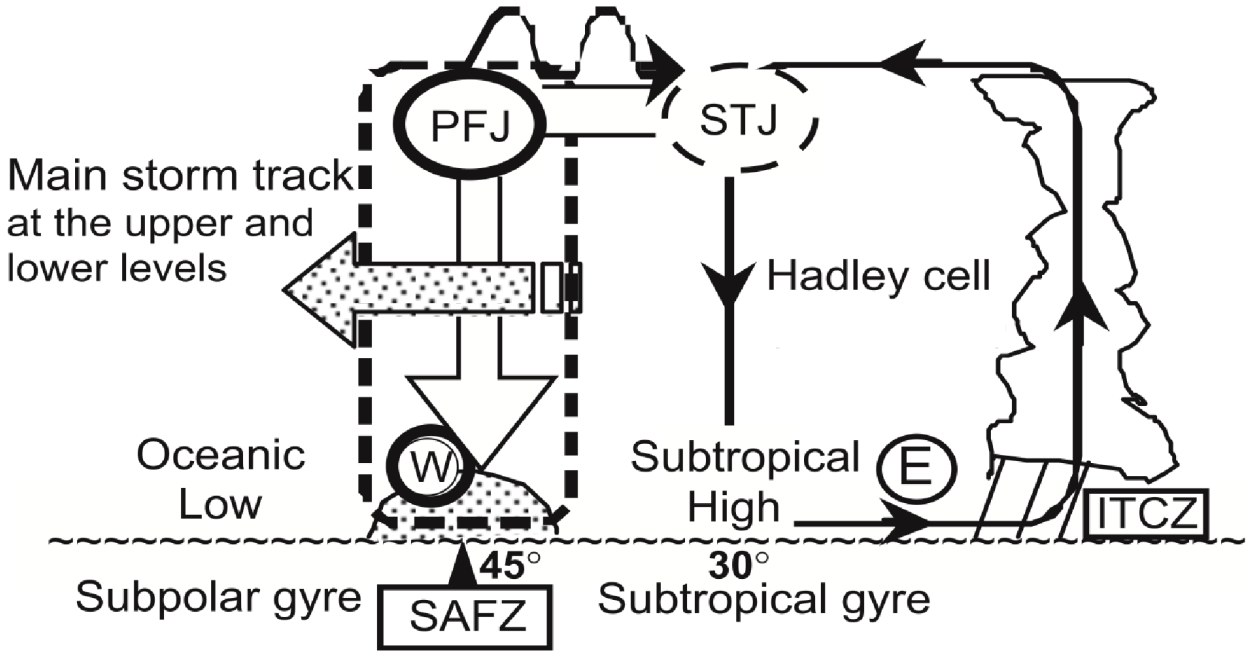

Figure 1.9. Schematics of tropospheric general circulation over an ocean basin with an SST front at 45°, denoted as a subarctic frontal zone (SAFZ). The main storm track (thick dashed line) is formed over a surface baroclinic zone (stippling), which is anchored by the SST front. Wave-activity dispersion to the STJ (wavy arrow) leads to form a deep polar-front jet (PFJ) above the SAFZ. Eddy downward transport of the mean-flow westerly momentum (open arrow) associated with the poleward eddy heat flux (stippled arrow) maintains a surface westerly jet (circled W) along the SAFZ. Adapted from Nakamura et al. (2004).

b) Understanding of the tropospheric general circulation through aqua-planet experiments

The new conceptual model postulated by Nakamura et al. (2004) describes the fundamental picture of the tropospheric general circulation that would be realized even without landmass. The tropospheric circulation observed in the SH may be interpreted in this simple framework with slight modifications for the individual ocean basins (Nakamura et al. 2004). For the SH, the essential importance of the midlatitude SST gradient for the atmospheric circulation can be assessed through "aqua-planet" AGCM experiments where all the landmass and sea-ice are removed from the model lower-boundary and, in many cases, zonally uniform SST is prescribed. This idealized "aqua-planet" setting suppresses planetary waves forced by land-sea thermal contrasts and topography, while retaining synoptic-scale eddies and eddy-driven PFJ. Although any quantitative reproduction of the observed atmosphere is of course impossible under the idealized aqua-planet setting, the experiment nevertheless allows us to extract the essential features of the atmospheric general circulation and the active role of the ocean to the atmosphere.

To warrant the applicability of the aqua-planet setting to the real atmosphere, meticulous care should be taken in preparing the meridional SST profile, especially in the Tropics and subtropics. In aqua-planet experiments by Brayshaw et al. (2008) and Chen et al. (2010), for example, they adopt SST profiles with modest meridional gradients entirely over the extratropics and modify them in changing tropical/subtropical SST simultaneously with midlatitude SST (Figure 1.10). It is obvious that these modifications directly affect the Hadley Cell and associated STJ and indirectly the midlatitude stormtrack and eddy-driven PFJ (Lee and Kim 2003). Although their studies imply the significance of midlatitude oceanic frontal zones, they fail to extract it unambiguously from the impacts of the tropical SST.

To overcome this particular deficiency, Nakamura et al. (2008) utilized an alternative set of aqua-planet experiments using a well thought-out set of SST profiles (black lines in Figure 1.11). In their control experiment, the climatological SST profiles observed over the South Indian Ocean (60~80°E) for austral summer (Dec.-Feb.) and winter (Jun.-Aug.) are prescribed in the model NH and SH, respectively. The profile is characterized by a steep SST gradient associated with an

oceanic front, which is located at 45°S throughout the year in both hemispheres. To extract the significance of an SST front, they modified the profile only in the extratropics to smooth out the frontal SST gradient (green lines in Figure 1.11). In this modification, tropical SST is unchanged from their control experiment so as to avoid any direct impacts on the Hadley Cell and STJ, which allowing us to extract only the impacts of the midlatitude SST front on the stormtrack and PFJ. They revealed the crucial importance of the oceanic frontal zones for energizing and anchoring the transient eddies along the SST front and strengthening the eddy-driven PFJ at the poleward flank of the front as actually observed (Figures 1.12a, c). They pointed out the importance of the meridional contrast in the turbulent sensible heat supply from the ocean for the recurrent development of the transient eddies through maintaining the near surface baroclinicity (Figure 1.12b), referring the mechanism as “oceanic baroclinic adjustment”. The importance of the sensible heat supply for anchoring a stormtrack was also verified in a more sophisticated high-resolution coupled GCM (Nonaka et al. 2009) and a high-resolution regional atmospheric model (Taguchi et al. 2009). Sampe et al. (2010) further studied the mechanism through an extensive investigation of the aqua-planet AGCM experiments by Nakamura et al. (2008). They showed that the differential heat supply from the ocean across the front effectively restores the near-surface baroclinicity against the relaxing effect by the poleward heat flux by transient eddies, leading to the recurrent development of the transient eddies along the front (Figure 1.13). The critical importance of the sensible heat supply for the efficient restoration of surface baroclinicity observed along the stormtracks has been verified through a numerical study by Hotta and Nakamura (2011).

Recent studies investigated the importance of the latitude of an oceanic front for the transient eddy activity and midlatitude westerlies. Deremble et al. (2012) used a three-level quasi-geostrophic model to suggest the considerable dependence of the latitude of eddy-driven PFJ to the latitude of prescribed SST front. Their estimation of the surface sensible heat flux was, however, too crude to validate how the oceanic baroclinic adjustment is operative in their experiments. Furthermore, the quasi-geostrophic model without considering the spherical geometry failed to simulate a realistic STJ. These deficiencies have been overcome in aqua-planet AGCM experiments by Ogawa et al.

(2012), in which the observed SST profile virtually identical to that in Nakamura et al. (2008) was prescribed as the model boundary condition. In their sensitivity experiments, they shifted the SST front meridionally by keeping not only its width and strength but also the tropical SST unchanged (Figure 1.14), to extract the impacts of SST front separated from the change in the Hadley Cell and STJ. With this experimental design, assessment of the importance of the SST frontal latitude for the climatological mean state of the stormtrack and PFJ became possible for the first time. Ogawa et al. (2012) found the climatological-mean near-surface baroclinicity (red lines in Figures 1.15a-b) and lower-tropospheric stormtrack (green lines of Fig.1.15a-b) to be particularly sensitive to the latitude of the SST front in both hemispheres. Strong meridional gradient of the surface sensible heat flux acts to maintain the near surface baroclinic zone along the SST front, showing that the oceanic baroclinic adjustment operative around the SST front (Figures 1.15e-f). Interestingly, however, the feedback forcing by transient eddies cannot necessary drive the PFJ near the SST front in all of the experiments (Figures 1.15c-d). Specifically, in case of the subpolar SST front, PFJ tends to form far away from the front at the latitude that corresponds to the PFJ axis that would be realized in the non-front experiment by Nakamura et al. (2008). This is suggestive of the dominance of atmospheric internal dynamics as postulated by Robinson (2006) in the climatological mean state in case of a subpolar SST front. However, the interpretation for the weakening of the sensitivity of the climatological mean axial latitude of PFJ to the SST front was not fully addressed. Furthermore, the differences in the impacts of SST front on the atmosphere between the winter and the summer hemispheres were not fully understood, either.

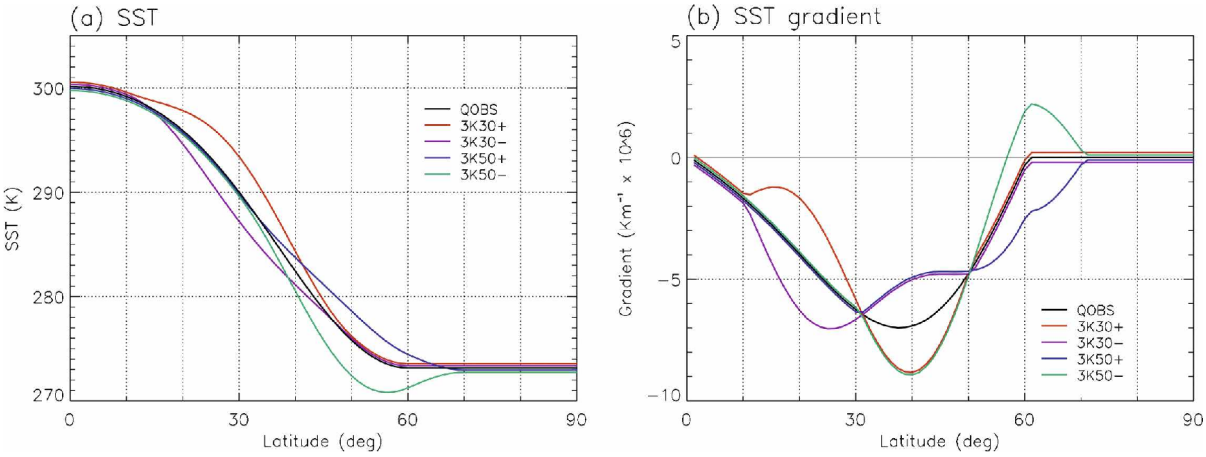

Figure 1.10. (a) SST profile and (b) SST gradient prescribed in Brayshaw et al. (2008).

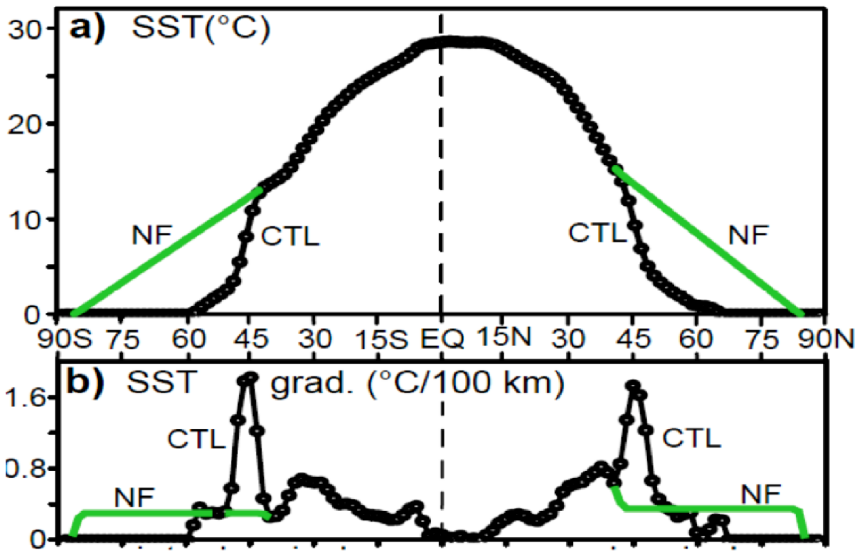

Figure 1.11. (a) SST profile and (b) SST gradient prescribed in Nakamura et al. (2008).

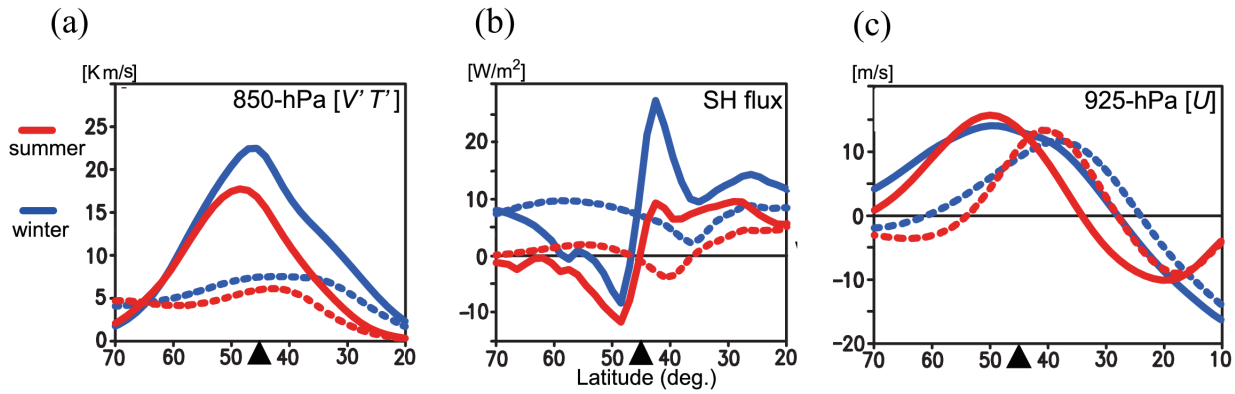

Figure 1.12. Climatological mean meridional profiles of zonal-mean (a) poleward eddy heat flux at 850hPa associated with subweekly disturbances, (b) upward turbulent sensible heat flux (positive: upward) (c) zonal wind velocity at 925hPa (positive: westerly) with (solid, CTL) and without (dotted, NF) SST front (triangle) for the summer (red) and winter (blue) hemispheres. Adapted from Nakamura et al. 2008.

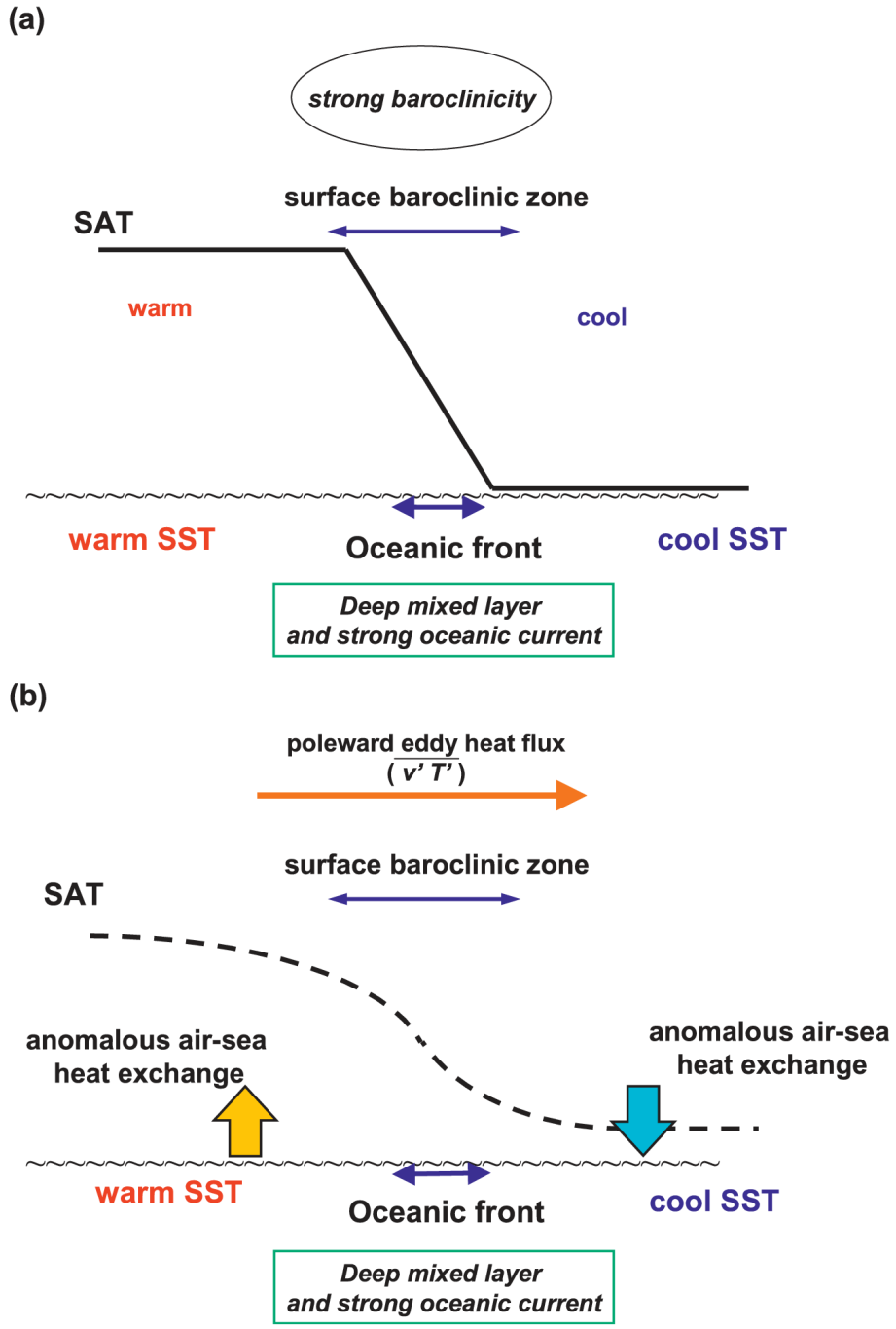

Figure 1.13. Schematic diagrams showing the oceanic baroclinic adjustment, the restoration of near-surface baroclinicity anchored by an oceanic front through surface sensible heat flux from the ocean against the relaxation by horizontal eddy heat transport. (a) An oceanic front forms a strong SAT gradient (solid line) which induces rapid baroclinic eddy growth. (b) SAT gradient is relaxed by poleward eddy heat flux and then restored by turbulent sensible heat flux at the surface corresponding to the air–sea temperature difference. Adapted from Sampe et al. (2010).

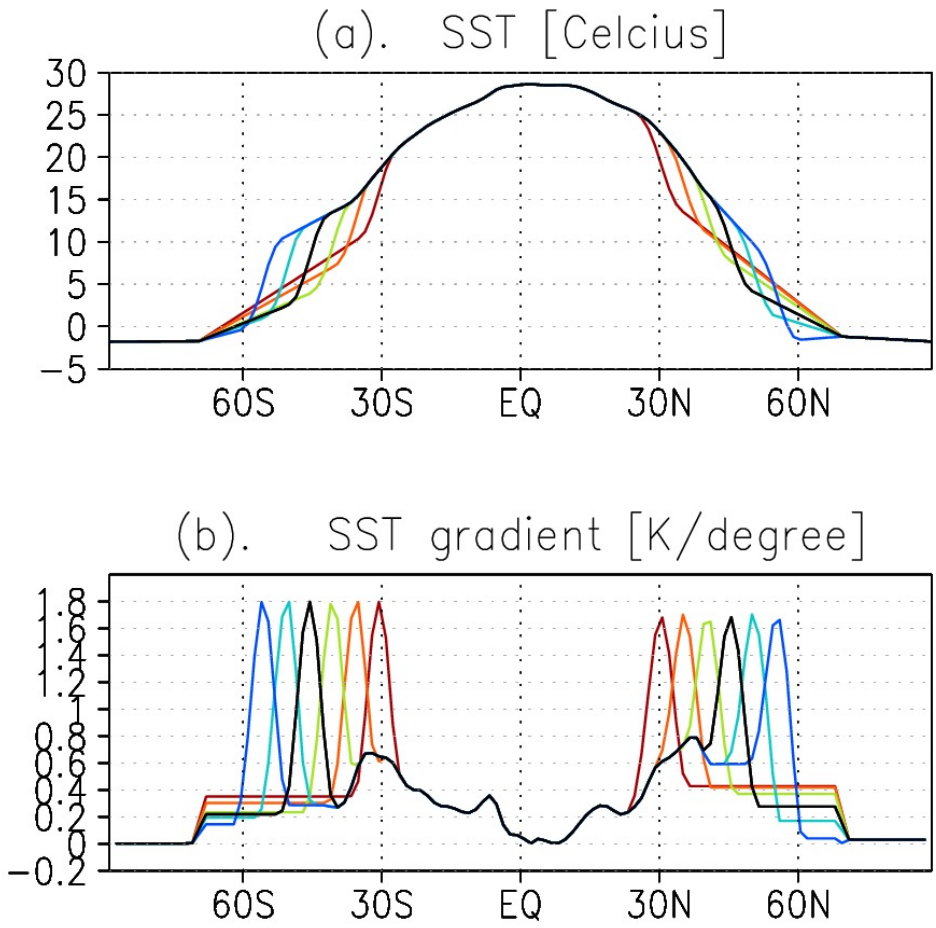

Figure 1.14. (a) SST profile and (b) SST gradient prescribed in Ogawa et al. (2012).

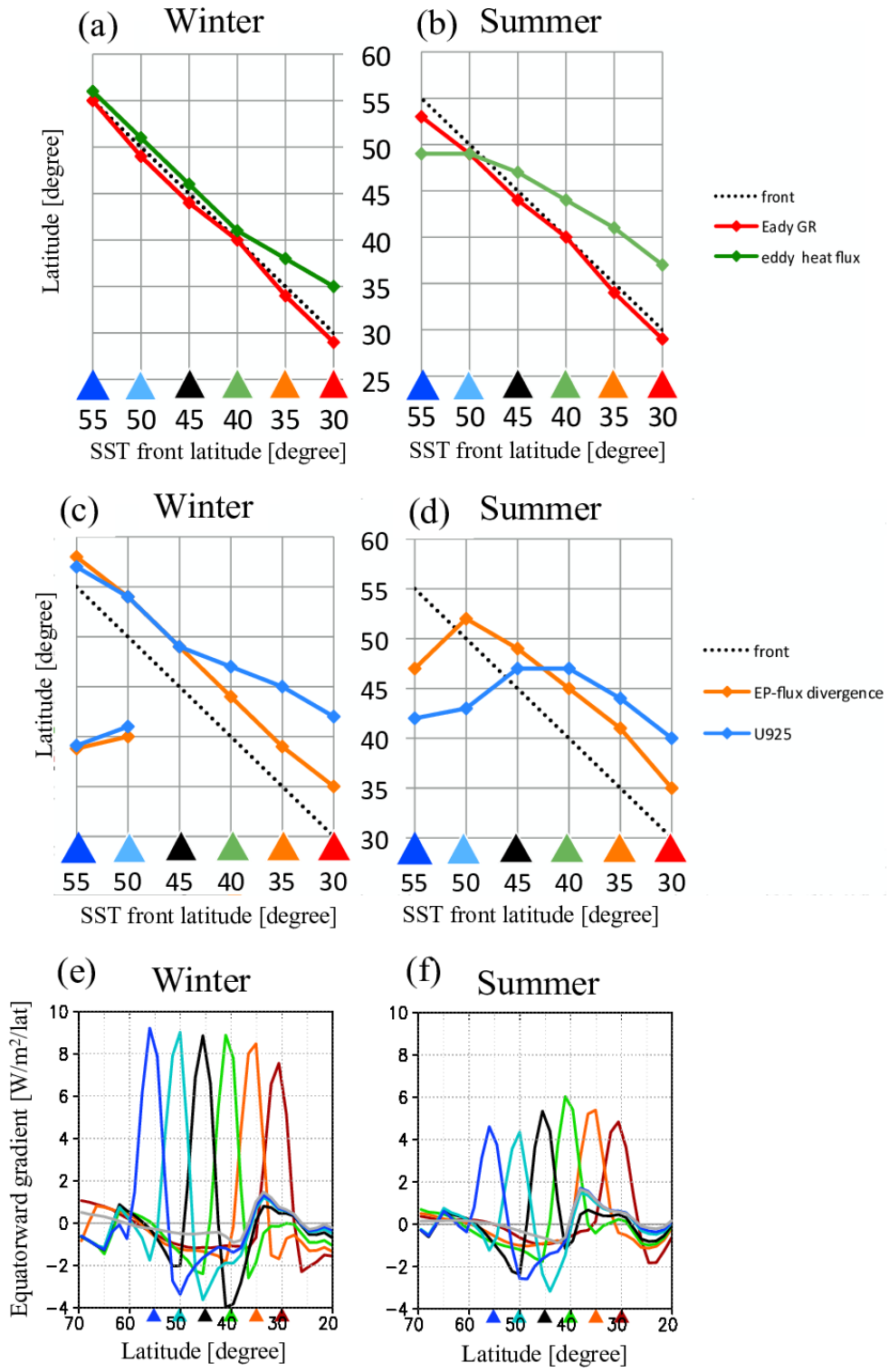

Figure 1.15. (a) Diagram showing the climatological-mean latitudes (ordinate) of zonally averaged maximum baroclinicity (red) and poleward heat flux (green) for the winter hemisphere as function of the frontal latitude (abscissa; also dotted line). (b) As in (a), but for the summer hemisphere. (c) As in (a), but for the latitudes of maximum zonal wind (blue) and eddy westerly acceleration (orange) derived from the E-P flux divergence (Edmon et al. 1980), both at the 925 hPa level. Gray dashed line indicates the maximum of zonal wind as 925-hPa simulated in the NF experiment by Nakamura et al. [2008] with SST profile with no frontal gradient. (d) As in (c), but for the summer hemisphere. Adapted from Ogawa et al. (2012). (e) Meridional profiles of the mean states of the meridional gradient of turbulent upward sensible heat flux from the surface in the winter hemisphere. (f) As in (e), but for the summer hemisphere.

1.4. Potential importance of oceanic frontal zones for the annular mode

Nakamura et al. (2008) pointed out through their aqua-planet AGCM experiments that the significant changes in transient eddy activity and PFJ between the midlatitude SST profiles with and without the frontal SST gradient might affect the behavior of the annular mode. In fact, Sampe et al. (2013) demonstrated through extensive analysis of the aqua planet experiments by Nakamura et al (2008) that the meridional structure and amplitude of the annular mode simulated in the presence of SST front is similar to what is observed whereas the amplitude is reduced by nearly 50% and the meridional structure is considerably distorted by the removal of frontal SST gradient in midlatitudes (Figure 1.16). These previous studies suggest the necessity to consider a midlatitude oceanic frontal zone in understanding not only the climatological-mean state of PFJ but also the annular mode variability. While the climatological significance of the stormtrack and PFJ has been pointed out by several studies (e.g., Ogawa et al. 2012), no study has demonstrated the dependence of the annular mode to the latitude of SST front. The influence of oceanic frontal zones on the tropospheric annular mode may exert significant impacts on the vertical coupling of the annular mode with the stratospheric variability, but no study has addressed the problem yet, either.

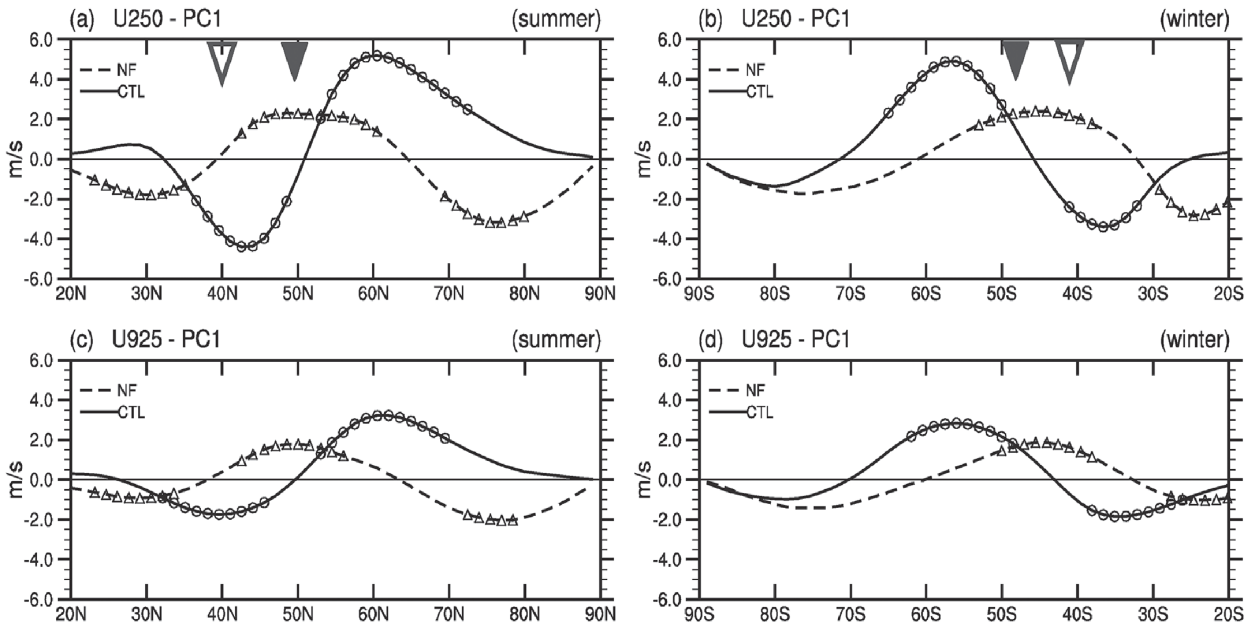

Figure 1.16. Zonal-mean zonal wind anomaly [m/s] at the (a,b) 250-hPa and (c,d) 925-hPa levels associated with the annular mode in a set of aqua-planet experiments for (a, c) the summer hemisphere and (b, d) the winter hemisphere. Solid (dashed) lines are for the experiment in the presence (absence) of the SST front. Small circles and triangles are plotted for a correlation greater than 0.5. Filled and open large triangles on the upper fringe of the upper panels indicate the axial latitudes of the climatological-mean storm track at 250-hPa in the presence (absence) of the SST front. Adapted from Sampe et al. (2013).

1.5. Purpose of this study

Recent studies have suggested the importance of the midlatitude oceanic frontal zones for the annular mode variability (Nakamura et al. 2008; Sampe et al. 2013), whereas the annular mode signature may be sensitive to the climatological-mean state of the westerly (Eichelberger and Hartmann 2007), whose sensitivity to the latitude of the oceanic frontal zone has been pointed out (Ogawa et al. 2012). That suggests the necessity of considering the latitude of SST front to understand the annular mode dynamics. The first aim of this study is therefore to investigate the dependence of the annular mode characteristics to the latitude of SST front. As in the previous studies, we utilize aqua-planet AGCM experiments to address this issue, which enables us to extract the essential features of the stormtrack and PFJ by suppressing planetary waves. In spite of its simplicity, the results may help the understanding of the real atmosphere in the SH (Sampe et al. 2013). Understanding the dependency of the annular mode on the latitude of SST front should help us understand the counterintuitive climatological dependency of the PFJ latitude discussed in Ogawa et al. (2012). The second aim of this study is to investigate another important aspect, the overlooked significance of the midlatitude oceanic frontal zone in activating stratosphere-troposphere dynamical coupling. As a relevant example of the vertical coupling through the annular mode, surface climatic trends induced in the SH during the late 20th century by the stratospheric ozone depletion are targeted in this study. While the advance in understanding of the SAM and its vertical coupling has contributed to deepening the understanding of the ozone-induced trends observed in the summertime SH, the potential importance of the SST front for the trends has not been addressed yet.

This dissertation is structured as follows. In chapter 2, the dependence of the annular mode on the latitude of SST front will be discussed, where the importance of the turbulent sensible heat supply will be addressed. In chapter 3, the impacts of SST front on the climatic trend induced by stratospheric ozone hole are discussed, where the importance of the SST front for the vertical coupling of the annular mode will be addressed. Discussions and concluding remarks are given in

chapter 4, where the comprehensive understanding of the impact of SST front on the annular mode will be discussed, including their seasonal dependence.

Chapter 2. Importance of midlatitude oceanic frontal zones for the regime-like behavior of the wintertime annular mode

2.1. Experimental design and analysis procedure

The AFES, AGCM for Earth Simulator (Ohfuchi et al. 2004), is used for our numerical experiments in this study. The original code of AFES was developed jointly by the (former) Center for Climate System Research (CCSR) of the University of Tokyo and the Japanese National Institute for Environmental Studies (NIES), but the code has been modified substantially for the particular architecture of the Earth Simulator. The model has 56 levels up to 0.09 hPa. Its horizontal resolution for our experiments is T79, corresponding approximately to 150km grid intervals both longitudinally and latitudinally. Though not sufficient for fully resolving meso-scale features of SST distributions within a oceanic frontal zone prescribed as the model lower-boundary condition, this resolution is still enough to resolve frontal SST gradient across an oceanic frontal zone that is crucial for realistic representation of both the climatological-mean state and annular mode variability in aqua planet experiments (Nakamura et al. 2008; Ogawa et al. 2012; Sampe et al. 2010, 2013).

The lower boundary of the AGCM in this study is set as the fully global ocean with different latitudinal profiles of zonally uniform SST (Figure 2.1a). As in the previous studies (Nakamura et al. 2008; Sampe et al. 2010,2013; Ogawa et al. 2012), one of these SST profiles was taken from the OI-SST data (Reynolds et al. 2007) for the South Indian Ocean [60~80°E] (black line in Figure 2.1a), where the warm Agulhas Return Current is confluent with the cool Antarctic Circumpolar Current to maintain frontal SST gradient. The profile for austral winter (Jun.-Aug.) was assigned to the model Southern Hemisphere (SH) and the corresponding summertime profile (Dec.-Feb.) to the model NH. With this SST profile characterized by the frontal gradient at 45° latitude in both hemispheres, the AGCM was integrated for 120 months under insolation fixed to its solstice condition after six-month spin-up. For sensitivity experiments, the frontal gradient of SST is shifted

from the latitude of 30° to 55° by 5° (Colored lines in Figures 2.1a,b), as in Ogawa et al. (2012). In the modifications, not only the intensity of the frontal gradient but also the SST equatorward of 25° was kept unchanged (Figure 2.1b), so as not to modify the tropical convection which drives the Hadley cell. We believe such a care for tropical SST is necessary to separate the impact of a midlatitude SST front from that of tropical SST, which is actually missing in many previous aqua-planet studies (Brayshaw et al., 2008; Chen et al., 2010). The SST profiles in this study are designed to highlight the dependence of the annular mode variability on the latitudinal position of an oceanic frontal zone. For deepening our understanding, another experiment is performed by using a "non-front (NF)" SST profile (Nakamura et al. 2008; Sampe et al. 2010, 2013). In each of the experiments with a frontal zone the SST gradient poleward of the frontal zone is the same as in the "NF experiment" (dashed line in Figures 2.1a,b). It should be noted that our idealized experiment is not designed for reproducing the observed atmospheric circulation in the SH, but aimed to highlight the essential features of the extratropical circulation.

In this chapter, our main focus is placed on the wintertime annular mode. Sampe et al. (2013) found the meridional structure of the summertime annular mode to be essentially unchanged regardless of the midlatitude SST gradient, except for the latitudinal shift of its entire structure corresponding to the latitudinal shift of climatological-mean PFJ axis in midlatitudes. They also found that the structure and amplitude of the wintertime annular mode are altered substantially with the removal of SST front. In spite of little variability in a well-defined STJ in the presence of SST front as in the observations (e.g., Lorenz and Hartmann 2001), the removal of the SST front changes the wintertime annular mode signature into a seesaw-like variability in intensity between the STJ and PFJ. In this chapter, sensitivity to the latitude of SST front is assessed for the wintertime annular mode and its association with high- and low-frequency fluctuations. These fluctuations are extracted through digital filtering with the half-power cutoff period of 8 days.

The climatological-mean states of storm tracks and westerlies simulated in our experiments are almost identical to the results in Ogawa et al. (2012) (compare Figure 2.2a with Figure 1.15c; see also Ogawa et al. 2012). In the lower troposphere (Figure 2.2a), the axial latitude of

climatological- mean [U] shows a counterintuitive low sensitivity to the subpolar SST front despite the high sensitivity in stormtrack latitude (Figure 1.15a), with a hint of dual peak in the westerly axis as found in Ogawa et al. (2012). The sensitivity is more ambiguous in the upper troposphere with the nearly constant latitude of PFJ around 45°(Figure 2.2b). In the following sections, sensitivity to the latitude of the SST front is discussed not only for the annular mode variability but also for the climatological-mean state to interpret the counterintuitive findings by Ogawa et al. (2012). A possible application of our findings in the numerical experiment to the observed wintertime SAM is also discussed.

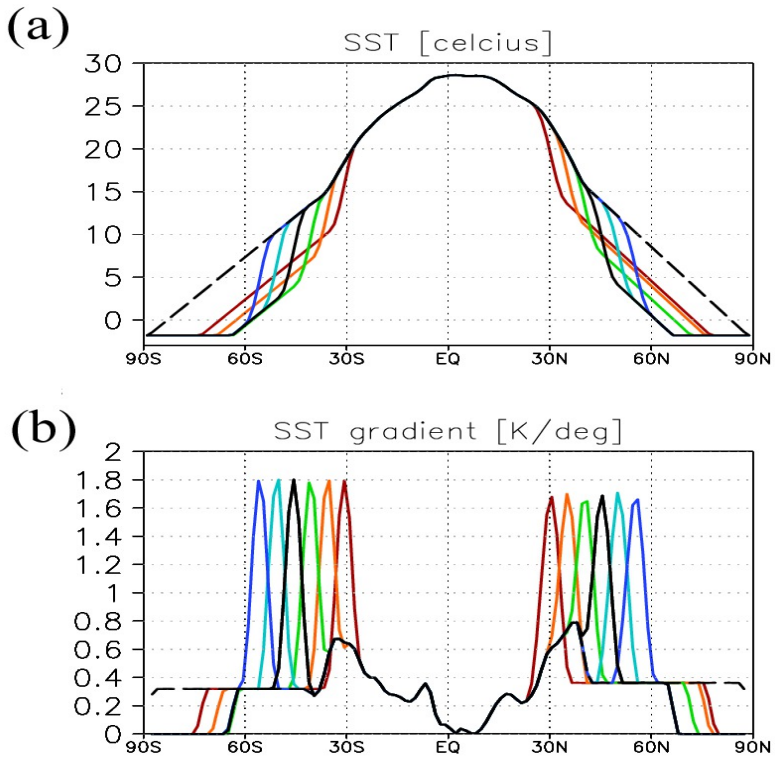

Figure 2.1. Latitudinal profiles of (a) SSTs and (b) its meridional gradient prescribed zonally symmetrically as the lower-boundary condition of AGCM.

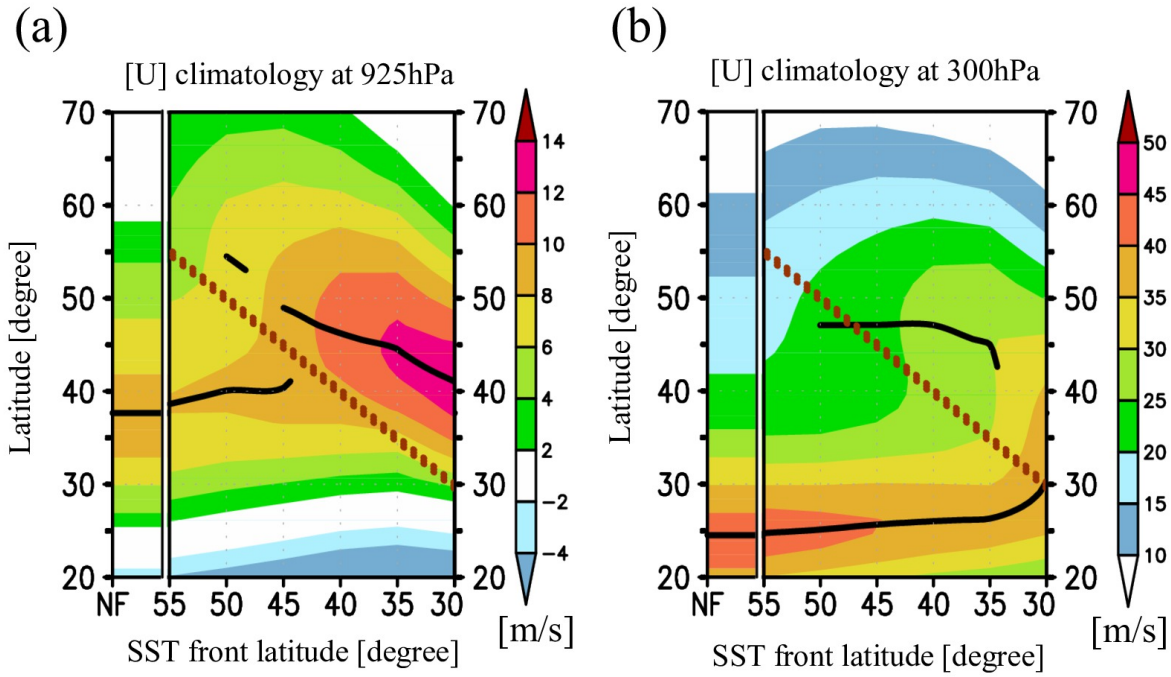

Figure 2.2. Climatological-mean profiles of [U] simulated at (a) 925hPa and (b) 300hPa in the individual experiments. The abscissa indicates the prescribed latitude of SST front. The vertical axis indicates latitude. Color shading indicates the zonal wind speed [m/s]. Axial latitudes of [U] are indicated with black lines. Latitude of the SST front is also indicated with a dotted line.

2.2. Low-frequency annular variability simulated in aqua-planet experiments

To extract low-frequency variability, an 8-day butter-worth filter was applied to the zonally averaged zonal wind ([U], where square bracket represents zonal-mean statistics) at 925hPa, where the climatological-mean STJ is very weak. We chose this level to highlight the variability of PFJ. Latitudinal profiles of the [U] variance for all the experiments are compiled in Figure 2.3 as function of the frontal latitude. The variance is area-weighted with the cosine of latitude. For the SST front located at 30°, 35° or 40° between the subtropics and midlatitudes, the [U] variance is maximized at the poleward flank of the climatological-mean [U] axis (as indicated with red lines in Figure 2.3), which suggests that a latitudinal wobble of the PFJ axis is dominant in the low-frequency variability. For the SST front located at 45°, 50° or 55° (between midlatitudes and subpolar latitudes), however, the [U] variance tends to be maximized far away from the climatological-mean [U] axis around 40° (red lines), but rather near its secondary axis located on the poleward flank of the SST front (Figure 2.2a). In addition, another secondary maximum in the [U] variance is found around 40° in these experiments, with a hint of its correspondence with the primary climatological-mean [U] axis. The aforementioned findings indicate that characteristics of the zonally symmetric low-frequency variability are quite sensitive to the latitude of SST front. Meanwhile, the two maxima of the model [U] response in the NF experiment is located at 50° and 70°, both of them are far away from the climatological-mean axial latitude of [U] around 40°S.

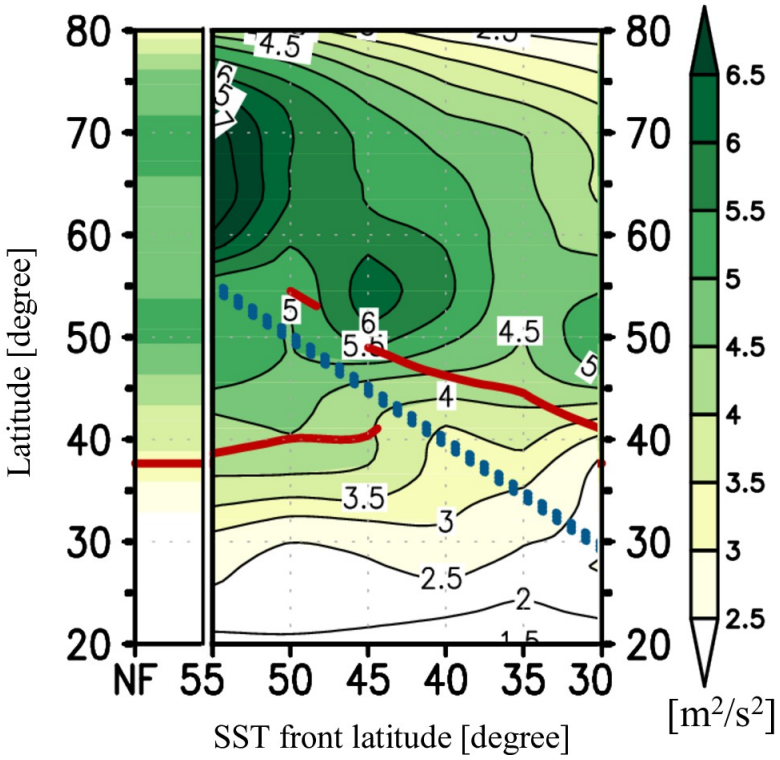

Figure 2.3. Climatological variances of [U] at 925 hPa simulated in individual experiments. Shading indicates the variance [m^2/s^2] weighted by cosine (latitude). Axial latitudes of climatological mean [U] are indicated with red lines. Latitude of SST front is also indicated with a dotted line.

2.3. Wintertime annular mode simulated in the aqua-planet experiments

a) Definition of the model annular mode

In order to identify the annular mode signature in the model extratropical troposphere, we applied an EOF analysis to 8-day low-pass-filtered anomalies of daily 925hPa [U] for the entire analysis period (3600 days) over the domain poleward of 20°S. In this EOF analysis, the [U] anomalies are weighted by the square root of the cosine of latitude. As observed (e.g., TW 2000), the model annular mode is defined as meridional wobble of the axial latitude of PFJ. The annular mode is extracted in EOF1 for all the experiments except the one with SST front at 35°, where EOF2 represents the annular mode. As in the convention, the "positive (negative)" phase represents poleward (equatorward) shift of the PFJ axis. Fractions of the total [U] variance explained by EOF1 and EOF2 are shown in Figure 2.4a. In the experiment with the SST front at 35°, the variance explained by EOF2 are comparable with that by EOF1. Indeed, the variance fraction accounted for by EOF2 (about 40%) for the SST front at 35° is larger than that by EOF1 in the experiments with the SST front at 30° (38%), 40° (37%) and 45° (39%).

b) Sensitivity of annular mode structure to the latitude of SST front

Instead of displaying the obtained EOF patterns, meridional profiles of composited differences in [U] between strong positive and negative events of the model annular modes for all the experiments are compiled in Figure 2.4b. The meridional structure of the annular mode shows strong sensitivity to the latitude of SST front. Centers of action in the [U] variability are located poleward and equatorward of the SST front, representing their seesaw relationship with the node situated around the SST front. The nodal latitude tends to be displaced almost linearly with the change in the latitude of SST front. The [U] anomaly at the poleward center is almost twice as strong as the equatorward counterpart. These two centers of action and the node in between are reflected in the meridional variance in [U] (Figure 2.3). Another EOF, which is EOF2 except for the experiment with the SST front 35° (EOF1 in this case), represents the variability in the strength of PFJ with little displacement in its latitude (Figure 2.4c). In the absence of SST front (i.e., the NF experiments), two centers of action located near 50° and 70° show much stronger [U] anomalies than another center in the subtropics, which is consistent with the [U] variance (Figure 2.3). Since the climatological-mean westerly axis is located at 38° (Figure 2.2a), EOF1 in the NF experiment represents not only meridional fluctuations of the midlatitude westerly axis but also the poleward extension/contraction of the midlatitude westerly belt.

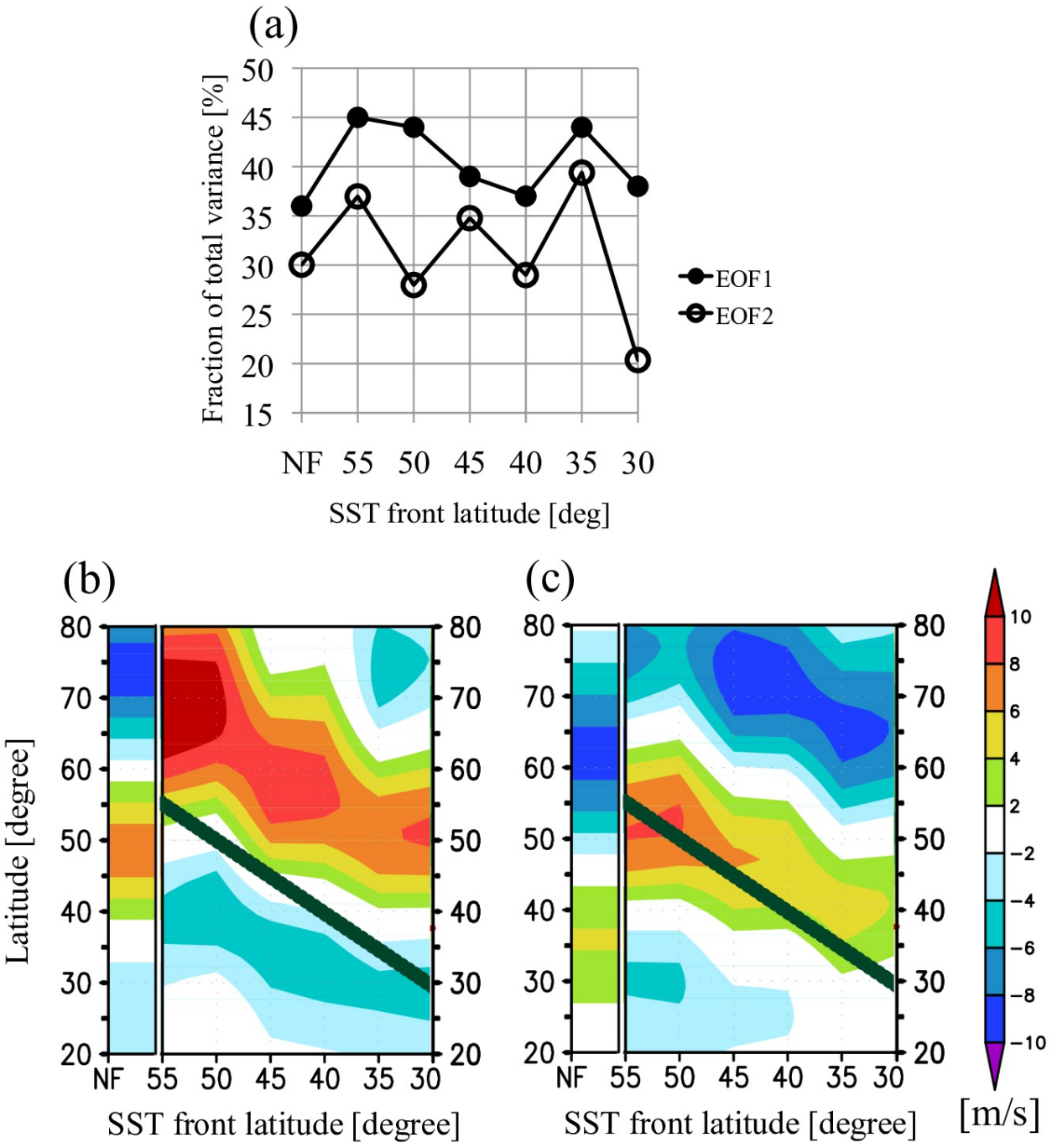

Figure 2.4. (a) Fractions of the variance associated with low-frequency [U] variability explained by EOF1 (closed circles) and EOF2 (open circles), as functions of the latitude of SST front. (b) Meridional profiles of [U] deference (m/s) at 925hPa between the composites of strong positive and negative events of the model annular modes when the absolute value of the principal component exceeds a unit standard deviation. (c) Same as in (b), but for EOF2 (EOF1 only for the experiment with SST front at 35°).

c) Characteristics of the annular mode in its positive phase

The meridional distribution of [U] anomalies associated with the model annular mode (Figure. 2.4b) suggests the sensitivity of its characteristics to the latitude of the SST front. In this section, typical behaviors of the PFJ and stormtrack for the positive phase of the annular mode are described. Figure 2.5a shows the meridional profiles of [U] at 925hPa composited for the periods in which the PC value exceeds a unit standard deviation. As the STJ is weak in the lower troposphere, the results mostly describe the variability of PFJ. In the positive phase, the latitude of the PFJ axis shows strong sensitivity to the latitude of the SST front, with a systematic poleward displacement relative to the front as observed climatologically over the Southern Oceans (Nakamura et al. 2004). This poleward displacement means that the near-surface westerly axis is inclined to stay on the cooler side of the SST front. The cooling of air parcels along the circumpolar westerly axis by the underlying ocean (Figure 2.5i) acts to displace them poleward (towards an isotherm with lower potential temperature) and thereby shrink the radius of the circulation circuit (Hoskins 1991), and this acceleration is necessary for the near-surface westerlies to be maintained against the frictional forcing. In the positive phase of the annular mode, the latitude of the near-surface stormtrack (Figures 2.5b-c) also shows its high sensitivity to the latitude of the SST front, and the stormtrack axis is closer to the SST front compared to the PFJ axis in all the experiments. Figure 2.5a indicates that the latitudes of PFJ and stormtrack in the experiments with subtropical SST front are also located systematically poleward of the SST front, which will be discussed later in this chapter.

In the positive phase of the annular mode, the upper-tropospheric axis of PFJ is distinct from STJ (Figure 2.5d), as in both the observations and previous model simulations (e.g., Hartmann and Lo 1998; Nakamura et al. 2008; Sampe et al. 2013). The latitudes of the upper-level axes of the stormtrack (marked as the peak variance of meridional wind fluctuations in Figure 2.5f or anomalous streamfunction in Figure 2.5h) and the eddy-driven PFJ (Figure 2.5d) almost coincide one another, and they show notable sensitivity to the latitudinal shift of the SST front, as their low-level counterpart. Their sensitivity is consistent with the same sensitivity found in the convergence maximum of upper-level poleward flux of westerly momentum associated with

transient eddies (Figure 2.5e). The poleward eddy momentum flux reflects the tendency for the major axis of each eddy component to tilt from southeast (SE) to northwest (NW), as indicated statistically as the positive correlation between the fluctuations in zonal and meridional wind velocities (Figure 2.5g). Interestingly, the positive correlation tends to be strongest at the SST front, and the domain of the positive correlation extends poleward even onto the poleward flank of the PFJ axis. On the equatorward flank of the PFJ axis, the anticyclonic westerly shear acts to yield deformation of eddy structure and thereby contribute to the maintenance of its SE-NW tilt. Figure 2.5g suggests that this tilt also tends to be observed even on the poleward of the eddy center with maximum anomalous wind velocity (Figure 2.5f) and of the PFJ axis as long as the cyclonic westerly shear is relatively weak (Figure 2.5d). From the viewpoint of energetics, this tilt acting on the cyclonic westerly shear yields slight positive conversion of kinetic energy (KE) from the PFJ into eddies. These characteristics of the horizontal structure of eddies in the positive phase of the annular mode are in agreement with both the observation and previous model simulations (Yu and Hartmann 1993; Hartmann and Lo 1998).

It should be stressed that, compared to the climatological-mean state shown in Ogawa et al. (2012), the latitudinal association among the stormtrack, PFJ and SST front is more evident in the positive phase of the annular mode, especially when the SST front is located at subpolar latitude. In other words, the their association in the climatological-mean state is likely a contribution from the positive phase of the annular mode.

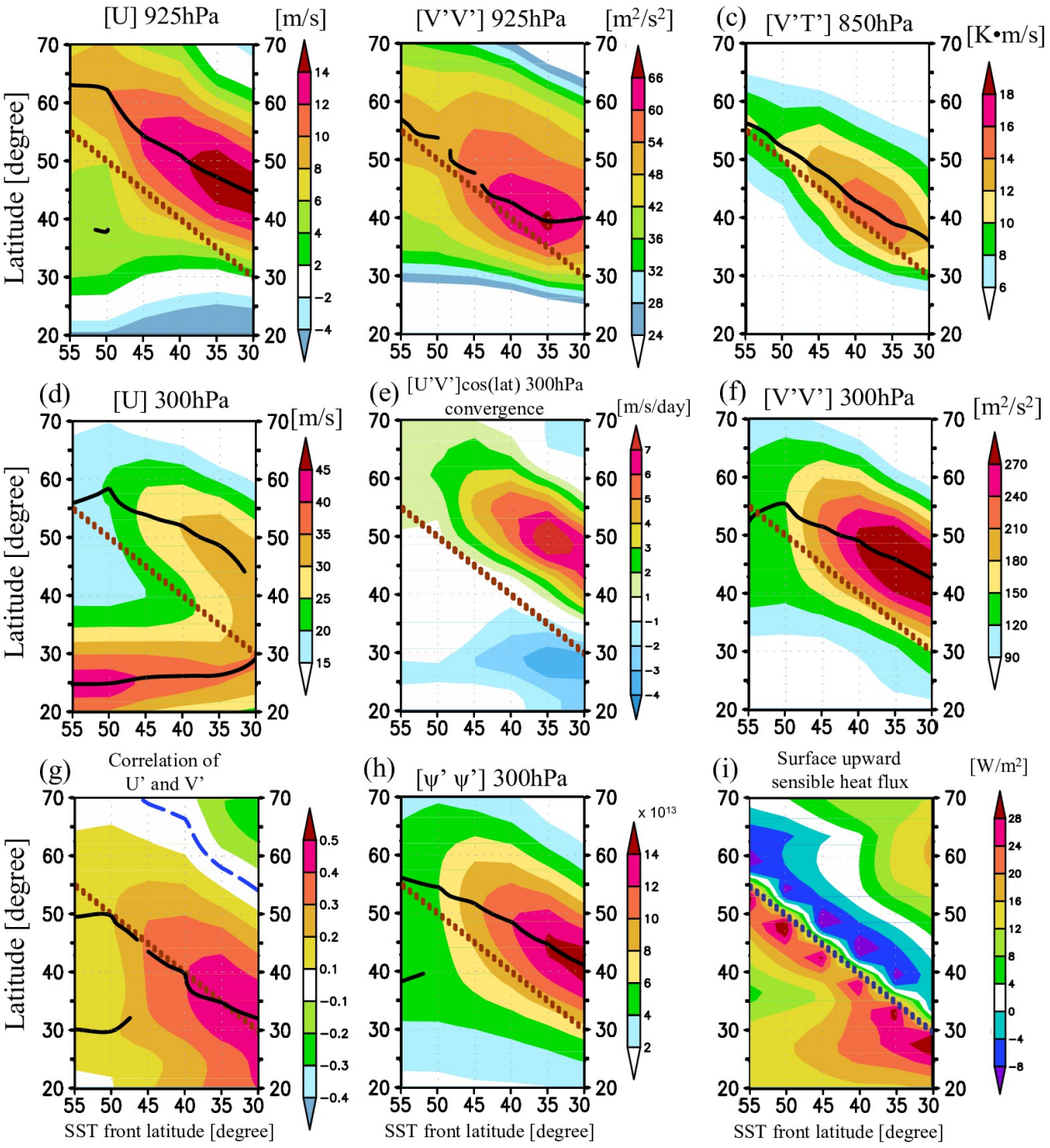

Figure 2.5. Composited meridional profiles of various zonal mean statistical values for the positive phase of the annular mode, compiled as functions of the latitude of SST front for individual experiments. (a) [U] at 925 hPa, (b) [V'V'] at 925 hPa, (c) [V'T'] at 850hPa, (d) [U] at 300hPa, (e) convergence of eddy momentum flux ([U'V'] cos(lat)), (f) [V'V'] at 300hPa, and (g) correlation coefficient of 8 day high-pass filtered U and V. Blue dashed line indicates zero. Primes indicate 8-day high-pass filtered quantities. (h) As in (f), but for the high-pass filtered stream function. (i) As in (f), but for the zonal-mean upward sensible heat flux.

d) Characteristics of the annular mode in its negative phase

Figure 2.6 shows the composited statistics for the negative phase of the annular mode. In sharp contrast to the positive phase (Figure 2.5a), the PFJ axis in the negative phase shows virtually no sensitivity to latitudinal shift of the SST front, and the axis stays around 40° for all the experiments (Figure 2.6a). Such an insensitivity of the PFJ axial latitude to the latitude of SST front has already been discussed by Ogawa et al. (2012), but for the climatological-mean primary PFJ axis simulated with the subpolar SST front (c.f. Figure 2.2a). They pointed out its latitudinal correspondence to the mean state of the NF experiments by Nakamura et al. (2008) and Sampe et al. (2010). Ogawa et al. (2012) argued that this latitudinal insensitivity of the mean PFJ might be due to the dominance of atmospheric 'internal' dynamics unrelated to the lower-boundary condition (Robinson et al. 2006). It is evident in Figure 2.6a that the PFJ axis in the negative phase of the annular mode in any of our experiments with frontal SST gradient well corresponds to the climatological-mean PFJ axis in the NF experiment, as indicated with the white dashed line in Figure 2.6a. The latitudinal collocation between the SST front and the low-level stormtrack axis marked with the peak variance of meridional wind fluctuations is also much less evident than in the positive phase (Figure 2.6b). The stormtrack latitude thus defined tends to be located near the climatological-mean stormtrack latitude in the NF experiment, despite the tendency for 850hPa poleward heat flux associated with transient eddies, as a measure of their baroclinic development, to maximize in the vicinity of the SST front (Figure 2.6c). It is thus suggested that in the negative phase of the annular mode the latitudes of the stormtrack and eddy-driven PFJ tend to be determined by the atmospheric internal dynamics, at least for the experiments with a midlatitude or subpolar SST front.

In the negative phase of the annular mode, the [U] profile near the tropopause level in any of the experiments (Figure 2.6d) is characterized by the prominent STJ, and PFJ almost diminishes in midlatitudes. Regardless of the frontal latitude, the upper-level stormtrack axis is located around 40° (Figures 2.6f,h) near the climatological-mean axes in the NF experiment (white line), and associated eddy momentum flux convergence (Figure 2.6e) maintains the midlatitude westerlies as

in the NF experiment. Regardless of the frontal latitude, the positive correlation between the fluctuations in zonal and meridional wind velocities (Figure 2.6g) suggests that eddies tend to exhibit SE-NW tilt of their major axis in the midlatitude and subtropics, while at subpolar latitudes the tilt is from southwest (SW) to northeast (NE) as indicated by the negative correlation. This "banana shape" of eddies in the negative phase of the annular mode is consistent with the observation and previous model experiments (Yu and Hartmann 1993; Hartmann and Lo 1998). From the viewpoint of energetics, the NW-SE tilt occurring on the cyclonic westerly shear between the dominant STJ and weakened PFJ yields positive KE conversion into eddies. In the experiments with midlatitude SST front (at 40°, 45° and 50°), both upper-level stormtrack activity and poleward eddy momentum flux tend to be weaker in the negative phase of the annular mode than in its positive phase, which is consistent with the weaker PFJ.

For the experiments with the subtropical SST front (at 30° or 35°), the PFJ axis is closer to the SST front in the negative phase of the annular mode, by definition, than in its positive phase, making a sharp contrast to the situation in the other experiments. In fact, the stormtrack activity with the subtropical SST front (Figure 2.6b) tends to be stronger in the negative phase than its in the positive phase (Figure 2.5b), suggestive of the stronger influence of the surface baroclinicity above the SST front in the negative phase. The annular mode signature for the subtropical SST front is different from the counterpart for the subpolar or midlatitude SST front, as discussed more in detail later in this chapter.

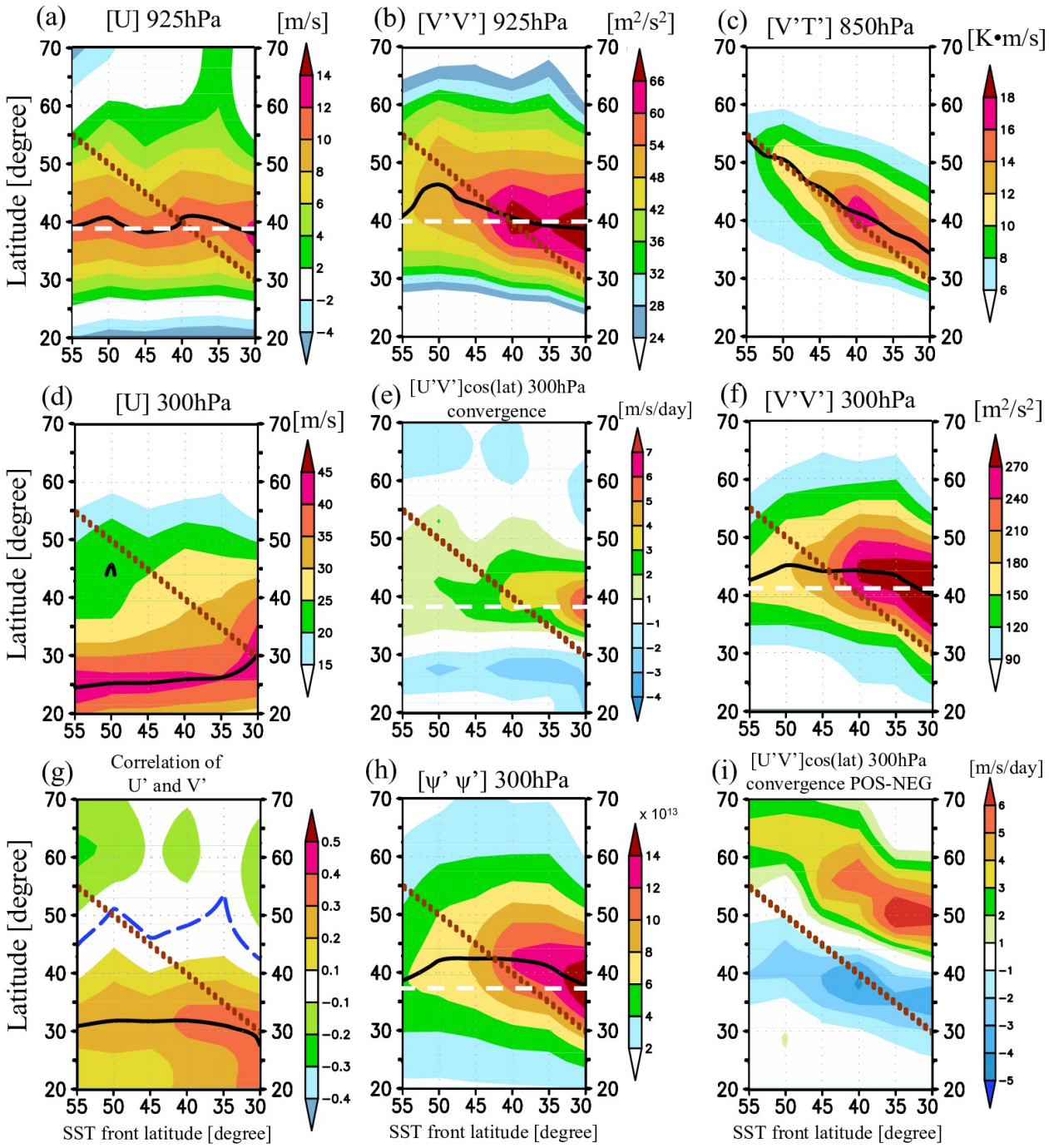

Figure 2.6. (a-h) As in Figures 2.5 (a-h), respectively, but for the negative phase of the annular mode. White dashed line in (a,b,e,f,h) indicates the climatological-mean peak latitude in the absence of SST front. Primes indicate 8-day high-pass filtered quantities. (i) Meridional profiles showing the composited difference in the convergence of eddy momentum flux ([U'V'] cos(lat)) at 300hPa between strong positive and negative events of the model annular modes for which the absolute value of the principal component exceeds a unit standard deviation.

e) Regime-like characteristics of the model annular mode and importance of sensible heat supply

As discussed in the preceding sections, the sensitivity of the annular mode characteristics to the latitude of SST front depends strongly on its phase. Latitudes of the PFJ and stormtrack axes show strong dependency on the latitude of SST front in the positive phase, while such a dependency become ambiguous in the negative phase. This suggests that the annular mode variability may be a manifestation of wobble of the extratropical atmospheric circulation between two "regimes" – one under the strong influence of SST gradient as the lower-boundary condition, and the other under the strong control by atmospheric internal dynamics with negligible influence of the boundary condition. In this section, we discuss the regime-like characteristics of the annular mode in the experiments with extratropical SST fronts.

Figure 2.7 shows the probability density of the latitude of the PFJ axis at 925hPa as a function of the latitude of the SST front. For the experiments with midlatitude or subpolar SST fronts (45°~55°), distinct dual peaks are found with a well-defined probability minimum in between. One of the peaks is located poleward of the SST front with displacement of about 5°, while the other is located equatorward of the front and around the same latitude as a distinct single peak in the NF experiment. Dual peaks are hinted also for the experiment with the SST front at 40°. Bimodality of the probability density distribution in the physical space can be regarded as a representation of two regimes of the zonal mean circulation. Latitudes of these two peaks correspond to those of composited [U] for the individual phases of the annular mode (compare Figure 2.7 with Figures 2.5a and 2.6a). In fact, for each of the experiments, the mean residence time of the [U] maximum at given latitude (Figure 2.8) tends to maximize around the latitudes of the dual probability peaks (Figure 2.7). These facts thus suggest two distinct quasi-equilibrium states of the model extratropical circulation in the presence of an extratropical SST front. Therefore, the variability associated with the model annular mode may be interpreted as a regime shift between these two quasi-equilibrium states or "regimes".

The higher sensitivity of PFJ and stormtrack to the SST front in the positive phase of the annular mode implies a stronger anchoring effect by the SST front on them. Previous studies (e.g.

Nakamura et al. 2008; Hotta and Nakamura 2011) demonstrated the importance of the meridional contrast of the surface turbulent sensible heat flux across an SST front in maintaining the surface baroclinicity and thereby allowing the recurrent development of synoptic eddies along the SST front (referred to as “oceanic baroclinic adjustment” in these studies). Nakamura et al. (2008) found in their aqua-planet experiment that zonally averaged sensible heat flux has strong gradient above the SST front (Figure 1.12b) in the climatological-mean state. In the experiments by Ogawa et al. (2012), such a strong peak in the equatorward gradient of zonal-mean upward sensible heat flux is also found climatologically in all the experiments regardless of the latitude of the SST front (Figures 1.15e,f). To discuss the variability of the anchoring effect associated with annular mode in this study, the anomalous equatorward gradient of upward sensible heat flux associated with the annular mode is investigated. Figure 2.9 shows the difference between the composited gradients of zonal-mean sensible heat flux between the two phases of the annular mode (positive minus negative). For each of the experiments, the heat flux gradient across the SST front is indeed stronger in the positive phase than in the negative phase, which suggests more efficient oceanic baroclinic adjustment operative in the positive phase.

The aforementioned regime-like characters of the wintertime annular mode in the presence of an oceanic frontal zone can be illustrated clearly by comparing the composites for different principal component (PC) values. Figure 2.10 shows the meridional profiles of [U] at 925hPa and 300hPa, stormtrack activity at 850hPa and 925hPa, the convergence of westerly momentum flux associated with both high- and low- frequency eddies, and the equatorward gradient of the surface sensible heat flux, all of which are based on the experiment with the SST front at 55° and composited separately for the individual spans of PC values. In the positive phase (for positive PC values), westerly axes in both the lower and upper troposphere are located poleward of SST front (Figures 2.10a-b) as already depicted in Figure 2.5a, as a manifestation of the well-defines of PFJ separated from the STJ. In this phase, the stormtrack axis near the surface is located along the SST front (Figure 2.10c), where baroclinic growth of transient eddies is active (Figure 2.10d). The convergence of poleward eddy momentum flux associated with migratory high-frequency eddies

(Figure 2.10e) occurs poleward of the PFJ axis, and in extreme events the flux is even divergent near the axis (Figures 2.10a-b). Meanwhile, the corresponding flux convergence associated with low-frequency wave disturbances (Figure 2.10f) occurs just along the PFJ axis and on its equatorward side. When the contributions from the two frequency bands are combined, eddies act to maintain the PFJ, and thus association among the stormtrack, PFJ and SST front is clear in the positive phase.

In the negative phase, however, the PFJ axis at 925hPa is located around 38°, far equatorward of the SST front (Figure 2.10a). In the lower troposphere, the westerlies near the SST front are very weak or even easterlies are simulated with the SST front at 30°, which suggests the overshadowed influence of the SST front on the extratropical circulation. In the upper troposphere (Figure 2.10b), PFJ is merged into STJ to form a broad single jet, in contrast to the double-jet structure in the positive phase. Correspondingly to the shift of PFJ, the low-level stormtrack defined as the variance of meridional wind fluctuations is also displaced equatorward from the SST front by 10~15° in latitude (Figure 2.10c), although the baroclinic growth of eddies as indicated by poleward eddy heat flux still maximizes at the SST front (Figure 2.10d). The peak latitude of the upper-level eddy momentum flux convergence is also displaced equatorward (Figures 2.10e-f), but still collocated with the low-level PFJ axis. The midlatitude westerlies are thus eddy-driven even in the negative phase of the annular mode, although the association of the PFJ and stormtrack with the SST front is broken down.

Indeed, probability for the latitude of the [U] maximum near the surface plotted in Figure 2.10g as a function of PC values clearly indicates that the [U] maximum tends to be located at either poleward of the SST front at 55° or equatorward around 38°. An unambiguous minimum between the probability peaks suggests the annular mode variability as a manifestation of the regime shift between the two distinct quasi-equilibrium states. In fact, the anchoring effect of the near-surface baroclinicity through meridional gradient in the surface sensible heat flux across the SST front at 55° is stronger (weaker) in the positive (negative) phase (Figure 2.10h), consistent with the stronger (weaker) baroclinic eddy growth along the front (Figure 2.10d). It should be noted that the association suggests nothing about the cause and effect between the stormtrack formation and the

effective restoration of near-surface baroclinicity through anomalous turbulent sensible heat flux. As suggested by Limpasuvan and Hartmann (2000), the stormtrack and PFJ axes can shift into the vicinity of the SST front without any anomalous sensible heat supply from the ocean. Once the PFJ and stormtrack shift into the vicinity of the SST front for any reason, the enhanced poleward eddy heat flux across the SST front acts to relax the cross-frontal SAT gradient and thereby augment the cross-frontal contrast of the surface sensible heat flux (Nonaka et al. 2009; Sampe et al. 2010). This augmentation efficiently restores the surface baroclinicity (Hotta and Nakamura 2011), to allow recurrent development of baroclinic eddies for anchoring the stormtrack and eddy-driven PFJ and thereby to prolong the residence time of [U] axis (Figure 2.8). Interestingly, the westerly axis tends to stay equatorward of the SST front even when the PC value is weakly positive (Figures 2.10a-b).

Figure 2.11 shows latitudinal profiles of probability density of the latitude of the near-surface [U] maximum, based on daily sampling for the four experiments with SST fronts at 55°, 50°, 45° and 40°, as well as for the NF experiment. Three different profiles of the probability density plotted in each of the panels in Figure 2.11 are based on separate samplings over the positive and negative events of the annular mode and over the entire experimental period. In the experiments with the SST front at 55°, 50° and 45°, the probability based on the whole-period sampling (black line) exhibits dual peaks, as consistent with Figure 2.7 (also for Figures 2.8 and Figure 2.10a for the front at 55°). Obviously, the PFJ axis in the positive phase of the annular mode (red line) tends to be located in the vicinity of the poleward peak, which corresponds to the period when the extratropical atmospheric circulation shows strong sensitivity to the SST front. In contrast, the [U] axis in the negative phase of the annular mode (blue line) tends to be located at the equatorward peak located around 38°, which corresponds to the distinct single peak of the probability of the [U] maximum over the entire period for the NF experiment (black line in Figure 2.11e). The dual-peak feature in the probability density is weaker in the experiment with SST front at 40° (Figure 2.11d), but still a weak peak is found at 38° separately from the dominant peak at 45°. These results support the notion that the annular mode simulated with a midlatitude or subpolar SST front represents a regime shift between the two quasi-equilibrium states, where the effectiveness of the oceanic baroclinic adjustment along the SST front is essentially different.

The regime-like behavior is suggested also in the probability density of PC values. As evident in Figure 2.12a, the probability density of the PC value in the experiment with the SST front located at 55° is apparently skewed negatively, deviating substantially from the normal distribution (shown by dashed line in Figure 2.12a), as actually observed for SAM (Hartmann and Lo 1998). Indeed, the skewness (-0.37) is statistically significant at the 95% confidence level, according to White (1980). The deviation of the probability density from the normal distribution shown in Figure 2.12b have two peaks in the positive and negative phases, consistent with the regime-like characteristic. Moreover, the negative kurtosis (-0.26) of the probability density suggests less likely occurrence of PC values with small absolute values. In fact, the negative kurtosis tends to become stronger as the SST front shifts poleward, suggestive of the more apparent regime-like behavior of the annular mode. It should be noted that the bimodality in PC values is not always identified with high statistically significance in spite of the regime-like character of the annular mode (Itoh et al. 1999). In fact, the skewness of PC1 values in the experiments with SST fronts at 45° or 50° does not reach the 95% confidence level, in spite of the clear bimodality in the physical space as shown in Figures 2.11b and 2.11c. Therefore, the experiment with SST front at 55° can be regarded as an ultimate case where regime-like characteristics of the annular mode can be identified in both the physical and phase spaces.

Figure 2.13 shows meridional sections of typical quasi-equilibrium states of the zonal-mean stormtrack activity and PFJ as realized during extreme events of the positive and negative phases of the annular mode in the presence of the SST front at 55°. In a regime represented by the positive phase of the annular mode (Figure 2.13a), PFJ is located slightly poleward of the SST front with strong stormtrack activity around the SST front with enhanced upward E-P flux as an indicator of baroclinic growth of eddies. In the other regime represented by the negative phase of the annular mode, by contrast, eddy activity is not well organized as a stormtrack and PFJ are weaker located at around 40° (Figure 2.13b). The situation is similar to the climatological-mean state in the absence of SST front (Figure 2.13c), indicative of the dominance of atmospheric internal dynamics for their maintenance in this regime.

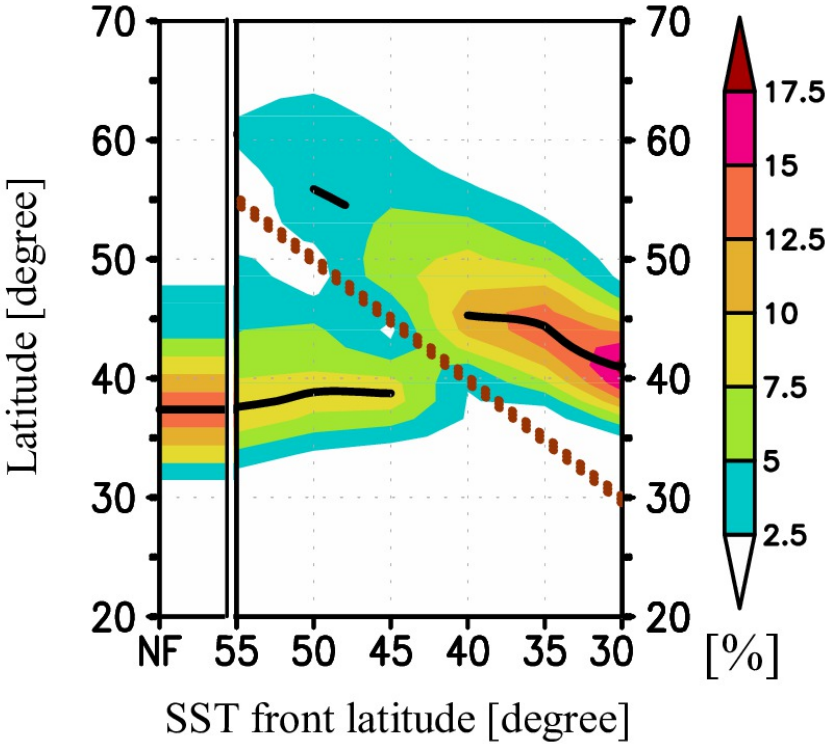

Figure 2.7. Climatological probability density [%] for the latitude of the [U] maximum as a function of latitude of the prescribed SST front, as indicated along the abscissa and dotted line.

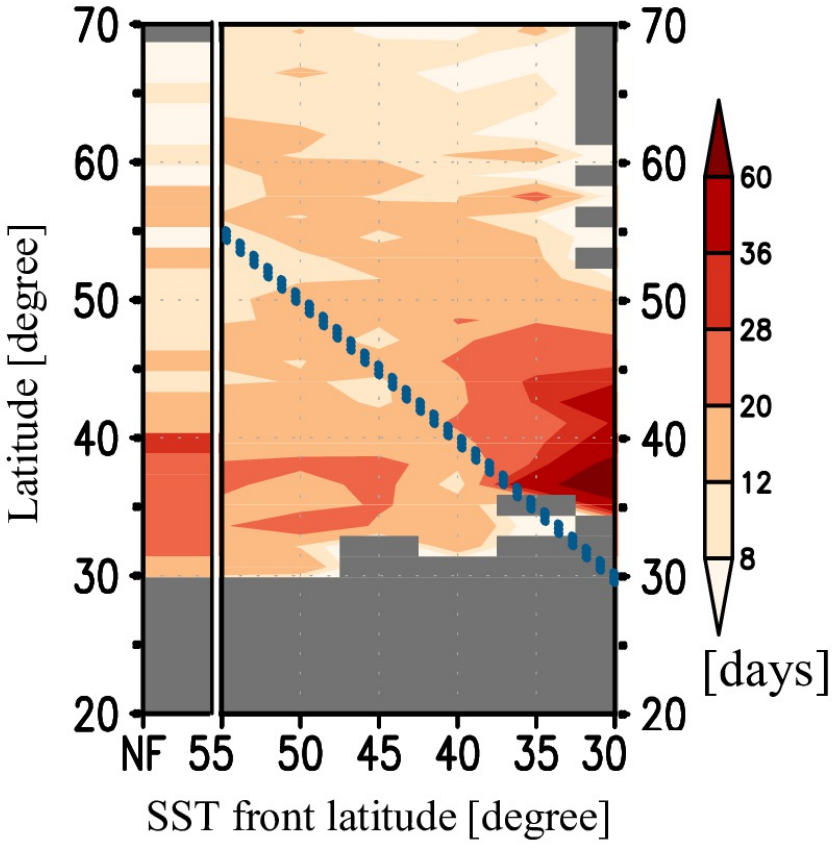

Figure 2.8. Latitudinal profiles of climatological-mean residence time [in days] of the [U] maximum (shaded) as a function of latitude of the prescribed SST front, as indicated along the abscissa and by dotted line. Gray shading indicates the absence of the [U] axis throughout the experimental period.

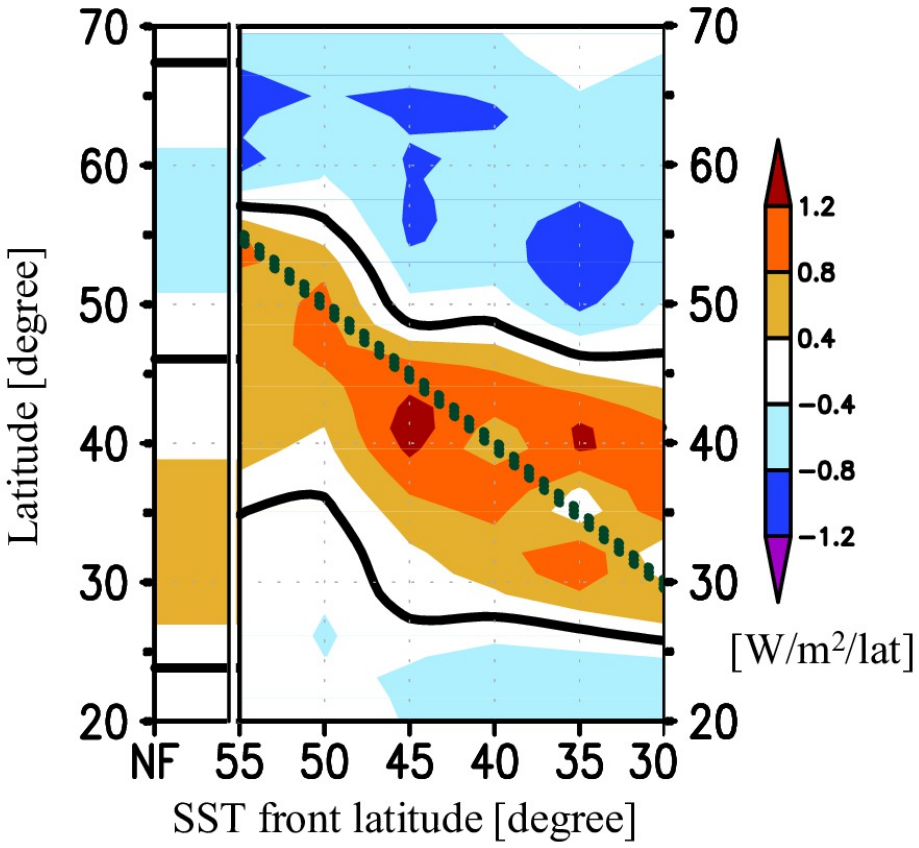

Figure 2.9. Composited difference in the equatorward gradient of zonal-mean sensible heat flux [W/m^2/lat] between the phase and negative events of the annular mode (pos. minus neg.) defined as the periods in which the absolute value of the principal component exceeds a unit standard deviation. The latitude of the prescribed SST front is indicated along the abscissa and by dotted line.

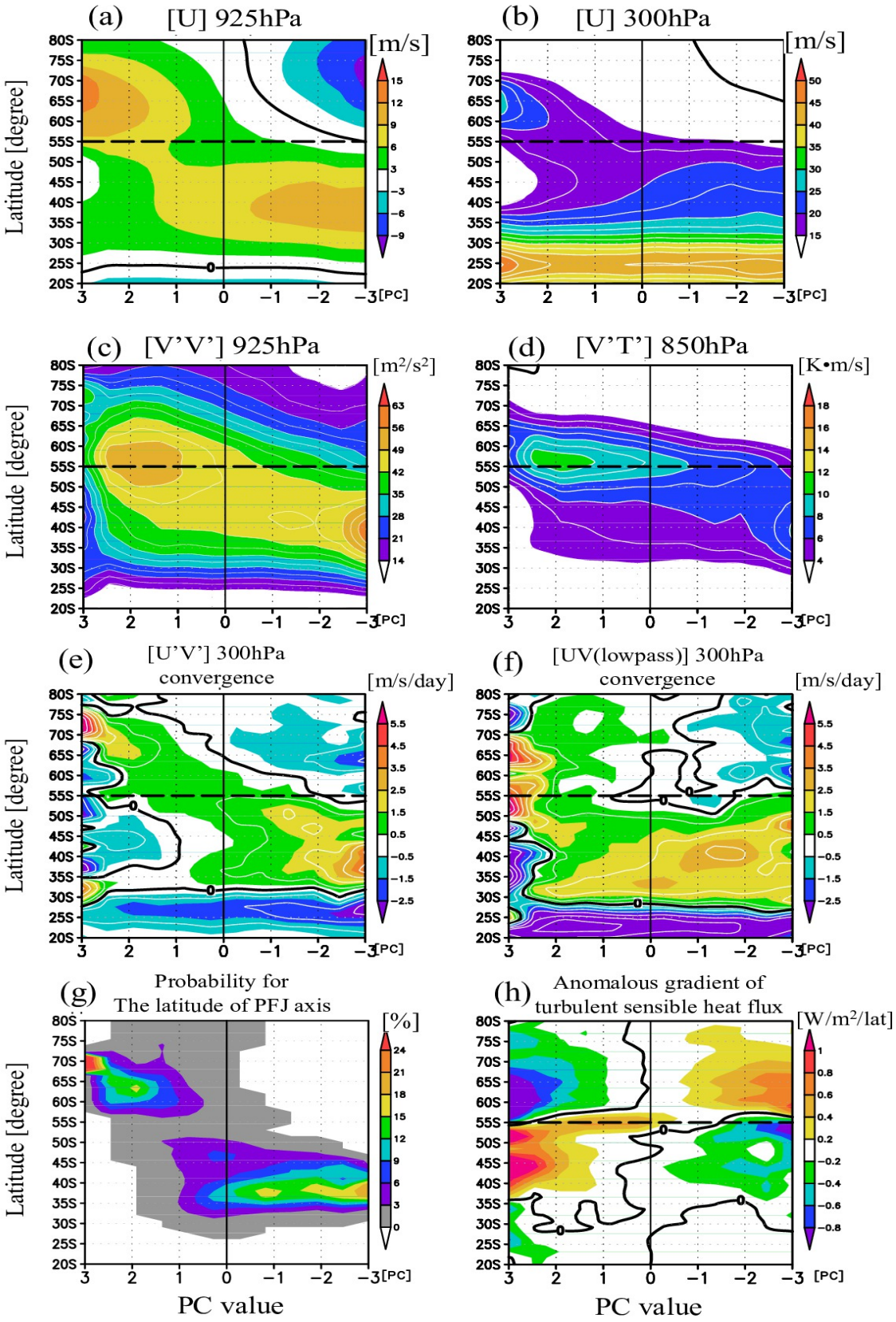

Figure 2.10. Meridional profiles of (a, b) [U] at 925hPa and 300hPa, (c) [V'V'] at 925 hPa, (d) [V'T'] at 850hPa, (e) convergence of eddy momentum flux ([U'V']) associated with 8-day high-pass filtered fluctuations (denoted with primes), (f) associated with 8-day low-pass filtered fluctuations, (g) probability for the [U] maximum at every latitude and (h) anomalous equatorward gradient of surface sensible heat flux, as functions of PC values that represent the magnitude and phase of the model annular mode in the experiment with the SST front located at 55°.

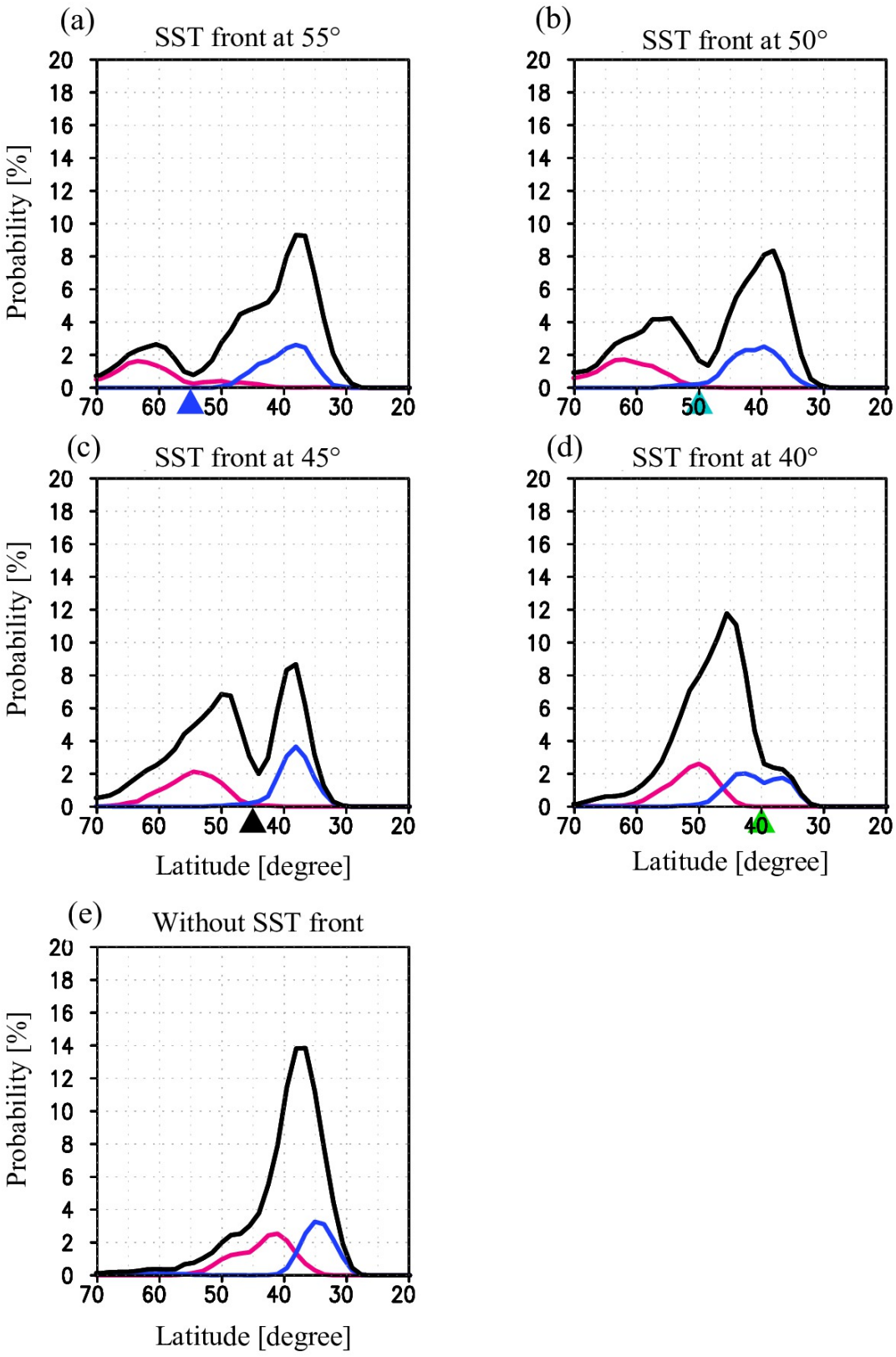

Figure 2.11. Probability densities (%) of the latitude of the 925hPa [U] maximum (abscissa) based on the sampling for the whole period (black line) and for strong positive (red line) and negative (blue line) events, separately, simulated in the experiments with SST front at (a) 55°, (b) 50°, (c) 45° and (d) 40°, in addition to (c) the NF experiment. The strong events are defined as the periods when the absolute value of the principal component exceeds a unit standard deviation.

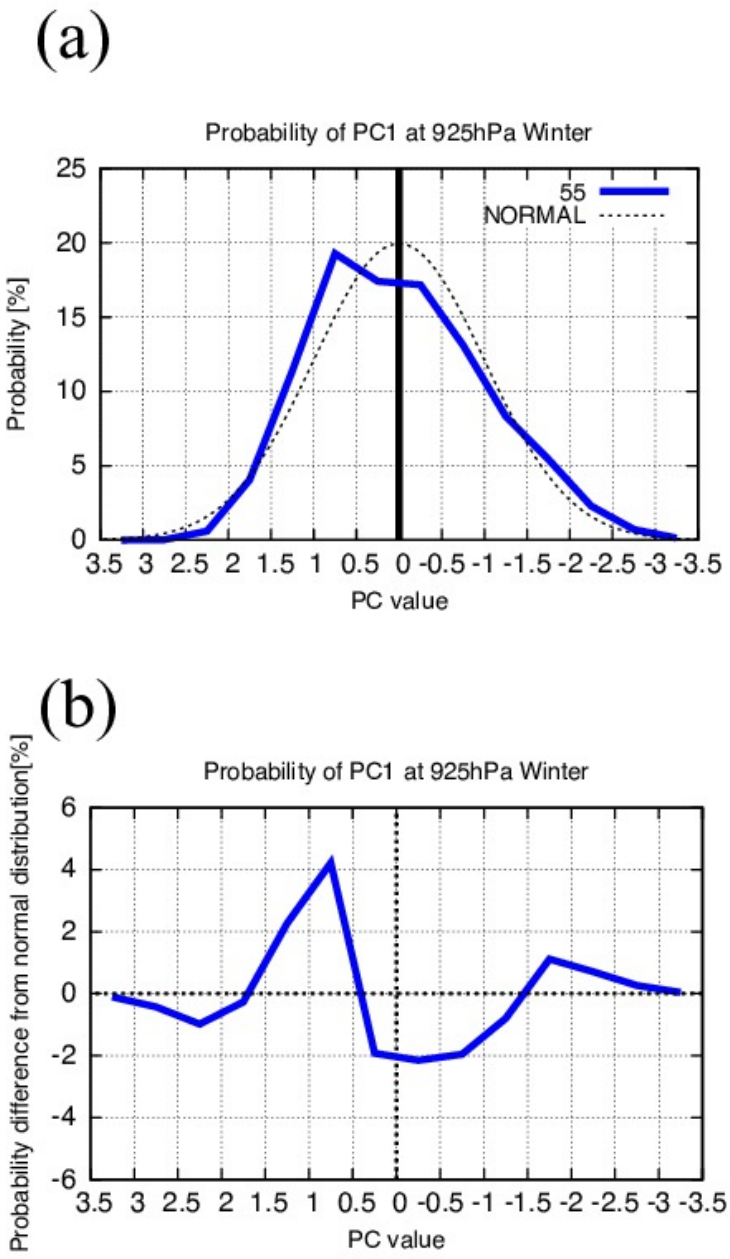

Figure. 2.12. (a) Probability density (%) of the normalized PC value (abscissa) in the experiment with the SST front located at 55°, and (b) its deviation that of from the normal distribution.

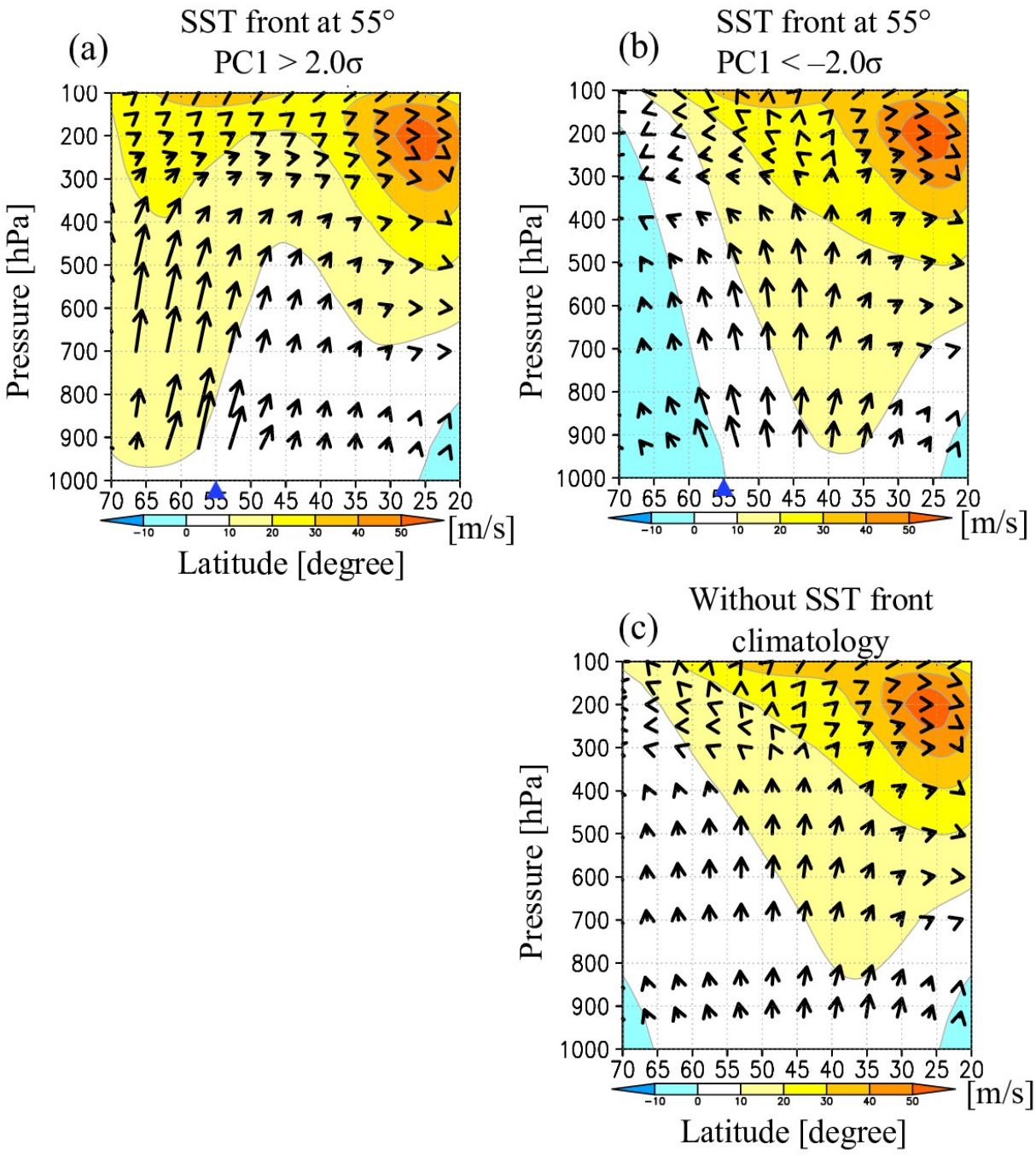

Figure 2.13. Composites of zonal-mean zonal wind (shading) and EP-flux (arrows) associated with 8-day high-pass filtered disturbances for the days on which the standardized PC1 time series is (a) above +2 and (b) below –2 in the experiment with SST front located at 55°. (c) As in (a), but for the climatological-mean state without SST front.

f) Role of low-frequency wave disturbances in the phase transition

As discussed in the preceding subsection, high-frequency baroclinic eddies are important in maintaining the PFJ in both the positive and negative phases of the annular mode, but quasi-stationary wave disturbances with lower frequency may be of certain importance in the transition from one phase to another. In fact, Shiogama et al. (2005) suggested the importance of low-frequency waves for inducing anomalous eddy momentum flux in phase shifts of the observed wintertime SAM. Likewise, Lorenz and Hartmann (2001) demonstrated the positive contribution of low-frequency waves to the decay of the zonal wind anomalies associated with SAM.

Figure 2.14a shows the evolution of PFJ and transient wave activity in phase transition from a strong negative event to a strong positive event of the model annular mode in the experiment with the SST front at 55°. The PC value during this transition is shown in Figure 2.14b, where Day 0 in corresponds to the timing of the sign reversal. This is the most pronounced transition in the particular experiment where the normalized PC value increases monotonically from below -1.5 to above +1.5 within 10 days or so. In this transition, both the PFJ and stormtrack axes shift from 38° at Day -3 to 65° at Day +4, with the distinct westerly acceleration and deceleration in equivalent barotropic structure (Figure 2.14c). The anomalous eddy poleward flux of westerly momentum and its convergence associated with high- and low- frequency wave disturbances are shown in Figures 2.14d-e. In this transition, the enhancement of poleward flux of westerly momentum that can contribute positively to the poleward PFJ shift arises mainly from low-frequency wave disturbances (Figure 2.14e), whereas high-frequency wave disturbances yield the reduction of that flux in the early stage of the transition (Day –4 through Day 0; Figure 2.14d). The anomalous amplitude of the low-frequency wave is plotted in Figure 2.14f, and the horizontal correlation of low-pass-filtered zonal and meridional wind anomalies are plotted in Figure 2.14g as an indicator of the orientation of the major axis of the disturbances. Although the time evolution of the anomalous amplitude of low-frequency wave disturbances (Figure 2.14f) is not quite consistent with the evolution of the anomalous poleward eddy momentum flux, especially on the poleward side of the SST front (Figure 2.14e), the time-evolution of the correlation shows considerable correspondence to that of the flux

almost over the entire extratropics and the entire transition period (Figure 2.14g). Therefore, the phase shift of the annular mode in this particular event is contributed to substantially by the spontaneous changes in the horizontal structure of low-frequency wave disturbances. Meanwhile, Figure 2.14h suggests a certain contribution from the enhanced equatorward gradient in the surface sensible heat flux accompanied by the enhanced baroclinic development of high-frequency transient eddies along the SST front. These features are consistent with Figures 2.10d and 2.10h. In fact, the upper-level westerly acceleration around 70° (Figure 2.14c) in the later stage (after Day 0) is contributed by enhanced eddy heat and momentum fluxes associated with high-frequency waves (Figures 2.14d and 2.14h), which act to maintain the PFJ axis around the latitude (Figure 2.14a).

Another phase transition of the annular mode, which is from a strong positive event to a strong negative event, is also investigated (Figure 2.15). During this transition, the PC value decreased monotonically from above +1.5 to below -1.5 within 10 days or so (Figure 2.15b). In this transition, a substantial contribution of anomalous low-frequency wave disturbances through their structural changes for the transition is also suggested (Figures 2.15c,e,g). Compared with the other transition discussed earlier, a contribution from anomalous eddy momentum flux associated with high-frequency wave is more evident (Figure 2.15d), which is consistent with the observations by Shiogama et al. (2005). In the early stage of the transition (Day –4 through Day 0), the anomalous poleward and equatorward eddy momentum fluxes on the just poleward flank of the SST front and at higher latitudes are convergent where baroclinic eddy development is enhanced (Figures 2.15h), to maintain the PFJ situated poleward of the front (Figure 2.15a). In the later stage (after Day 0), baroclinic eddy development weakens poleward of the SST front, and the poleward eddy momentum flux is reduced around the SST front, yielding the anomalous flux convergence around 40° as a positive contribution to the equatorward shift of the PFJ. In this transitional event, the evolution of the momentum and heat fluxes associated with high-frequency transient eddies (Figures 2.15d,h) are rather complicated, partly because this period verges immediately onto another transition into the positive phase (Figure 2.15b). The particular transition is preceded by the enhancement of equatorward gradient of sensible heat flux around Day +5, followed by the

augmentation of poleward eddy momentum flux around the SST front and on its poleward side. It should be stressed that, as in the other transitional period discussed earlier, low-frequency wave disturbances also play an important role especially in the early stage (before Day 0). The peak latitude of poleward momentum flux associated with them shifts gradually equatorward associated with the spontaneous changes in the horizontal structure of those waves (Figure 2.15g), yielding a similar latitudinal shift in the anomalous westerly acceleration to the equatorward side of the front as a positive contribution to the equatorward shift of the PFJ (Figures 2.15c and 2.15e).

The role of low-frequency wave disturbances in the aforementioned transition events is further investigated in Figures 2.16 and 2.17. At Day 0 of the event toward the positive phase, 300hPa zonal-mean tendency (Figure 2.16b) is westerly (easterly) in high (mid-) latitudes, to which anomalous poleward westerly momentum flux associated with low-frequency wave disturbances contributes mainly (Figures 2.14e and 2.16c-d). The zonal wind tendency is not zonally symmetric, however. Longitudinal profiles of the westerly tendency averaged in the latitudinal bands of the positive and negative tendencies (black lines in Figures 2.16e-f) indicate that contributions from the longitudinal sector from the 100°E to 60°W dominate in the zonal-mean westerly and easterly tendencies in high and mid-latitudes (Figures 2.16c-d), respectively. Meanwhile, high-latitude westerly forcing by low-frequency wave disturbances (red line in Figure 2.16f) occurs mainly between 70°E and 140°E, whereas midlatitude easterly forcing by those disturbances is strongest around 130°E. The eddy forcing is found to be associated with a quasi-stationary Rossby wave train propagating from high latitudes to midlatitudes within the longitudinal sector between 60°E and 150°E, illustrated as the northeastward-pointing flux of Rossby wave activity (Takaya and Nakamura 2001) averaged from Day –3 to Day +3 (Figure 2.16g). The northeastward group velocity is consistent with the SE-NW tilt of phase lines of the streamfunction anomalies and thereby the southward translation of westerly momentum that contributes to the phase transition of the annular mode. The dominant zonal wavenumber of the low-frequency wave disturbances is approximately 3 (Figure 2.16g). This is consistent with the observations by Shiogama et al. (2005) for the observed phase transition of the SAM, to which forcing on stationary wave disturbances

owing to the land-sea thermal contrasts in the SH may contribute substantially, unlike in our aqua-planet experiment. Though undulated, PFJ marked as the near-surface westerly axis is located around 40° before this transition (Day –6, Figure 2.16h) and then shifted to around 70° (Figure 2.16j). PFJ is fairly symmetric in the zonal direction before and after the transition (Figures 2.16h and 2.16j), but it appears to be less symmetric during the transition (Day 0, Figure 2.16i) on the presence of the Rossby wave train.

It is noteworthy that the quasi-stationary wave train simulated in the positive transitional event shows notable equatorward propagation, while the eastward emanation is dominant in the negative transition event (Figures 2.16g and 2.17g). In fact, such differences as simulated in the propagation characteristics of quasi-stationary wave trains between the two opposing transition events were actually observed by Shiogama et al. (2005), although the meridional propagation is noticeable over the South Pacific in any of the opposing transitional events. The stronger meridional propagation in the observations than in our model simulation is presumably due to either the effects of land-sea thermal contrasts and/or remote influence from the tropics.

In the other transition event, which was depicted in Figure 2.15, the PC value decreases most rapidly at Day +1. At this stage, the zonal-mean tendency is easterly in high latitudes while nearly zero in midlatitudes (Figure 2.17b). The easterly tendency is simulated at almost every longitude, whereas the easterly forcing by low-frequency wave disturbances maximizes around 100°E (Figure 2.17f). In fact, the wave-activity flux is pointing southeastward between 90°E and 140°E (Figure 2.17g), as an indication of equatorward translation of westerly momentum from high latitudes by the wave disturbances. In midlatitudes, by contrast, the zonal-mean westerly tendency is rather weak, and so is the westerly forcing associated with low-frequency wave anomalies (Figure 2.17e). During this transition, tropical OLR anomalies normalized locally are generally weak (Figure 2.17k) and therefore unlikely to force the Rossby wave train in midlatitudes simulated between 60°E and 140°E (Figures 2.17g). As shown in Figures 2.17i, zonal asymmetry of PFJ appears to be stronger during the transition than before or after (Figures 2.17h and 2.17j). Therefore, at least in those events discussed in Figures 2.16 and 2.17, phase transitions of the annular mode are

triggered by the emanation of quasi-stationary Rossby wave trains, rather than a zonally uniform westerly forcing.

The importance of low-frequency wave disturbances in the phase transition of the annular mode can also be identified statistically. Figures 2.18 and 2.19 show the meridional profiles of [U] at 925hPa and 300hPa and the convergence of westerly momentum flux associated with both high- and low- frequency eddies for different values of PC1 based on the experiment with the SST front at 55°, composited separately for the days for positive (Figures 2.18a-b; 2.19a-c) and negative (Figures 2.18c-d; 2.19d-f) tendencies of PC1 (hereafter denoted as dPC/dt). The [U] profiles at a given PC value are very similar regardless of the sign of dPC/dt (Figures 2.18a,c). The corresponding profiles of the convergence of poleward flux of westerly momentum associated with migratory high-frequency eddies are also very similar regardless of the sign of dPC/dt (Figures 2.19b,e). For low-frequency wave disturbances, by contrast, the convergence of the associated poleward momentum flux shows notable dependency on the sign of dPC/dt, especially for small absolute values of PC (Figures 2.19c,f). When the PC value is between –1 and +1, for example, the upper-level eddy westerly forcing peaks between 60° and 70° for positive dPC/dt (Figure 2.19c), in good correspondence with the acceleration of upper-level PFJ into the positive phase (Figure 2.19a). In the particular latitudinal sector by contrast, high-frequency transient eddies in these small PC values exert no systematic acceleration on the background westerly (Figure 2.19b). The transition toward the positive phase of the annular mode appears to be driven mainly by low-frequency disturbances. For negative dPC/dt in small PC values (between –1 and +1), low-frequency wave disturbances act to decelerate the upper-level westerlies between 60° and 70° (Figure 2.19f), acting to distract the persistency of the annular mode (Lorenz and Hartmann 2001). The disturbances also act to accelerate the westerly around 40°, where the PFJ is accelerated into the negative phase (Figures 2.18a,c). Though similar, the corresponding contribution from by high-frequency transient eddies is much smaller for small absolute values of dPC/dt (Figure 2.19e), suggesting that low-frequency disturbances are the main driver also for the transition of the annular mode toward the negative phase. The importance of low-frequency waves in the phase transition of the annular

mode is also found in the experiments with the SST front at 45° and 50° (not shown).

It should be noted that the stronger (weaker) meridional contrast in the upward surface sensible heat flux in the positive (negative) as discussed in Figure 2.9 does not necessarily mean that it triggers the phase transition of the annular mode. Figures 2.20a and 2.20e show anomalous equatorward gradient in the surface upward sensible heat flux as a function of PC values based on the experiment with the SST front at 55°, composited separately for the days for positive and negative dPC/dt, respectively. Along the SST front, the equatorward gradient becomes stronger (weaker) in the positive (negative) phase of the annular mode regardless of the sign of dPC/dt, indicative of its stronger (weaker) restoring effect on the near-surface baroclinicity (Figures 2.20b and 2.20f). Interestingly, the Eady growth rate itself is slightly weaker in the positive phase than in the negative phase, although it still exhibits a prominent peak along the SST front (Figures 2.20b and 2.20f). The lower baroclinicity in the positive phase compared to the negative phase is consistent with both the slightly weaker meridional SAT gradient (Figures 2.20c,g) and slightly higher static stability (Figures 2.20d,h). During the transition when the PC values are between –1 and +1, the anomalous meridional gradient of upward sensible heat flux are similar between the positive and negative transitions (Figures 2.20a and 2.20e). It can therefore be considered that the anomalous sensible heat flux does not trigger the phase transition. It is nevertheless noteworthy that the equatorward gradient of the upward sensible heat flux tends to be enhanced around the SST front during the transition either into the positive or negative phase, acting to shift the stormtrack towards the front. This tendency implies that the anomalous sensible heat flux helps the phase transition of the annular mode toward the positive phase triggered by low-frequency wave disturbances, while it tends to counteract the transition toward the negative phase.

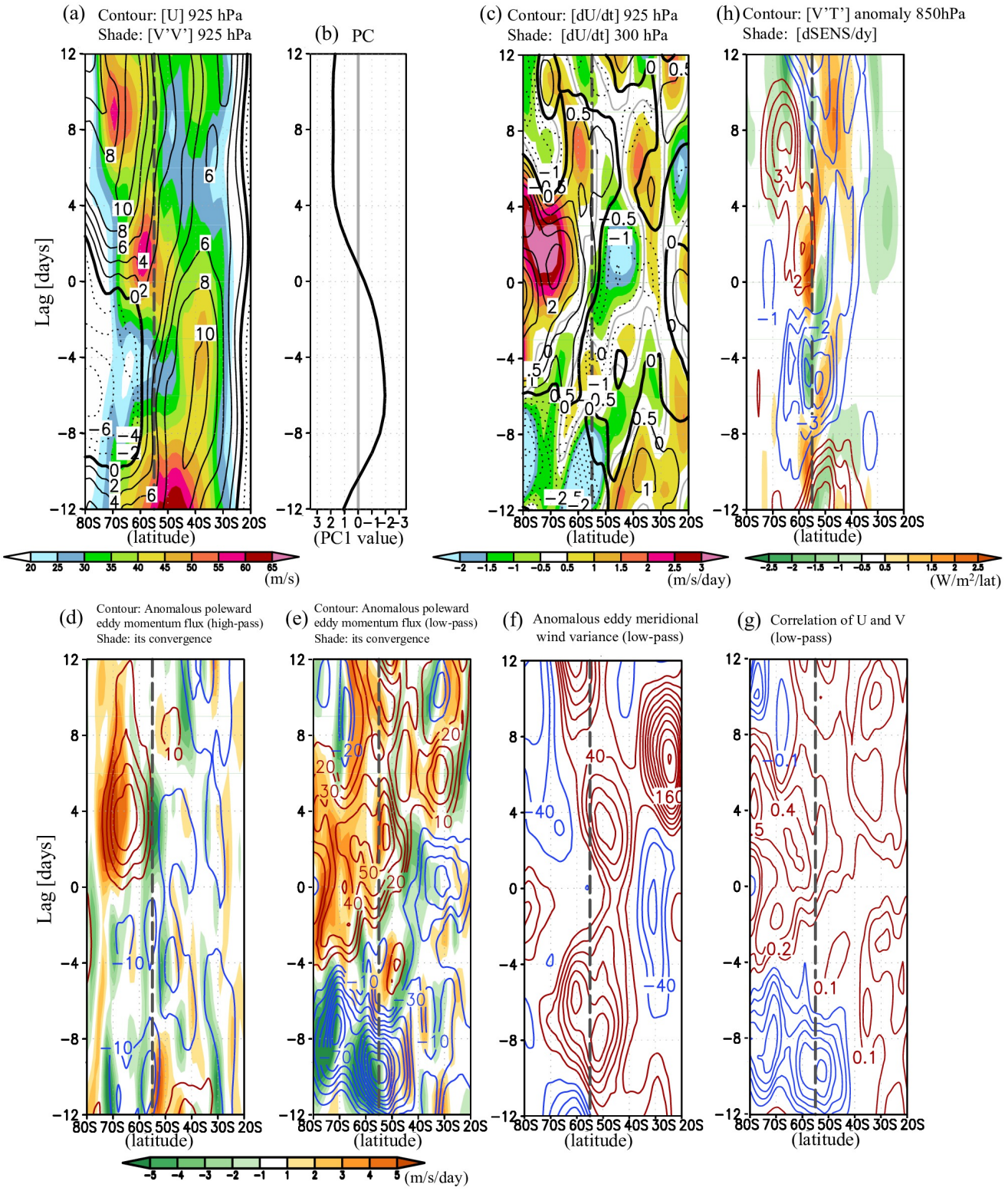

Figure 2.14. Transition from a strong negative event to a strong positive event of the model annular mode in the experiment with SST front at 55° (vertical dashed line). (a) [U] (contour) and [V'V'] (shade) at 925 hPa, (b) PC value (Day 0 corresponds to the timing of the sigh reversal), (c) simulated acceleration rate of [U] at 925 hPa (contour) and 300 hPa (shade), (d) anomalous poleward momentum flux (contour) and its convergence (shade) associated with 8-day high-pass filtered fluctuations, (e) as in (d), but for 8-day low-pass filtered fluctuations, (f) anomalous variance in the eddy meridional wind associated with 8-day low-pass filtered fluctuations, (g) horizontal correlation of 8day low-pass filtered zonal wind and meridional wind, and (h) anomalous poleward eddy heat flux associated with 8day high-pass filtered fluctuations (contour) and anomalous equatorward gradient in the surface sensible heat flux (shade).

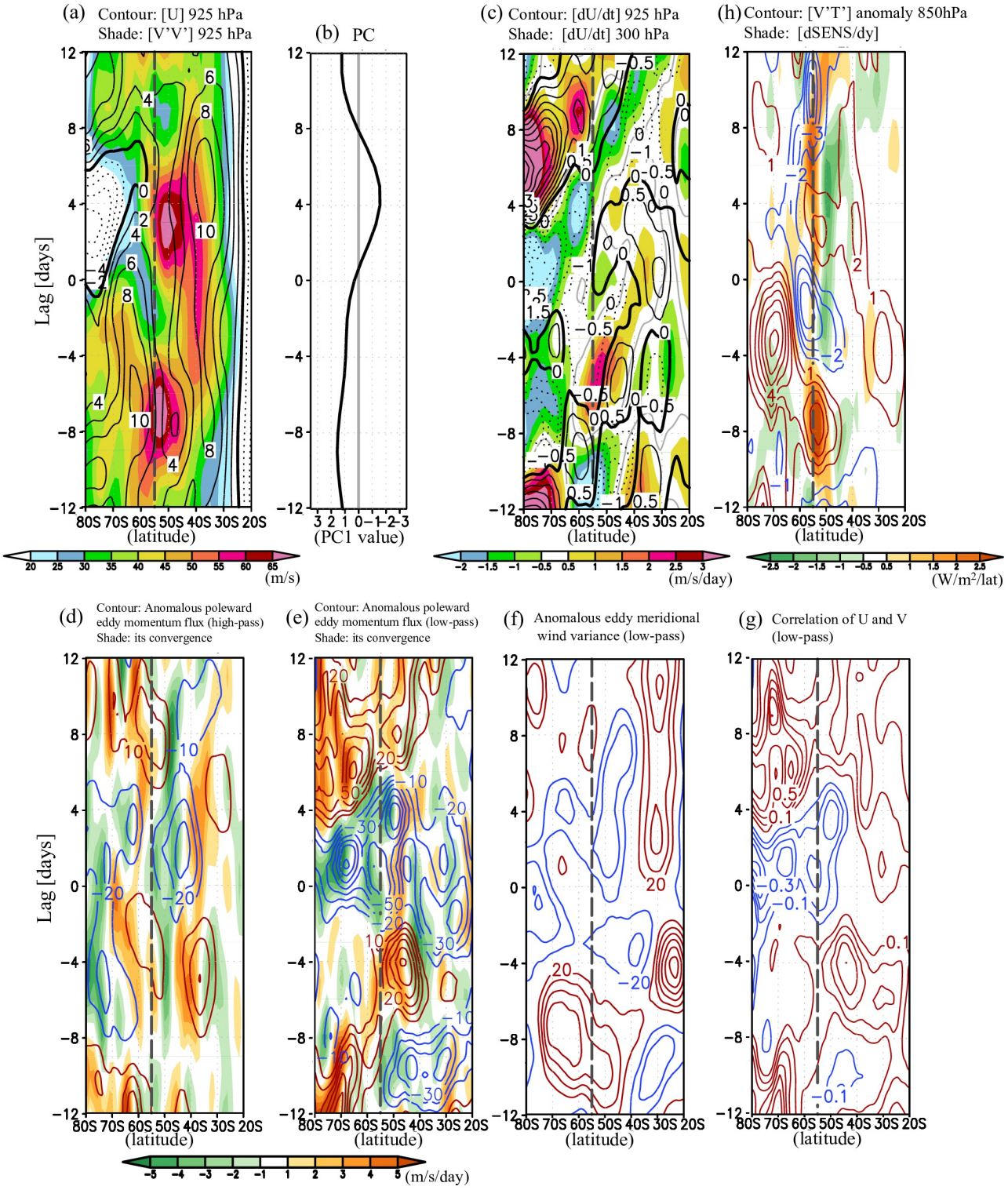

Figure 2.15. As in Figure 2.14, but for another transition (Day 0) from a strong positive event to a strong negative event of the model annular mode.

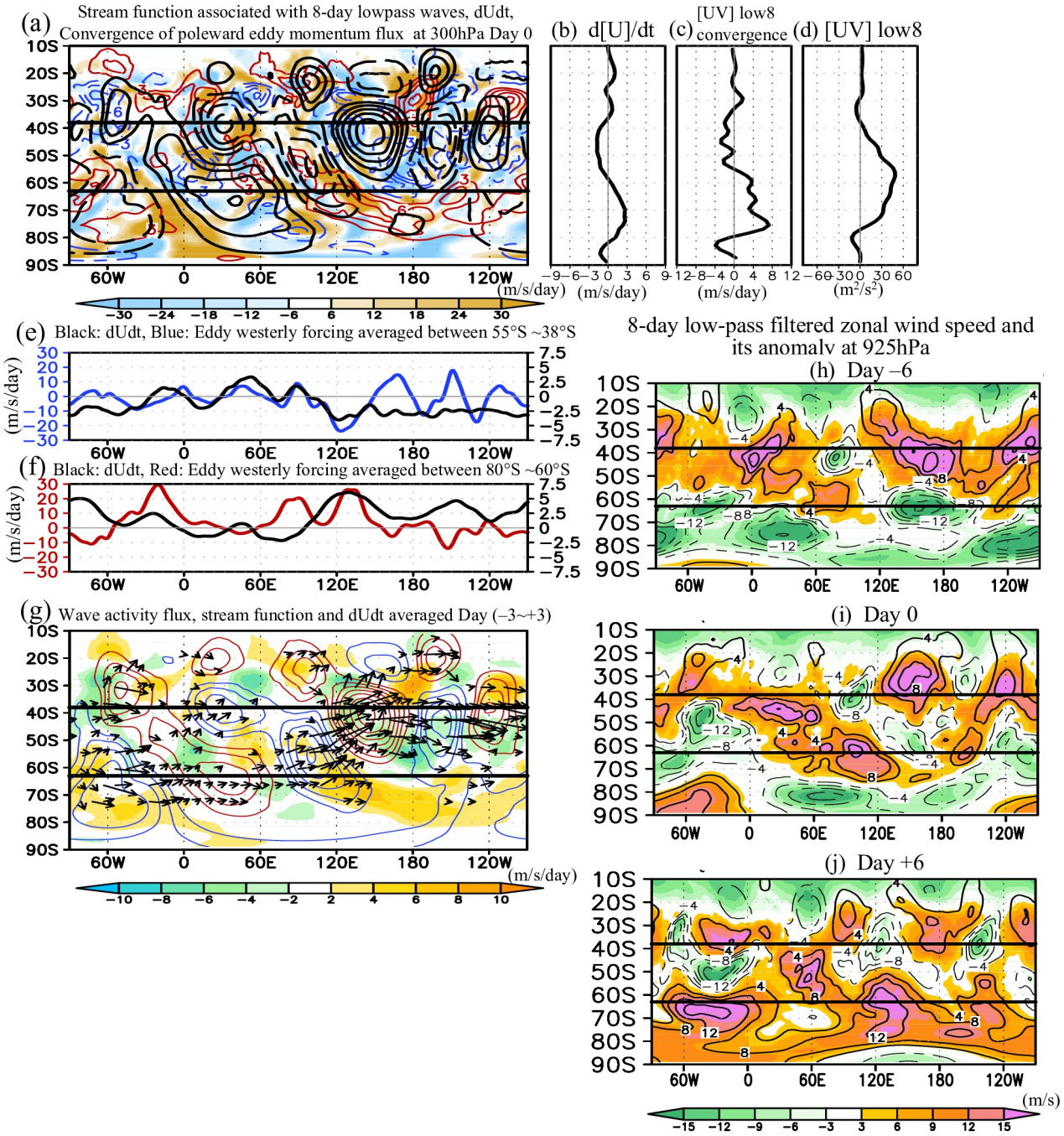

Figure 2.16. (a) Anomalies in geostrophic streamfunction (black contour for every $7x10^6$ m^2 s^{-1}; dashed for negative) and eddy westerly forcing estimated as local convergence of poleward eddy flux of westerly momentum due to 8-day low-pass filtered disturbances, superposed on the low-pass-filtered zonal wind tendency (contoured for every 3 m s^{-1}/day; red for westerly, blue for easterly) at Day 0 of the transition event depicted in Figure 2.14. (b) Zonally averaged zonal wind tendency plotted in (a). (c) As in (b), but for the eddy westerly forcing. (d) As in (b), but for the poleward eddy momentum flux. (e) Longitudinal profiles of zonal wind tendency (black line) and eddy westerly forcing (colored line) in (a) averaged between 38°S and 55°S. (f) As in (e), but for the latitudinal averages between 60°S and 80°S. (g) Anomalies in streamfunction (colored contours) and eddy westerly forcings (shade) in (a) but for the 7-day average from Day -3 to +3, with the horizontal flux of Rossby wave activity flux (arrows; Takaya and Nakamura 2001) averaged over the 7 days. (h-j) 925hPa zonal wind velocity and its anomaly at (h) Day –6, (i) Day 0 and (j) Day +6. Heavy horizontal lines in (a) and (g-j) signify the latitudes (63°S and 38°S) of the PFJ axis in the positive and negative phases (Figures 2.5a and 2.6a), respectively.

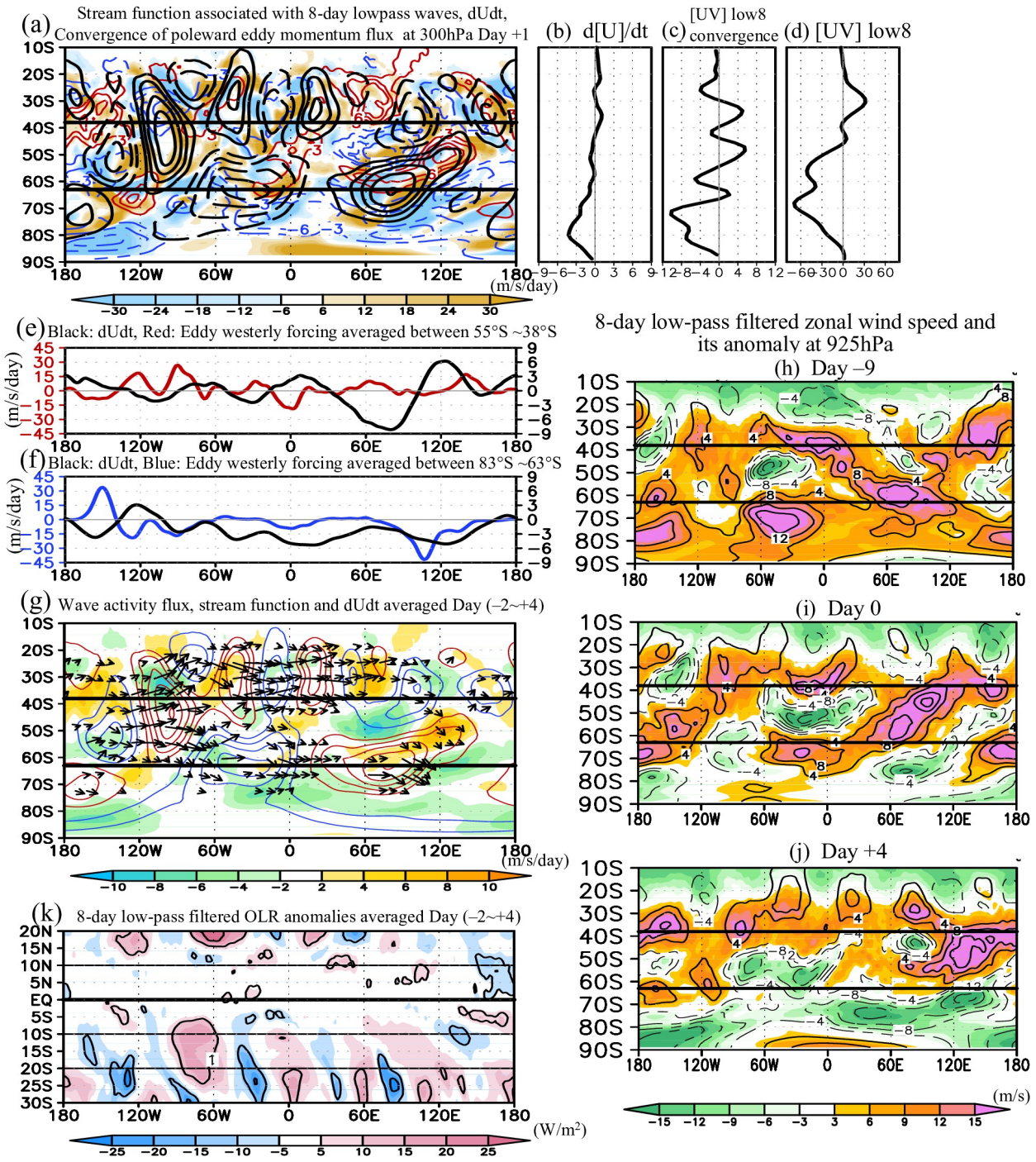

Figure 2.17. (a-j) As in Figure 2.16 (a-j), respectively, but for the negative transitional event as discussed in Figure 2.15b. Reference date for (a-f) is Day +1, and in (g) 7-day statistics are taken from Day -2 to +4. (k) As in (g), but for 8-day low-pass filtered anomalies of outgoing long-wave radiation (OLR, shading) as a measure of the anomalous convective activity (negative values for enhanced convective activity). Contours indicate the same anomalies but normalized locally by their standard deviation.

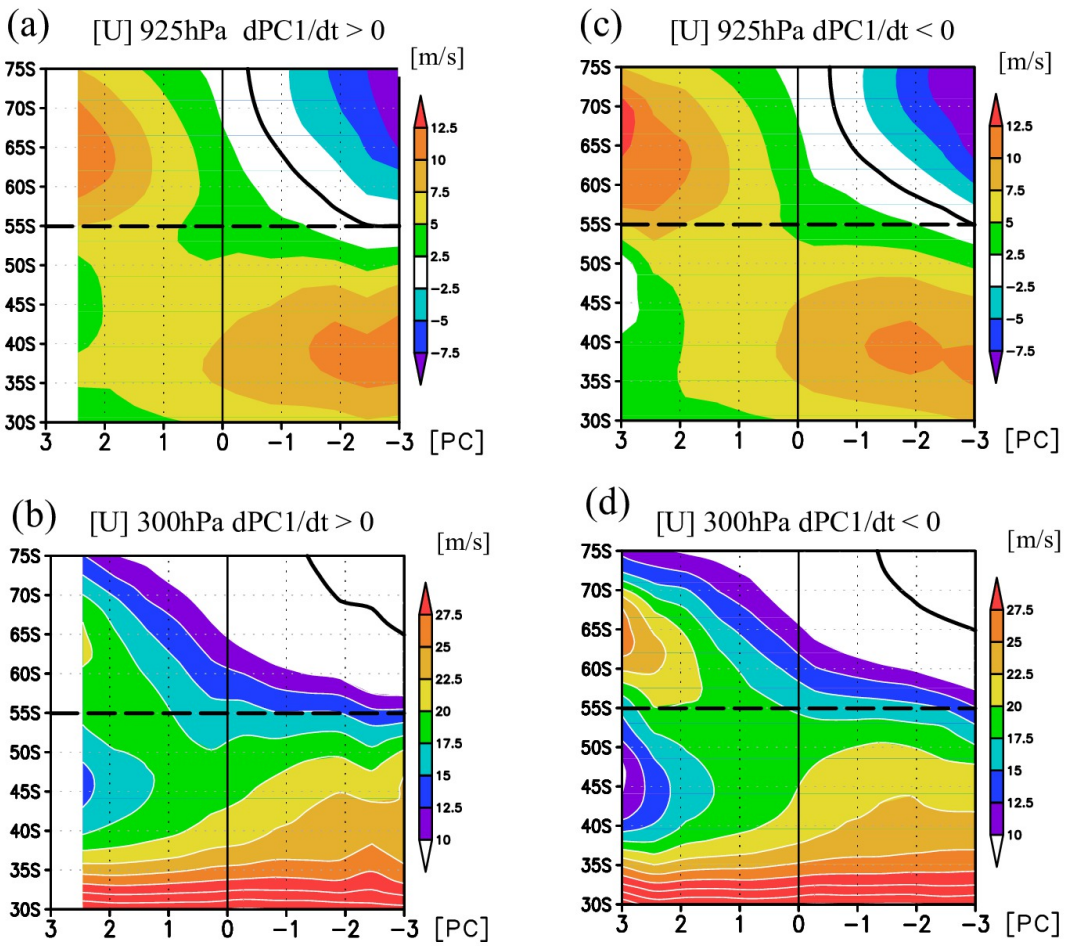

Figure 2.18. (a-b) As in Figures 2.10a-b, respectively, but for the days for positive PC1 tendency (m/s). (c-d) As in (a-b), respectively, but for the days for negative PC1 tendency.

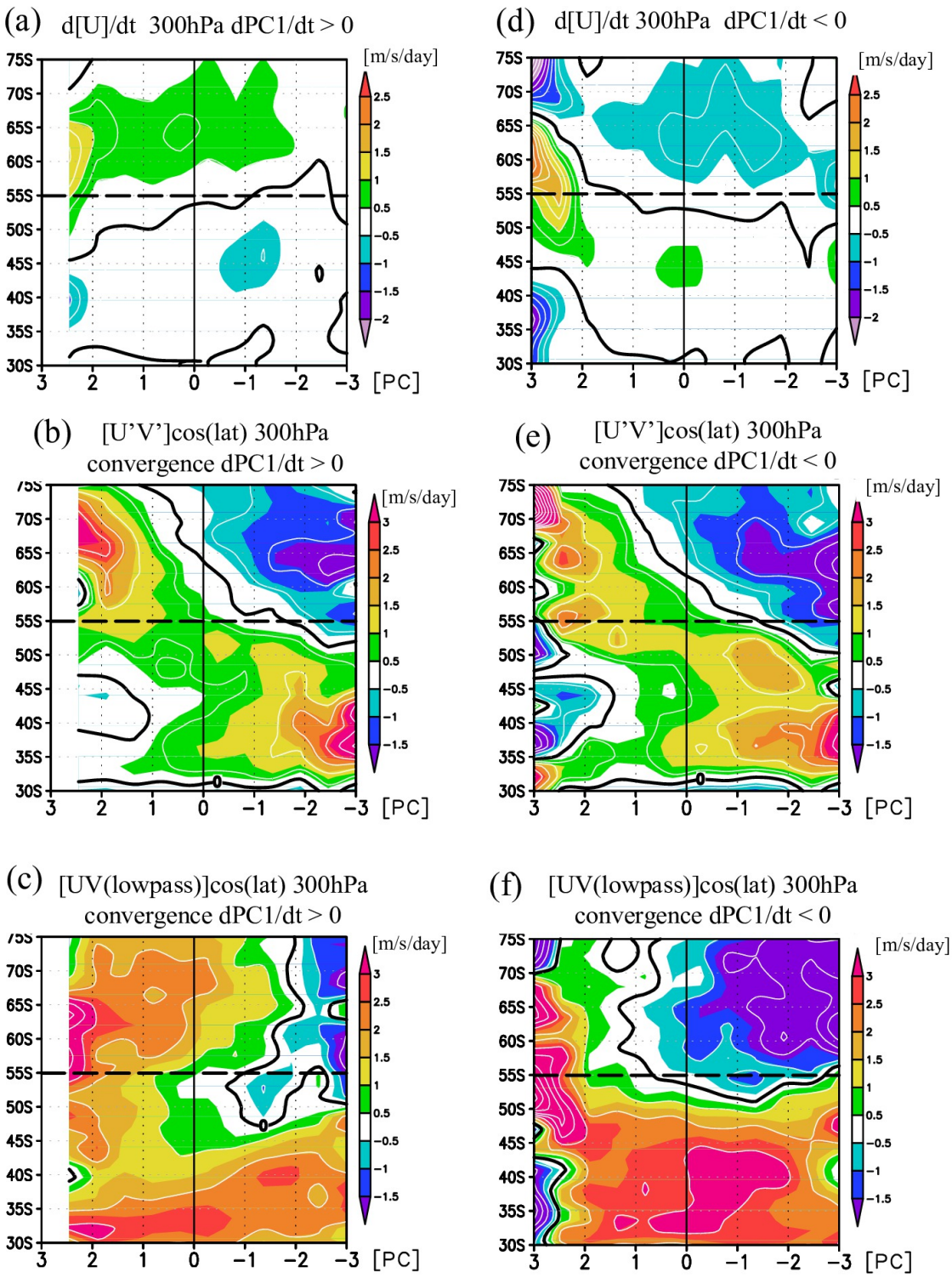

Figure 2.19. (a-c) As in Figure 2.18a, but for (a) low-pass-filtered zonal-mean zonal wind tendency, (b) convergence of eddy momentum flux ([U'V']) associated with 8-day high-pass filtered fluctuations and (c) 8-day low-pass filtered fluctuations, for the days for positive PC1 tendency. (e-g) As in (a-c), respectively, but for the days for negative PC1 tendency.

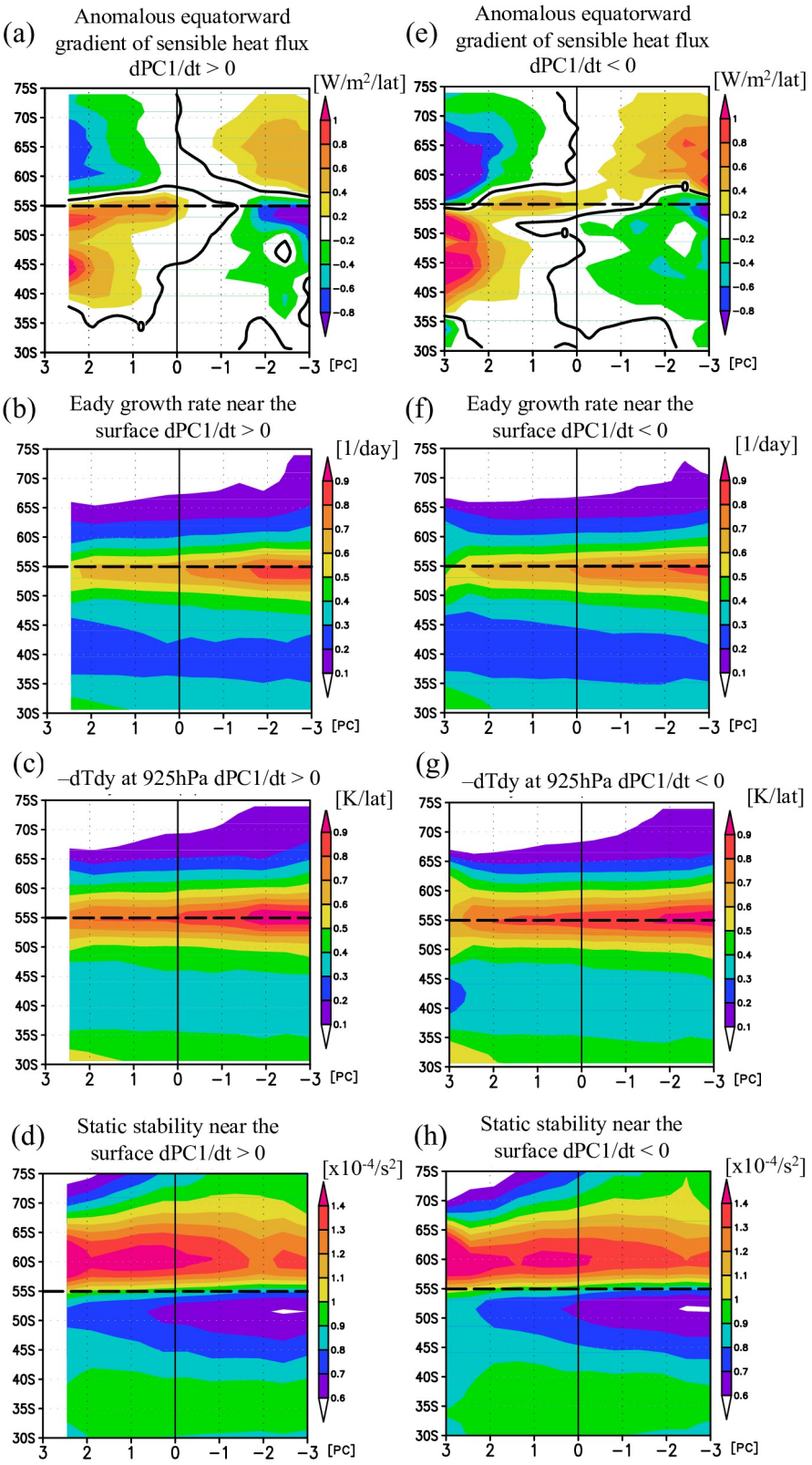

Figure 2.20. (a,b) As in Figures 2.18a, but for (a) the anomalous equatorward gradient of the surface upward sensible heat flux and (b) Eady growth rate averaged below 850hPa, respectively, composited only for the days for positive PC1 tendency. (c) As in (b), but for equatorward temperature gradient at 925hPa. (d) As in (b), but for the squared Brunt–Väisälä frequency averaged below 850hPa. (e-g) As in (a-d), respectively, but for the days for negative PC1 tendency.

g) Characteristics of the annular mode with subtropical SST front

As implied from Figure 2.7, regime-like behavior almost diminishes for the model annular mode in the presence of a subtropical SST front, marking sharp contrast to the case of a midlatitude or subpolar SST front. For the subtropical SST front at 30° or 35°, the probability density for the latitude of the 925hPa [U] maximum shows a single peak as in the case of the NF experiment (Figure 2.7). Figures 2.21a and 2.21b shows the same probability density as in Figure 2.7, but separately for the experiments of SST front at 30° and 35°, respectively, as a counterpart of Figure 2.11. The annular mode represents a wobble of the near-surface PFJ axis around its climatological-mean position, which is similar to the case of the NF experiment (Figure 2.11e). Interestingly, the likelihood of the PFJ axis between 50° and 60° is lower in the experiment with an SST front at 30° than in any other experiments, and the probability density is therefore more symmetric about the mode than in any other experiments including the NF experiment. In the presence of SST front at 30°, SST gradient poleward of 40° is the same as in the NF experiment, but SST itself is about 5°C lower (Figure 2.1a). Owing to its coolness, moisture supply from the ocean is less than in the NF experiment, resulting in the weaker stormtrack activity and thereby the reduction of probability of the eddy-driven PFJ axis in the subpolar region.

Variability in [U] near the tropopause level associated with the annular mode is different in the experiments with a subtropical SST front from the experiments with a midlatitude or subpolar SST front. Figure 2.22 shows the meridional profiles of [U] at 300hPa composited for the periods when the PC values exceed a unit standard deviation positively (red line) or negatively (blue line) in all the experiments. Nakamura et al. (2008) and Sampe et al. (2013) showed through their aqua-planet experiments that the annular mode signature near the tropopause level changes between the cases in the presence of an SST front at 45° and in its absence. They pointed out that, in the absence of SST front, fluctuations in the STJ intensity are incorporated into the annular mode variability, which essentially represents the PFJ variability in the presence of the SST front at 45°. In our experiments with the SST front at 45°, the annular mode signature is consistent with these previous studies, representing the variability in PFJ with little changes in STJ. In fact, the annular

mode characteristics in the presence of a subpolar SST front (at 50° or 55°) are similar. In the presence of a subtropical SST front (at 30° or 35°), by contrast, the annular mode accompanies relatively large variability in the strength of STJ (Figures 2.22a,b), which is similar to the NF experiment (Figure 2.22g). The variability in STJ is also hinted in the experiment with an SST front at 40° (Figure 2.22c). In this experiment (Figure 2.11d), the near-surface signature of the annular mode represents a mixture of the regime-like behavior of the PFJ axis as in the cases with SST fronts at higher latitudes and simple meridional wobble of the PFJ as in the NF experiment.

The differences in the annular mode characteristics in the presence of a subtropical SST front from those in the presence of an SST front at higher latitude can arise from multiple factors. One of them may be the tendency for the stormtrack to form closer to the STJ, and therefore upper-level transient eddies that have amplified along the stormtrack and then propagate equatorward can shortly reach the STJ without substantial decay to transport westerly momentum poleward from the STJ. Momentum flux convergence and divergence associated with this transport are stronger in the positive phase (Figure 2.5e) than in the negative phase (Figure 2.6e), and their differences between the two phases are strongest in the presence of the subtropical SST fronts (Figure 2.6i). Another factor may be relatively strong stormtrack activity in the presence of a subtropical SST front compared to the case of a subpolar SST front (Figures 2.5f and 2.6f), probably because of plenty of moisture supply from the warm ocean into cyclonic transient eddies migrating along the stormtrack.

It should be pointed out that in the presence of a subtropical SST front, the formation of the stormtrack and eddy-driven PFJ occurs under the influence of the strong downward motion associated with the Hadley Cell. Figure 2.23 compiles the meridional profiles of climatological-mean mass-streamfunction at 500hPa simulated in the individual experiments. The zero line marks the poleward extent of the Hadley Cell and thus the latitude of the strongest downward motion. Therefore, the latitude tends to coincide with the axis of the subtropical high-pressure belt, as observed (Nakamura and Shimpo 2004; Nakamura et al. 2004), with the near-surface westerlies at higher latitudes. The downward motion acts to retard both the baroclinic

eddy growth (Sampe et al. 2010) and associated driving of the surface westerlies. It is thus quite unlikely for the surface [U] axis to be located near a subtropical SST front even in the negative phase of the annular mode, despite the enhancement of high-frequency transient eddy activity (Figures 2.5a and 2.6a). In the presence of a subtropical SST front, the [U] axis tends to be situated around the latitude at which the axis forms in the NF experiment (compare the peak latitudes of lines in Figures 2.21a,b with 2.11e). The displacement of the [U] axis associated with the annular mode is consistent with the displacement of the mass-streamfunction (Figure 2.23) and the poleward extension of the Hadley Cell. In climatology, westerly acceleration associated with the poleward motion of the Hadley Cell is balanced with westerly deceleration by eddies associated with the enhanced transient eddy activity in the presence of a subtropical SST front (Figure 2.24), to which higher SST and enhanced moisture supply into individual transient eddies may be able to contribute.

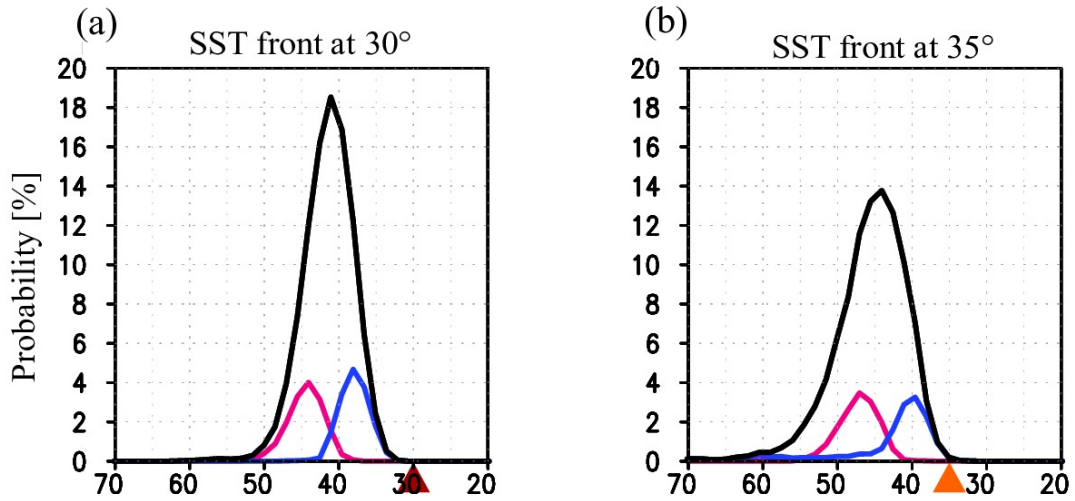

Figure 2.21. As in Figure 2.11, but for the experiments with SST front at (a) 30° and (b) 35°.

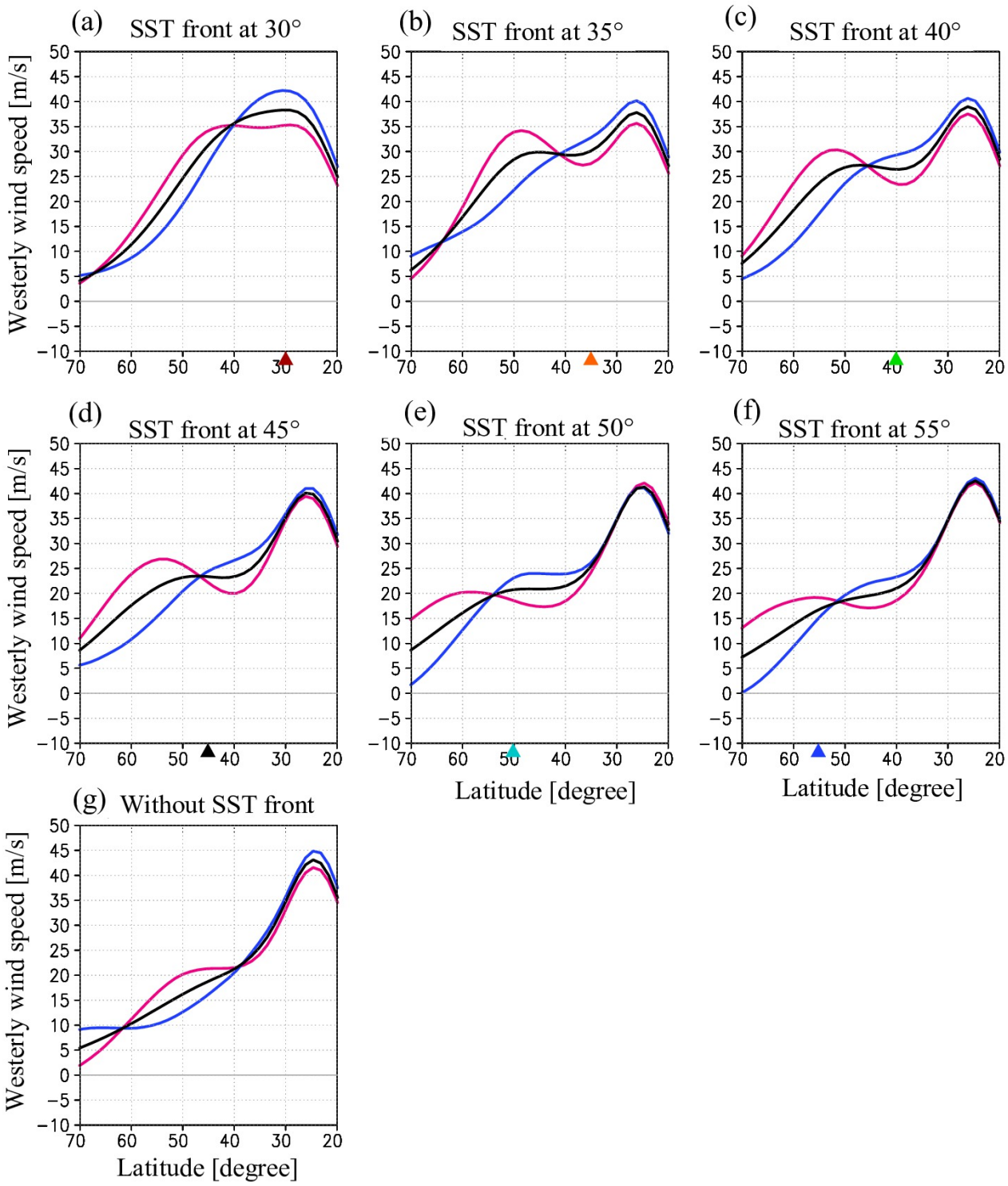

Figure 2.22. Meridional profiles of 300hPa [U] [m/s] in the climatological mean state (black line) and in the composites for the strong positive (red line) and negative (blue line) events in which the absolute values of the principal component exceed a unit standard deviation.

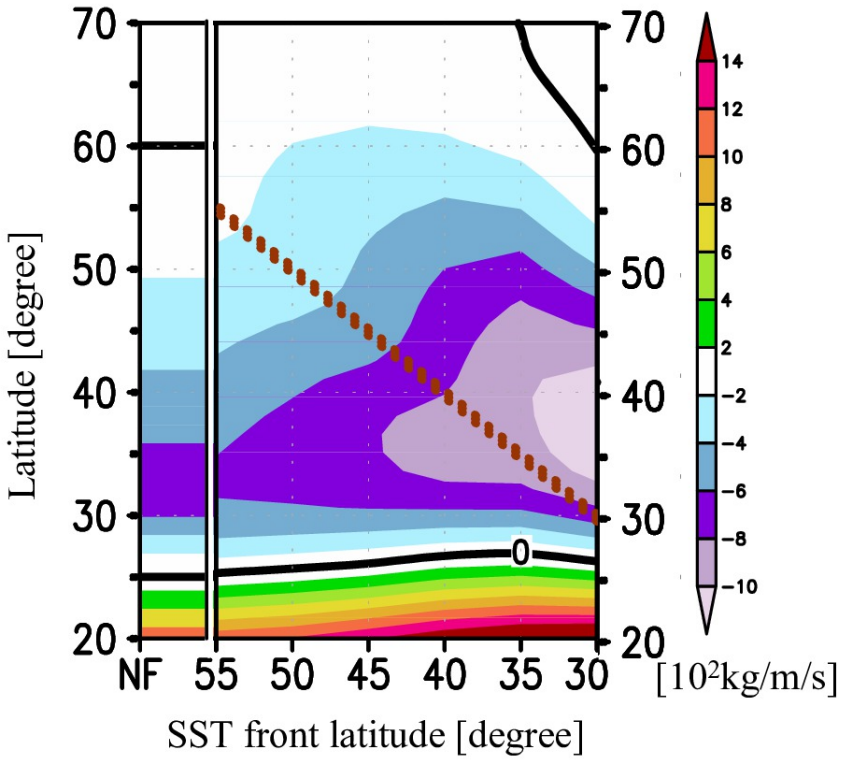

Figure 2.23. Climatological-mean state of the zonal-mean mass-streamfunction at 500 hPa [10^2 kg/m/s]. The latitude of SST front prescribed SST front is indicated in the abscissa and also by dotted line.

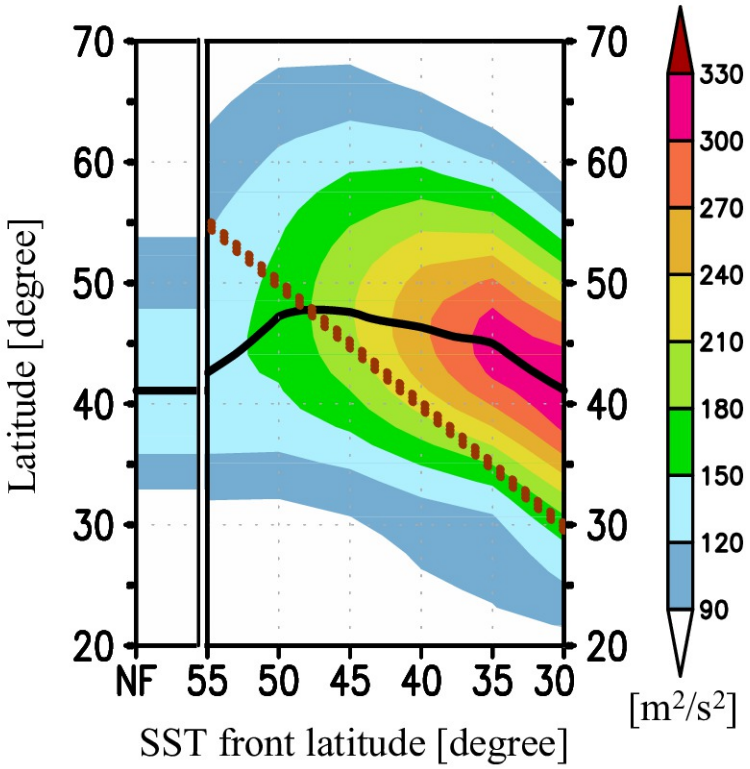

Figure 2.24. As in Figure 2.23, but for the variance of 300-hPa meridional wind [m^2/s^2] associated with 8-day high-pass-filtered fluctuations.

2.4. Implications for the observed wintertime Southern Annular Mode

a) Definition of Southern Annular Mode (SAM)

In this section, we argue that some of the characteristics of the wintertime annular mode revealed from our aqua-planet experiments are applicable to the observed wintertime SAM. In the SH winter, midlatitude oceanic fronts are located at different latitudes within the individual basins on the basis of the OISST data (Figure 2.25). The SST fronts in the South Atlantic and South Indian Ocean are located around 45°S, while the front is located around 55°S in the South Pacific. Monthly-mean atmospheric statistics derived from the JRA55 reanalysis dataset (Ebita et al. 2011) for the 55 years from 1958 to 2012 are used in this section, in addition to monthly-mean sensible heat flux based on the OA-flux dataset (Yu et al. 2008).

The SAM signature has been extracted through an EOF analysis that was applied to monthly-mean zonal wind anomalies poleward of 20°S from which the remote influence of ENSO (El-Nino/Southern Oscillation) had been statistically removed. Specifically, the EOF analysis was applied to monthly-mean zonally-varying U at 925hPa in austral winter (June, July and August), and the removal of the ENSO signal was based on the regression coefficient evaluated locally with the Southern Oscillation Index (SOI) available at the Japan Meteorological Agency (http://www.data.jma.go.jp/gmd/cpd/db/elnino/index/soi.html). As shown in Figure 2.26, the SAM signature extracted in our EOF1 represents virtually the same structure as extracted by the conventional definition by TW2000, although a wavy signature over the South Pacific is less emphasized because of the removal of the ENSO influence. The dominance of our EOF1, however, based on zonal wind anomalies (16% of the total variance explained) somewhat attenuates compared to the conventional definition (TW2000) based on geopotential height anomalies (28%). This may be because smaller horizontal structures tend to be more emphasized in the zonal wind variability than in the variability in geopotential height. Nevertheless, we define the annular mode based on near-surface zonal wind anomalies to highlight the dominant PFJ variability.

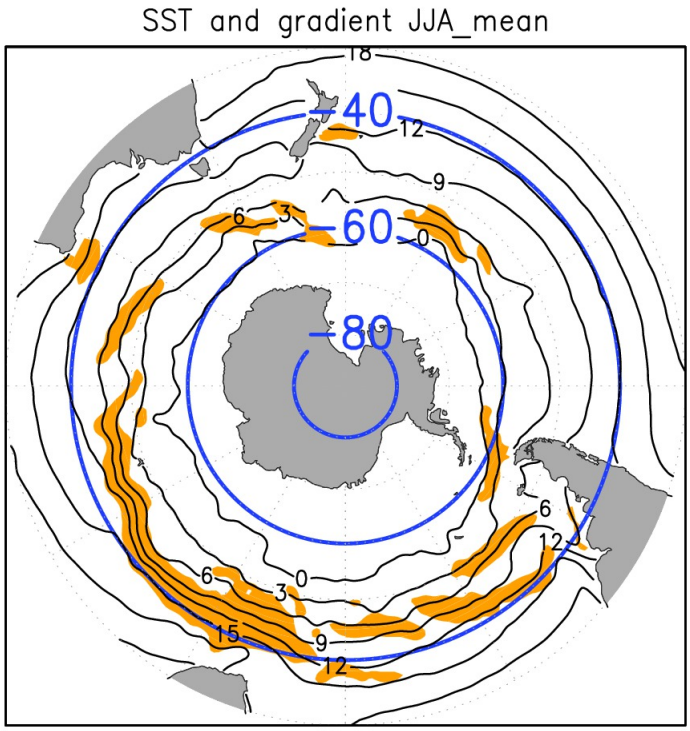

Figure 2.25. Climatological distribution of June-July-August mean SST [°C] (contoured) based on the OI-SST dataset from 1982 to 2012. Oceanic fronts where meridional SST gradient locally exceeds 1 [K/lat] are shaded. Thick solid lines indicate latitudinal circles.

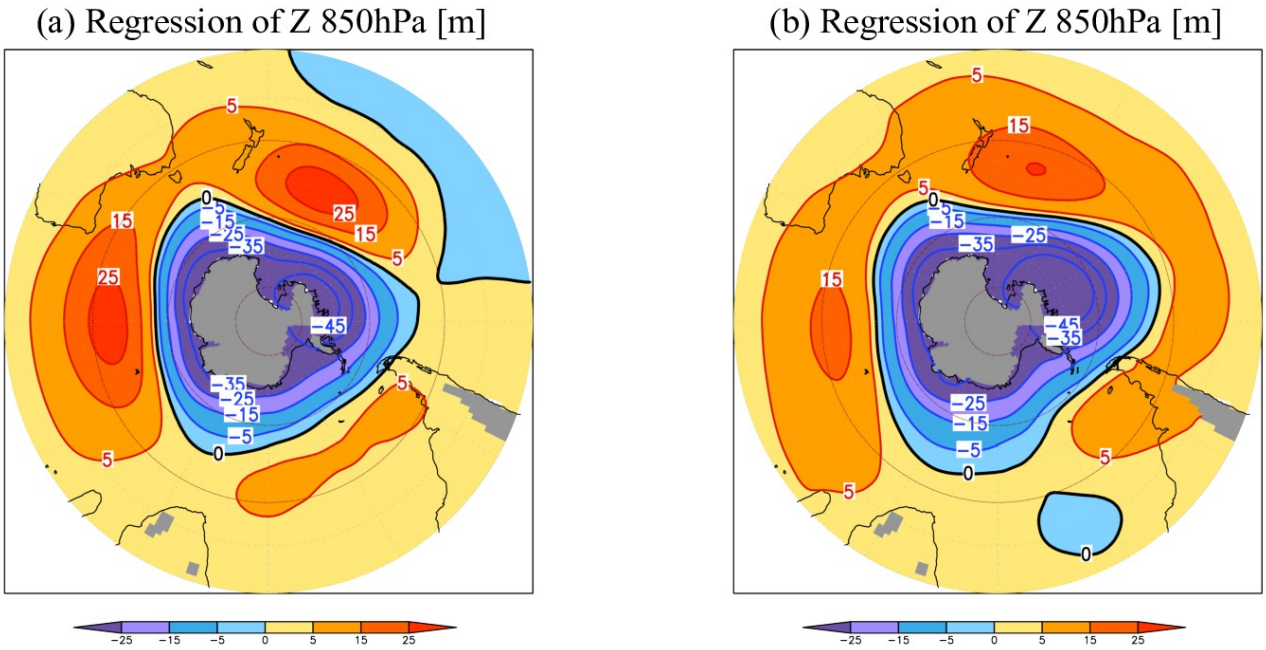

Figure 2.26. (a) Geopotential height anomalies [m] at 850 hPa regressed on the 1st principal component (PC1) of monthly anomalies of 925hPa zonal wind poleward of 20°S in austral winter (June-July-August). Remote influence of ENSO has been removed. (b) As in (a), but for geopotential height anomalies at 850 hPa regressed on the 1st principal component of the same anomalies, as derived by Thompson and Wallace (2000).

b) Consistency of the annular mode characteristics with the aqua-planet experiment

Monthly anomalies of 925hPa zonal wind as a wintertime SAM signature defined in the preceding sub-section are shown in Figure 2.27a. From a macroscopic viewpoint, the wind anomalies exhibit a high degree of zonal symmetry, representing a seesaw in zonal wind between the subtropical and subpolar latitudes. Nevertheless, the nodal latitude as well as the positions and strength of centers of action appear to differ in one ocean basin from another, following the SST fronts. While the moderate zonal asymmetry in the wintertime annular mode has already been pointed out in previous studies (e.g., Codron 2007), no study has discussed its relation to the underlying ocean. Figure 2.27b shows the relationship in longitudinally-averaged latitudes between an SST front and the node of 925hPa zonal wind anomalies associated with SAM for each of the ocean basins. In fact, the nodal latitude of the SAM-related zonal wind variability tends to be located more poleward with the latitude of SST front, which is consistent with the results in our aqua-planet experiments (Figure 2.27b). Furthermore, the regime-like characteristics found in our aqua-planet experiments are also found in the observed [U] composited separately for the strong positive and negative events of the SAM. As in Figure 2.28, the axial latitude of the zonal wind composited for the positive SAM events (Figures 2.28a,c) averaged over the Pacific is displaced latitudinally by ~10° relative to the counterpart for the Atlantic and Indian Ocean sectors, which is consistent with the aqua-planet experiment. The latitudinal difference of the zonal wind axis seems to be consistent with the difference in the SST front. For the negative SAM events, by contrast, the corresponding latitudinal differences in the latitude of the zonal wind at 925hPa among the three ocean basins are much smaller, which is again consistent with the aqua-plant experiments (Figures 2.28b,c). In fact, probability for the latitude of the observed wintertime U maximum averaged for South Pacific sector (170°W~120°W) exhibits two broad peaks in subpolar latitudes and midlatitudes (Figure 2.31a), suggestive of the regime-like behavior of the low-frequency U variability at least in this sector. Essentially the same argument can be made on the axial latitude of lower-tropospheric stormtrack, if applied to the composites for the positive and negative events (Figure 2.29). In fact, the equatorward gradient of upward sensible heat flux averaged within each ocean basin tend to be stronger across the SST front (Figure 2.30), which suggests the oceanic

baroclinic adjustment acts more efficiently in the positive phase than in the negative phase. Therefore, the modest zonal asymmetry of the wintertime SAM structure can be understood as the inter-basin differences in the SAM signature yielded by the corresponding differences in the SST front latitude.

It is noteworthy that the regime-like characteristics suggested by the probability for the latitude of PFJ axis is less evident in the South Indian sector (50°E~100°E; Figure 2.31b) with SST front at 45°S than in the aqua-planet experiment with the SST front at the same latitude (Figure 2.31d). It can be interpreted from a viewpoint of the relative latitudinal distance between the SST front and the particular latitude where the PFJ is driven by atmospheric internal dynamics. In fact, the latitude of the latter is different between the aqua-planet experiments (around 38°) and the observation (around 42°). Taken into account of the latitudinal difference by nearly 5°, it may be more reasonable to compare the aqua-planet experiments with SST front at 50° and 40° to the observed U in the South Pacific and South Indian Ocean, respectively. In fact, the probability for the latitude of [U] axis in the experiment with SST front at 50° (Figure 2.31e) also suggests the regime-like behavior as in the case with SST front at 55° (Figure 2.31c), whereas such a behavior is ambiguous with SST front at 40° (Figure 2.31f), as actually observed in the South Indian Ocean (Figure 2.31b).

The latitudinal excursion of the PFJ axis between the positive and negative phases of the SAM (as indicated by arrows in Figure 2.31) is greater over the South Pacific than over the South Indian Ocean, in agreement with the corresponding aqua-planet experiments. It is noteworthy that the observed difference is in better agreement with the comparison between the experiments with the SST fronts at 50° and 40° (Figures 2.31e,f) than with the fronts at 55° and 45° (Figures 2.31c,d). In terms of the latitudinal distance of PFJ from the particular latitude where the PFJ tend to be located in the negative phase of the annular mode and thus presumably determined by atmospheric internal dynamics, the observed distance in the positive phase for the South Pacific (South Indian Ocean) is closer to the corresponding latitudinal distance simulated in the aqua-planet experiment with SST front at 50° (40°) rather than 55° (45°) (Figure 2.28d), although such a subtle difference is less clear for the low-level stormtrack latitude (Figure 2.29d). For the regime-like behavior in the

wintertime annular mode, it is therefore important for the SST front to be situated poleward of the PFJ latitude determined by atmospheric internal dynamics by above a certain distance, as confirmed consistently in both aqua-planet experiments and observed facts (see arrows in Figures 2.31a-b and 2.31e-f).

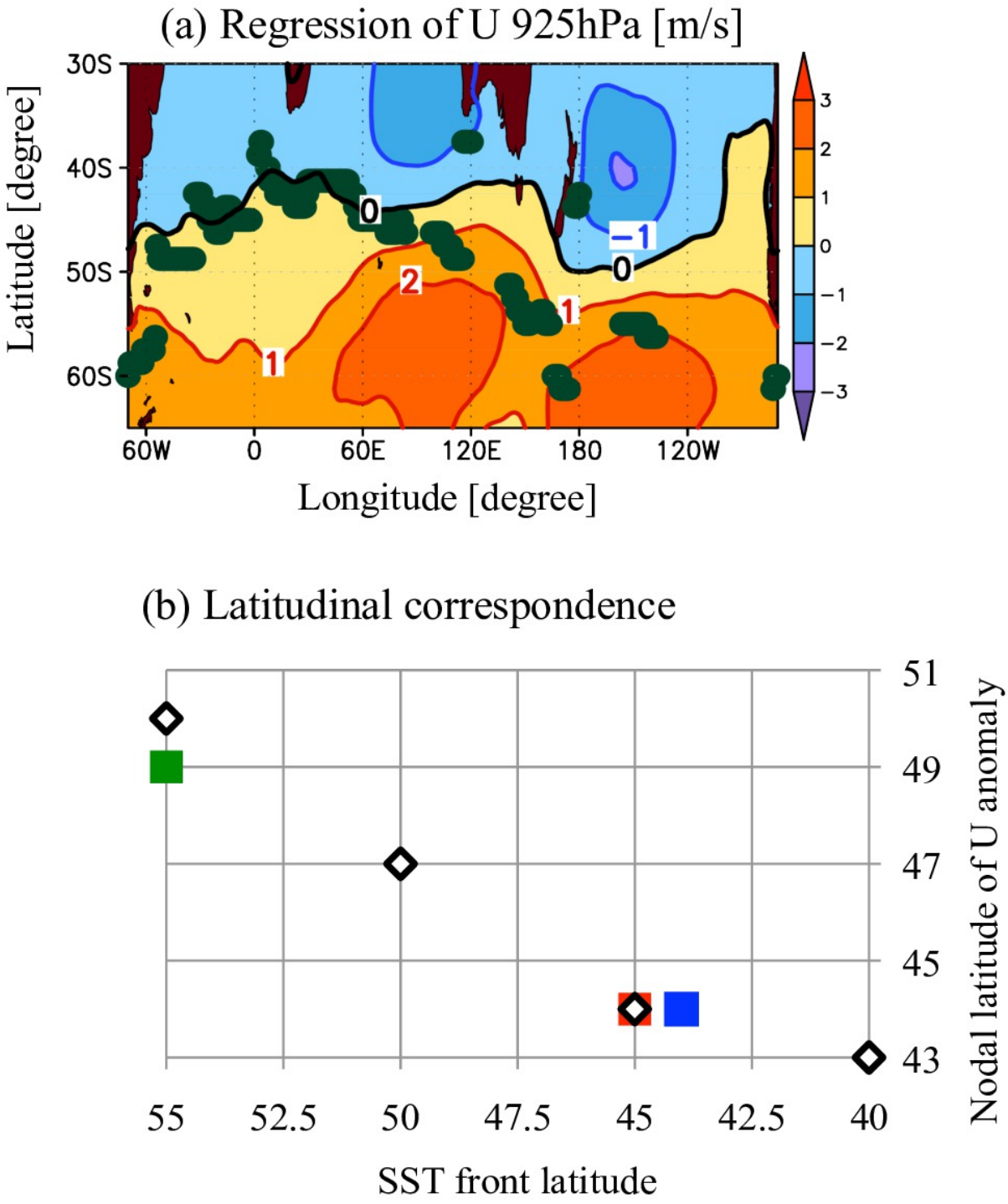

Figure 2.27. (a) Anomalies of 925hPa zonal wind [m/s] regressed on PC1 (shade), showing SAM signature in austral winter. Green dots indicate prominent oceanic fronts with meridional SST gradient exceeding 1 [K/lat]. (b) A scatter plot showing the relationship between the wintertime climatological latitude of the midlatitude oceanic front (abscissa) and the nodal latitude of 925hPa zonal wind anomalies based on (a) both averaged longitudinally over the Atlantic (40°W~10°E; blue), Indian (50°E~100°E; red) and Pacific (170°W~120°W; green) sectors (ordinate). Black symbols denote the corresponding results based on the aqua-planet experiments with the SST front located at 40°, 45°, 50° and 55°.

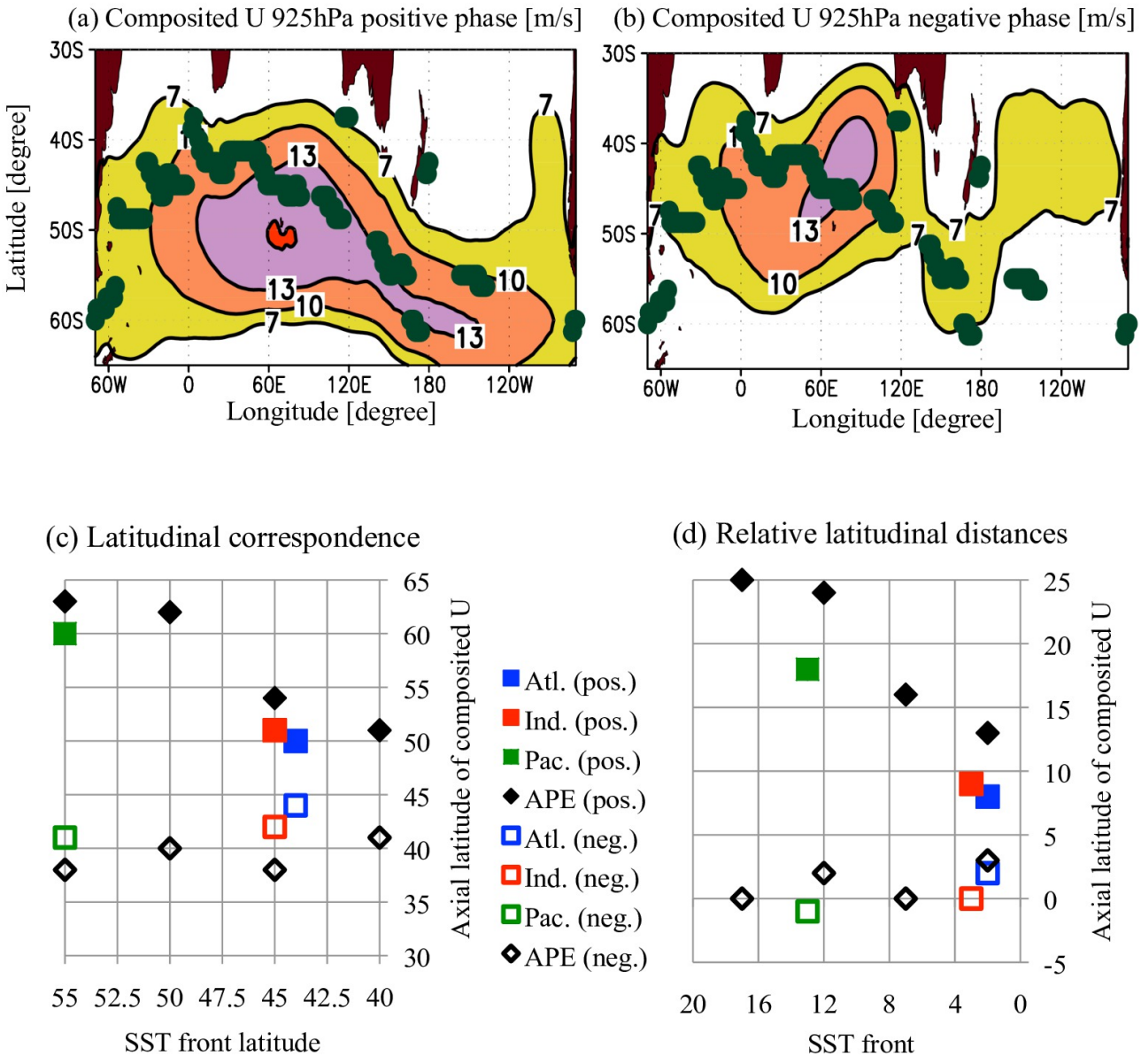

Figure 2.28. Zonal wind at 925hPa composited for (a) strong positive and (b) negative events are indicated by shading. Green dots indicate SST fronts with stronger meridional gradients than 1 [K/lat]. (c) A scatter plot showing the relationship between the wintertime climatological latitude of the midlatitude oceanic front (abscissa) and the latitude showing the maximum of the longitudinal averaged U for Atlantic (40°W~10°E), Indian (50°E~100°E) and Pacific (170°W~120°W) sectors (ordinate). Closed (open) mark corresponds to positive (negative) phase of the annular mode. (d) As in (c), but a plot between the axial latitudes of the composited U maximum (ordinate) and the SST front (abscissa), both relative to 38°S for aqua-planet experiments and 42°S for the observations. Latitudes of the SST front at 40°, 45°, 50° and 55° corresponds to the latitudinal differences by 2°, 7°, 12° and 17° from 38°S, respectively.

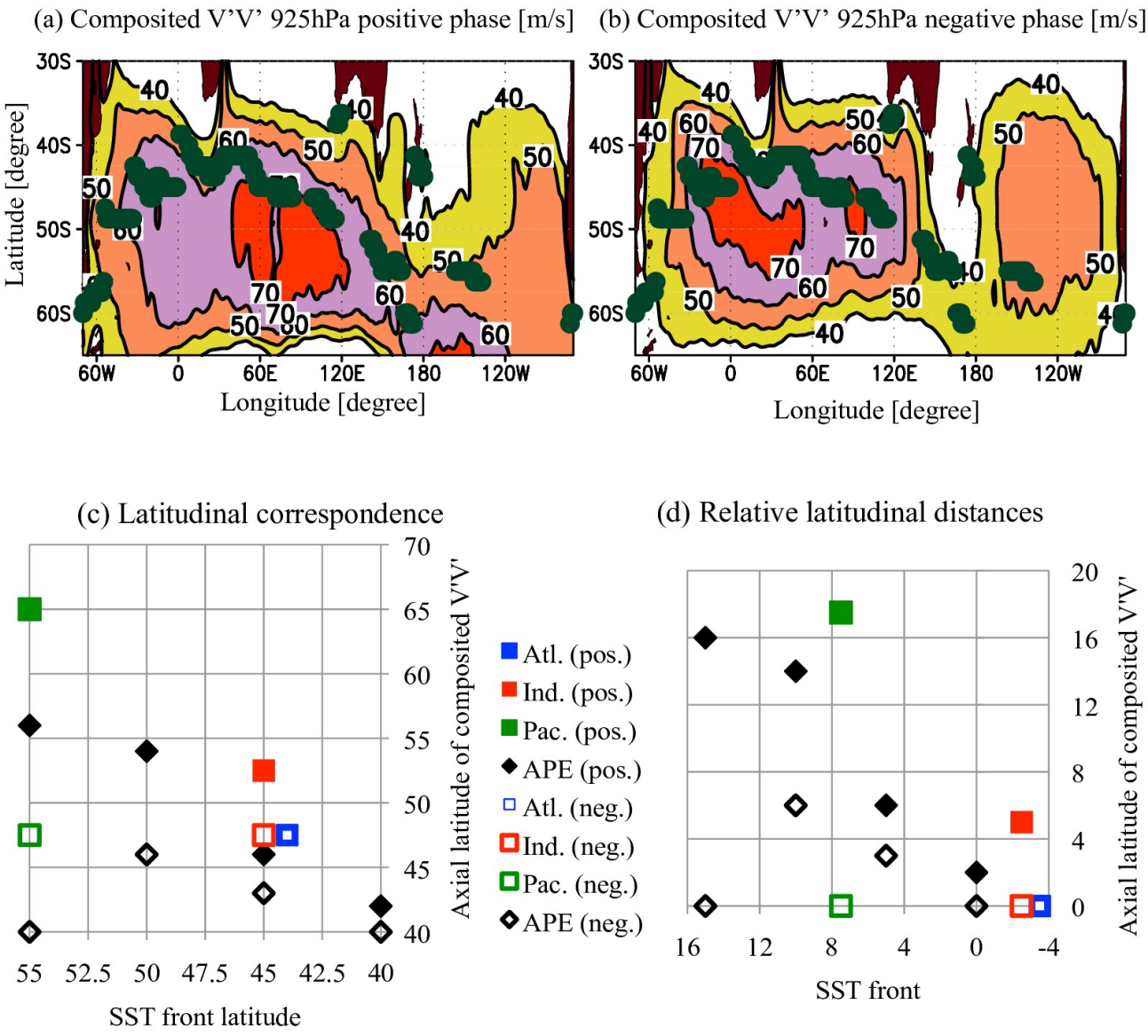

Figure 2.29. As in Figure 2.28, but for the variance in 925hPa meridional wind associated with 8-day high-pass-filtered fluctuations as a measure of stormtrack activity. In (d), the latitudinal difference is taken as the difference from 40°S (47.5°S) in the aqua-planet experiments (observations), respectively.

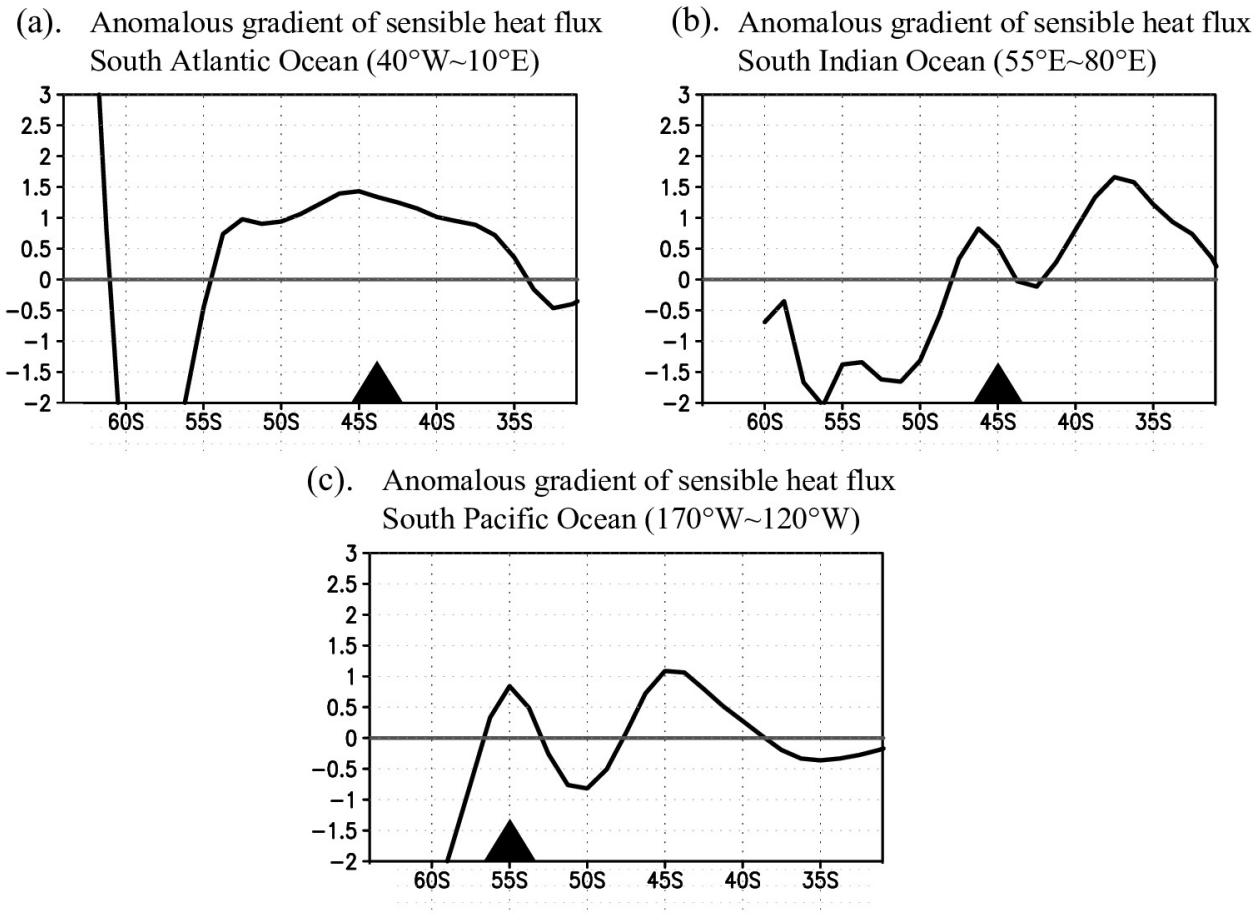

Figure 2.30. Difference in the composited gradients of the wintertime surface turbulent sensible heat flux between the strong positive and negative events of the annular mode defined as the periods during which the absolute value of the principal component exceeds 1.5 standard deviations, which is averaged for (a) Atlantic (40°W~10°E), (b) southwestern Indian (55°E~80°E) and (c) Pacific (170°W~120°W) sectors. The latitude of SST front prescribed SST front is indicated by the triangle at the bottom of each panel.

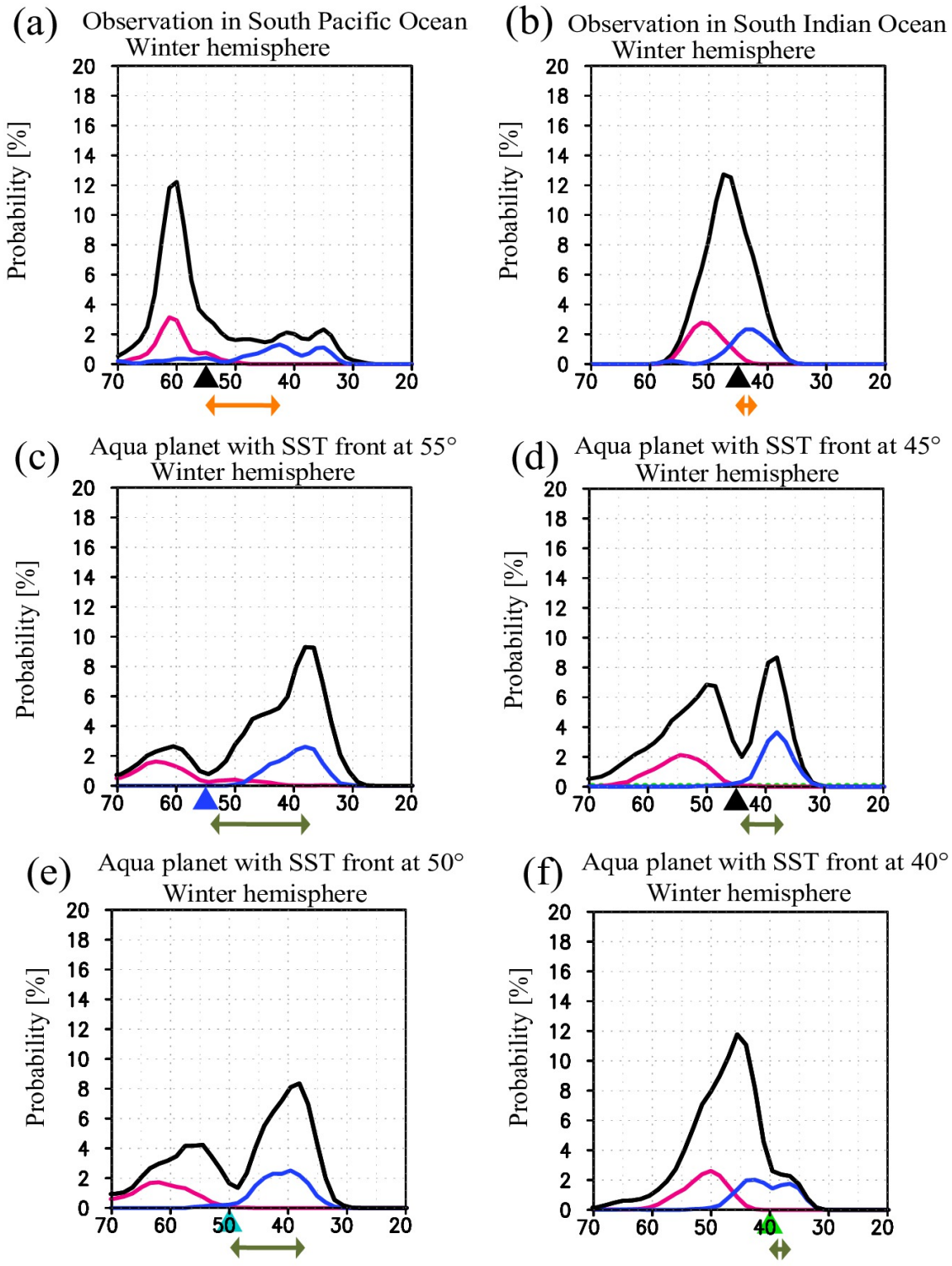

Figure 2.31. Probability for the latitude of [U] maximum at 925 hPa for all the monthly time steps (black line) and the periods of strong positive phase (red line) and negative phase (blue line) defined as the periods when the absolute value of the principal component value exceeds a unit standard deviation, displayed for the observed wintertime U averaged for (a) Pacific sector (170°W~120°W) and (b) South Indian sector (50°E~100°E). (c-f) As in (a,b), but sampled for all the daily time steps of the aqua-planet experiments with SST front at (c)55°, (d)45°, (e)50°, and (f)40°. Latitudinal distances between the SST front and the particular latitude where the PFJ is driven by atmospheric internal dynamics are indicated by orange (green) arrows for observations (aqua-planet simulations) below individual panels of (a-f).

2.5. Interpretation of the climatological-mean state

Regime-like characteristics in the wintertime annular mode have been found in the aqua-planet experiments with SST front at midlatitude or subpolar latitudes. The regime-like characteristics may leave some imprints also in some of the climatological-mean statistics, for example, as the distinct two peaks of the probability density of the latitude of the near-surface [U] maximum simulated in the aqua-planet experiments with a midlatitude/subpolar SST front (black lines Figure 2.11a-d). Figures 2.32a-d show the climatological-mean profile of 925hPa [U] (black line) and the composited profiles for the strong positive and negative events (red and blue lines, respectively) of the model annular mode in an experiment with an SST front located at 45°, 55°, 40° or 50°, respectively. Each of the climatological-mean profiles exhibits a hint of dual peaks that reflect two different quasi-equilibrium states, or "regimes", represented by the two phases of the annular mode, and the climatological-mean state can be interpreted as the superposition of the two regimes corresponding to the individual phases of the annular mode. The latitude of the equatorward peak in the climatological-mean state, though rather ambiguous for the SST front at 40° (Figure 2.32c), is almost the same among those experiments, corresponding to the negative phase of the annular mode represented in Figure 2.6a. In contrast, the latitude of the poleward peak differs from one basin to another, corresponding to the latitudinal difference of the SST front, which can be understood as an imprint of the positive phase represented in Figure 2.5a.

Furthermore, Figures 2.32b and 2.32d offers an interpretation for the counterintuitive weakness in the climatological sensitivity of the axial latitude of [U] to the latitude of an SST front, as found in Ogawa et al. (2012), especially if located at subpolar latitude. In fact, the equatorward peak of the climatological-mean [U] in the experiments with subpolar SST fronts (at 50° and 55°) is more representative of the negative phase of the annular mode. The particular phase represents a regime in which atmospheric internal dynamics is dominant, thus showing no sensitivity to the latitude of an SST front. This interpretation supports the argument by Ogawa et al. (2012) that the climatological weak sensitivity of the latitude of PFJ to subpolar SST fronts may be due to the

dominant contribution of atmospheric internal dynamics that is unrelated to the lower boundary condition (Robinson 2006).

The aforementioned interpretation is applicable to the wintertime climatological-mean state actually observed over the SH. Figures 2.32e and 2.32f show the meridional profiles of 925hPa [U] in the climatological mean and composited profiles for the individual phases of the SAM for the South Indian Ocean and the South Pacific, respectively. As pointed out by Nakamura et al. (2004), the wintertime climatological-mean axial latitude of [U] depends on the latitude of SST front in each of the ocean basins (black lines in Figures 2.32e-f). This dependence arises basically from the positive phase of the SAM (red lines in Figures 2.32e-f), but not from its negative phase (blue lines in Figures 2.32e-f), which is in good agreement with the aqua-planet simulations. Each of the climatological-mean zonal wind profiles observed over the South Indian Ocean and the South Pacific resembles the results of the experiments especially with SST front located at 40° and 50° (Figures 2.32c and 2.32d), respectively, rather than those with the SST front located at 45° and 55° (Figures 2.32a and 2.32b). We therefore argue that it is the meridional distance of an SST front from the latitude of PFJ determined by atmospheric internal dynamics in the negative phase of the annular mode that is important not only for the annular mode characteristics discussed in the section 2.4b but also important for the meridional structure of the climatological-mean state represented by the superposition of the two “regimes” represented by the positive and negative phases of the annular mode.

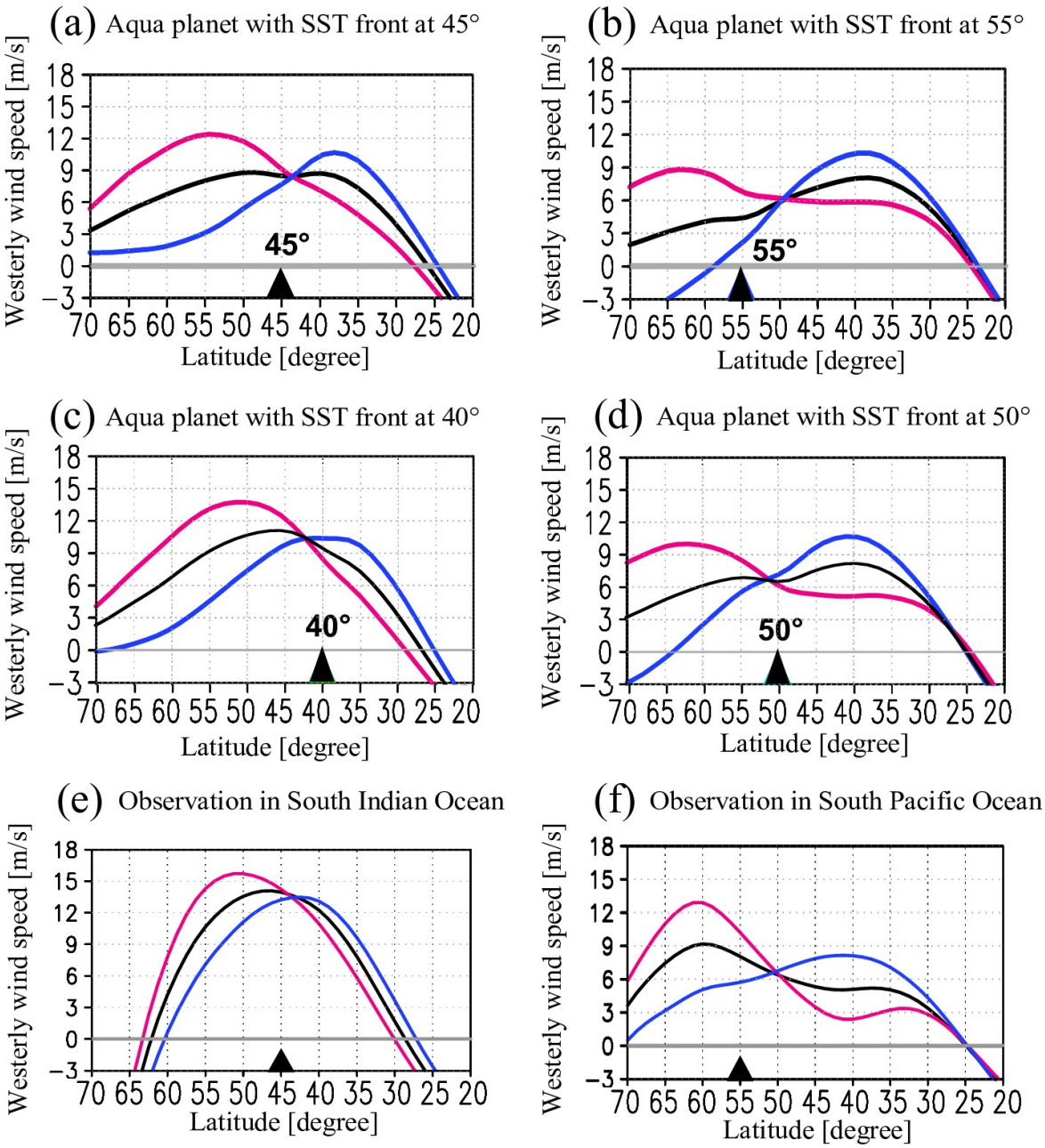

Figure 2.32. (a-d) Meridional profiles of 925hPa [U] [m/s] based on the climatological mean state (black line) and the composites for the strong positive (red line) and negative events (blue line) in which the absolute values of the principal component exceeds a unit standard deviation, from aqua-planet experiments with SST front at (a) 45°, (b) 55°, (c) 40°, and (d) 50°, respectively. (e,f) As in (a,b), respectively, but for observed wintertime U averaged longitudinally over the (c) South Indian Ocean (50°E~100°E) and (d) South Pacific (170°W~120°W).

2.6. Seasonal dependence in the annular mode characteristics

In this study, characteristics of the wintertime annular mode have been focused on. The regime-like character as revealed in the present analysis does, however, not seem to be applicable to the summertime annular mode signature. Figures 2.31d and 2.33b shows the latitudinal profile of the probability for the latitude of [U] maximum near the surface in the winter and summer hemisphere of the aqua-planet experiments with SST front at 45°. While the regime-like character is evident in the winter hemisphere (Figure 2.31d), this is not the case in the summer hemisphere as suggested by the fact that the dominant single peak at 47° is found for the whole period (black line) while the peak in the positive (negative) phase of the annular mode is located at the poleward (equatorward) skirt of the dominant peak. Similar seasonality in the observed SAM characteristics is evident particularly in the South Pacific sector (Figures 2.31a and 2.33a). In austral winter (June-July-August), the variability of PFJ as suggested by the probability diagram shows regime-like signature as discussed in the subsection 2.4b (Figure 2.31a). In the austral summer (December-January-February), however, the probability seems more like the simple meridional fluctuation of PFJ as suggested by the similarity of the probability to the normal distribution (Figure 2.33a). Therefore, regime-like characteristics of the annular mode influenced by the SST front seem to be unique in winter.

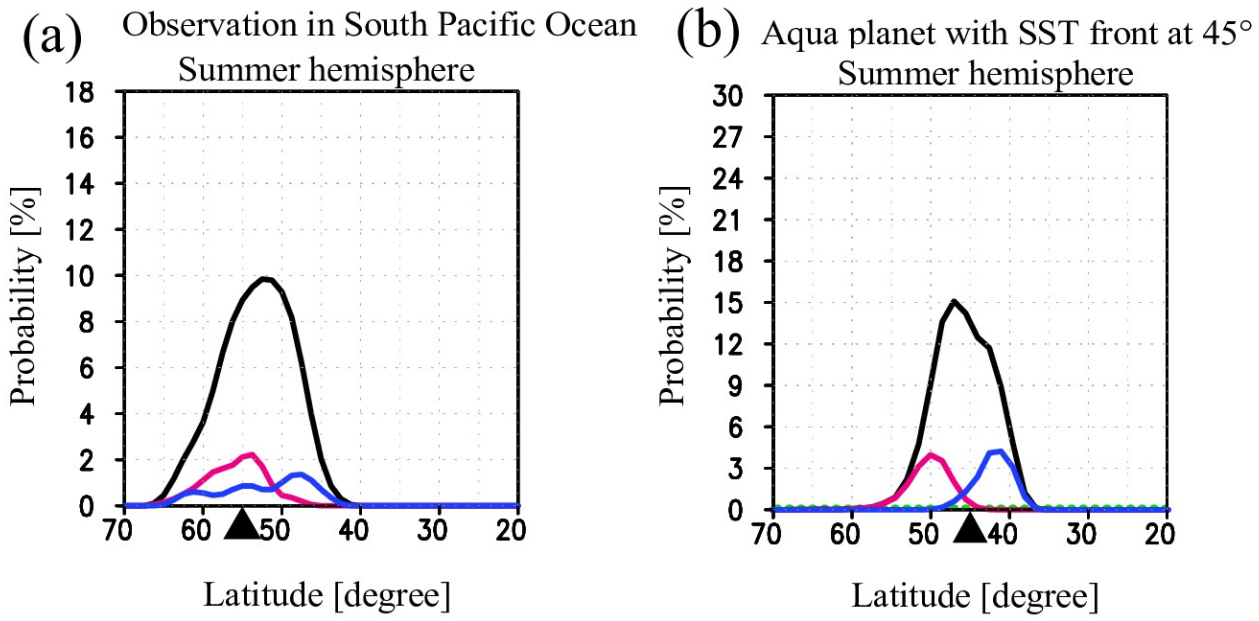

Figure 2.33. (a,b) As in Figures 2.31(a,d), but for summer hemisphere.

Chapter 3. Importance of midlatitude oceanic frontal zones for ozone-induced climatic trends in austral summer

3.1. Experimental design and analysis procedure

In this chapter, significance of midlatitude oceanic frontal zones in activating stratosphere-troposphere dynamical coupling is investigated. As a relevant example of the coupling in the form of the annular mode, our focus is placed on the surface climatic trends observed in the summertime SH induced by the stratospheric ozone depletion in the late 20th century, as discussed in section 1.2. In spite of many arguments in previous studies (see section 1.2; also Thompson et al. 2011), the mechanisms for the vertical coupling involved in the particular trends are still controversial, and the potential importance of the oceanic front has nonetheless been neglected.

Here a set of aqua-planet experiments is designed to assess how significantly the summertime surface climatic response observed in the SH during the late 20th century to the springtime stratospheric ozone depletion can depend on the midlatitude SST gradient. The Hamburg version of the European Centre AGCM (ECHAM5; Roeckner et al. 2003) is used in this chapter. Its horizontal resolution is T63 (equivalent to ~180km grid intervals), which is not particularly high but still sufficient for resolving the oceanic frontal zones. The model has 39 vertical levels up to 0.01hPa near the mesopause. A better representation of stratospheric processes is expected than using AFES used in chapter 2, whose top level (0.09hPa) is much lower in the mesosphere. While only 17 of the 56 vertical levels of AFES are located higher than the 100hPa level, as many as 23 of the 39 levels of ECHAM5 are higher than that level. As in the AFES experiments discussed in chapter 2, the lower boundary of the AGCM is set as the fully global ocean with different latitudinal profiles of zonally uniform SST taken from the OI-SST dataset (Reynolds et al. 2007). With this aqua-planet configuration, four AGCM experiments were performed with combinations of two SST profiles and two ozone concentration distributions. The two SST profiles are both zonally symmetric and seasonally varying, but different in their midlatitude gradient. One of the two SST

profiles given to the model was taken from the climatological-mean (1982-2007) monthly SST profile observed at 60°E in the South Indian Ocean, which is essentially the same as the reference profile used in the AFES experiments in chapter 2. It includes steep SST gradients associated with an oceanic front at 45°S throughout the year (black lines in Figure 3.1a-b and Figure 3.1c). Following the previous studies (Nakamura et al. 2008; Sampe et al. 2010; 2013) and in the same manner as in chapter 2, we linearly interpolated SST from the poleward flank (at 53°S) of the oceanic front toward the South Pole, where SST is set to 0°C and sea-ice is assumed to be absent. The other SST profile was produced to represent a "non-front (NF)" configuration through the interpolation of SST from the equatorward flank (at 40°S) of the front to the pole (green dashed lines in Figure 3.1a-b and Figure 3.1d) in the same manner as in producing the non-front SST in chapter 2. The profile in the model SH used for the NF experiments was prescribed in the model Northern Hemisphere (NH) after imposing the lag of 6 months. While the "non-front (NF)" SST profile in the Tropics and the model NH is thus kept the same as that in the "with-front (WF)" SST, SST gradients over the midlatitude SH are much weaker than in the WF profile throughout the year (compare Figure 3.1d with Figure 3.1c).

For each of the SST profiles, two experiments were performed with two different ozone profiles that are both zonally symmetric and seasonally varying. The ozone profiles had been produced by zonal averages of ozone concentration taken from the JRA-25 reanalysis data (Onogi et al. 2007) for the following two 3-year periods. One is from 1979 to 1981 that corresponds to the beginning of the ozone depletion, and the other from 1999 to 2001 when the ozone concentration reached its minimum over Antarctica. The two stratospheric ozone profiles prescribed for the experiments differ by nearly 50% over the polar region in September and October (Figure 3.2). Although the depletion analyzed in the JRA25 data is somewhat underestimated, its seasonality is consistent with the observed depletion (Figure 1.5a; Thompson et al. 2011).

Each of the four AGCM experiments was conducted for 49 years, after a 3-year spin-up. Climatological mean states in the presence and absence of the SST front are defined as the average over both the high- and low-ozone experiments, while responses in the atmospheric circulation to

the ozone depletion are defined as the differences between them under the same SST profiles. Owing to the aforementioned zonal symmetries in the SST and ozone profiles imposed to the model, the responses exhibit a high degree of zonal symmetry and we therefore discuss zonally averaged statistics throughout this chapter.

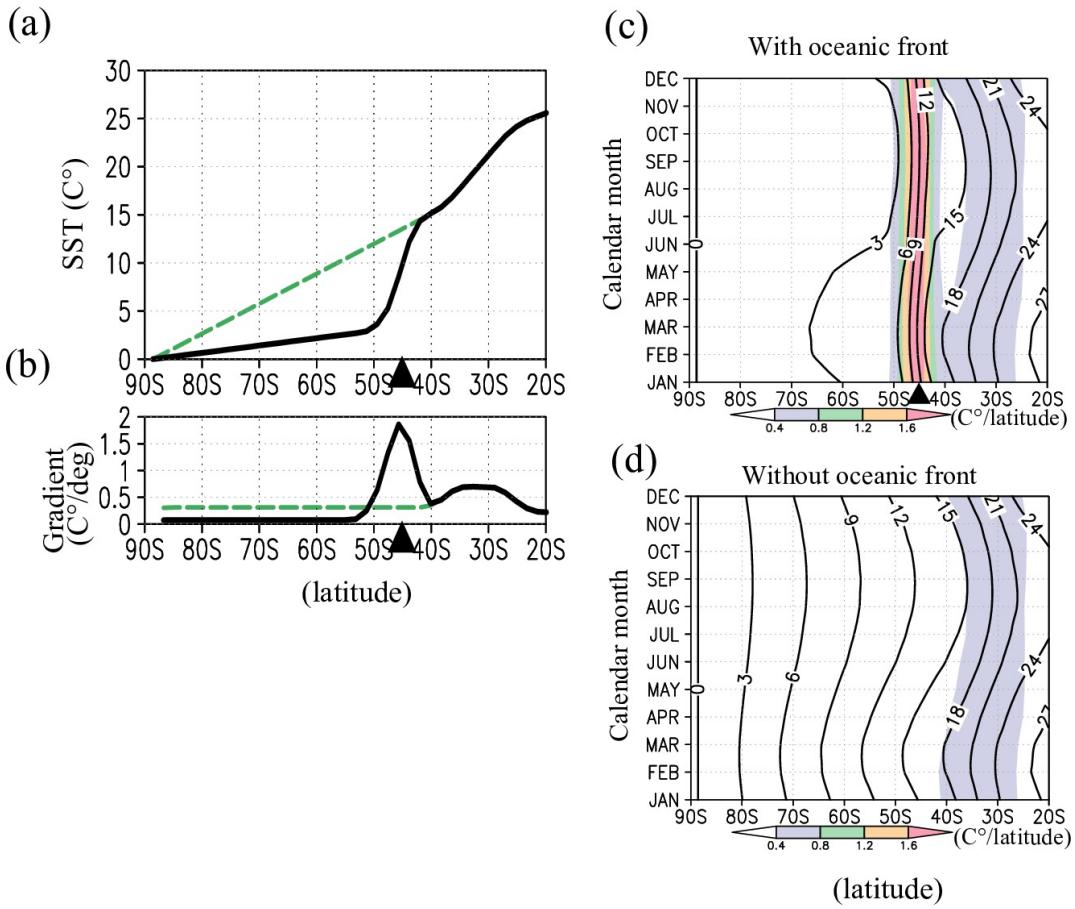

Figure 3.1. Latitudinal profiles of (a) prescribed SST and (b) its meridional gradient averaged from 1st November to 31st December for the experiments with (black) and without (green) the oceanic front. (c)-(d) Latitude-time sections showing the seasonal march of zonally symmetric SST prescribed for the AGCM experiments. Black triangle indicates the latitude of the oceanic front. Contours indicate SST (°C) and shading indicates its meridional gradient (°C/latitude) for the experiments (c) with and (d) without the oceanic front.

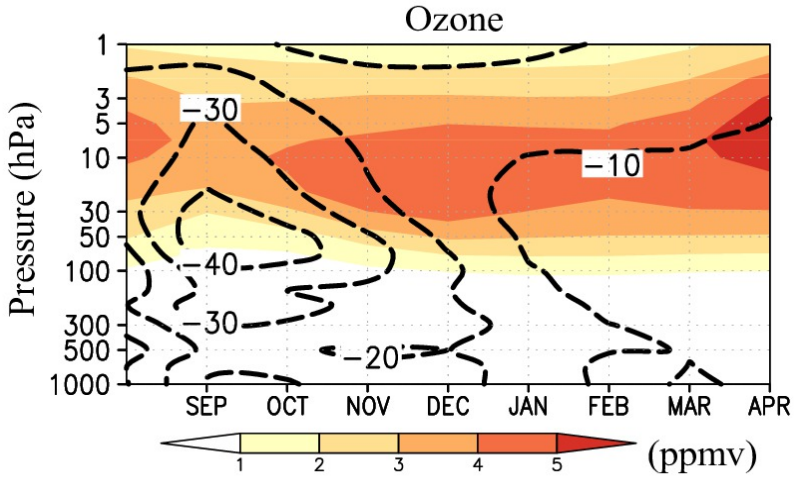

Figure 3.2. Prescribed height-time section of the zonally-uniform ozone concentration (ppmv; shade) averaged over the polar latitudes (75~90°S) for the low-ozone period and its fractional depletion (%) from the high-ozone period (contour).

3.2. Impacts of midlatitude oceanic frontal zones on the climatological-mean state over the Southern Hemisphere

As mentioned in section 1.3, previous studies (Nakamura et al. 2008; Sampe et al. 2010; Ogawa et al. 2012) demonstrated the vital importance of frontal SST gradient for the climatological-mean states of PFJ and stormtrack at least in midsummer and midwinter. It is shown here that the impacts of an SST front are distinct also in another season from spring to early summer, when the observed signal of the surface climate trend induced by ozone depletion over the extratropical SH is most pronounced (Figure 1.5c; Thompson and Solomon 2002).

Figure 3.3 shows the climatological zonal mean statistics averaged from 16th November to 16th December in both the WF and NF experiments. Lower-tropospheric stormtrack activity associated with synoptic-scale eddies is locally doubled in the presence of the SST front at 45°S (solid line in Figure 3.3a). The latitudinal correspondence between the well-defined stormtrack and SST front is consistent with the strong SAT gradient (corresponding to the surface baroclinic zone) anchored by the SST front and its maintenance through the "oceanic baroclinic adjustment" (Nakamura et al. 2008). Indeed, the meridional gradient in the surface turbulent sensible heat flux (solid line in Figure 3.3b) is prominent along the SST front. The stormtrack activity in the upper troposphere also shows a distinct peak slightly poleward of the SST front (solid line in Figure 3.3c). The eddy momentum flux convergence near the tropopause is thus maximized slightly equatorward of the SST front (solid line in Figure 3.3e), where eddies drive the well-defined PFJ away from the STJ (Figure 3.3f). The dynamical association among SST front, stormtrack, and PFJ in this season is thus evident in the presence of the midlatitude SST front.

In the absence of SST front, by contrast, the stormtrack in the lower troposphere is much less organized with no well-defined axis (dashed line in Figure 3.3a), which is consistent with weak meridional gradient of surface sensible heat flux in the lack of its well-defined maximum (dashed line in Figure 3.3b). Indeed, the lower-tropospheric stormtrack activity measured by 850hPa

poleward eddy heat flux is reduced by about 50%. In the upper troposphere (Figure 3.3c), the stormtrack is shifted equatorward by 7° with notable reduction of eddy activity between 40°S and 60°S. Indeed, the maximum stormtrack activity as estimated by the variance of meridional wind associated with synoptic waves is nonetheless reduced by about 40% around 50°S. The stormtrack in the NF experiments may be maintained through atmospheric internal dynamics unrelated to the lower-boundary condition (Robinson 2006). In the NF experiments, the peak latitude of poleward eddy momentum flux is also shifted equatorward with reduced amplitudes (dashed line in Figure 3.3d). Instead, equatorward momentum flux is enhanced in midlatitudes (Figure 3.3d), which yields the maximum flux convergence that is slightly stronger than in the WF experiments (Figure 3.3e). The peak flux convergence in the NF experiments is shifted equatorward (Figure 3.3d), and so is the axis of the eddy-driven PFJ by about 6° near the surface (Figure 3.3g). The stronger convergence of eddy momentum flux may be due to the change in the horizontal structure of the synoptic eddies into more like “banana shape”. This change which seems consistent with augmented meridional westerly shear in the NF experiments due to the notable weakening of the eddy-driven westerlies poleward of 40°S in the absence of the SST front (Figure 3.3h). In fact, the weakening of the tropospheric westerlies in summer by the removal of SST front (Figure 3.3h) is in common with the AFES experiment (Figure 3.4).

It should be noted that the particular smoothing of the frontal SST gradient in this study introduces artificial warming over the subpolar ocean and thus artificially enhances heat and moisture release into the atmosphere, which acts to enhance moist diabatic growth of storms. In the absence of SST front in our experiments, however, both the climatological storm-track activity and eddy-driven midlatitude westerlies weaken substantially (Figures 3.3a and 3.3h), indicative of the importance of the frontal SST gradient for shaping the climatological-mean atmospheric circulation in the extratropics.

Figures 3.5a and 3.5b show the climatological activity of planetary waves as defined by the zonal wavenumber 3 or less in the lower and upper troposphere, respectively. The poleward heat flux associated with the lower-tropospheric planetary waves is comparable between the experiments

with and without SST front (Figure 3.5a), and it is much weaker than that with synoptic-scale wave disturbances (Figure 3.3a), reflecting more barotropic structure of the planetary waves. The amplitude of the upper-tropospheric planetary waves increases with latitude and maximizes in the polar region, regardless of the presence of the midlatitude SST front (Figure 3.5b). In the presence of SST front, the amplitude is larger by 30~50% in the polar and subpolar regions, which can be interpreted as the amplification of the planetary waves through local nonlinear processes with energy cascade from active synoptic (or baroclinic) waves. The stronger upper-tropospheric planetary waves in the polar and subpolar regions in the presence of SST front can lead to their enhanced propagation into the stratosphere. In fact, the poleward eddy heat flux associated with the planetary waves around the tropopause, which is a measure of upward wave-activity propagation, is stronger by over 40% in the presence of SST front (Figure 3.5c) and consistently the stratospheric planetary waves are considerably stronger (Figure 3.5d) .

In recognition of certain ambiguities in the definition of the planetary waves, we construct the same statistics as above but with the inclusion of the contribution from the component with zonal wavenumber 4. Compared to its counterpart in Figure 3.5a, the inclusion of the zonal wavenumber 4 gives rise to a notable peak in the poleward eddy heat flux slightly poleward of the SST front (Figure 3.5e). In fact, the corresponding heat flux associated only with the zonal wavenumber 4 (Figure 3.5f) shows an even more notable peak near the SST front (solid line), indicative of active baroclinic growth of this wave component in the presence of SST front. The particular wave component may thus be regarded as baroclinic waves with similar characteristics as synoptic-scale waves typically with zonal wavenumber of 5 or 6. Hereafter the wave components with wavenumber 4 or more (3 or less) are referred to as synoptic (planetary) waves.

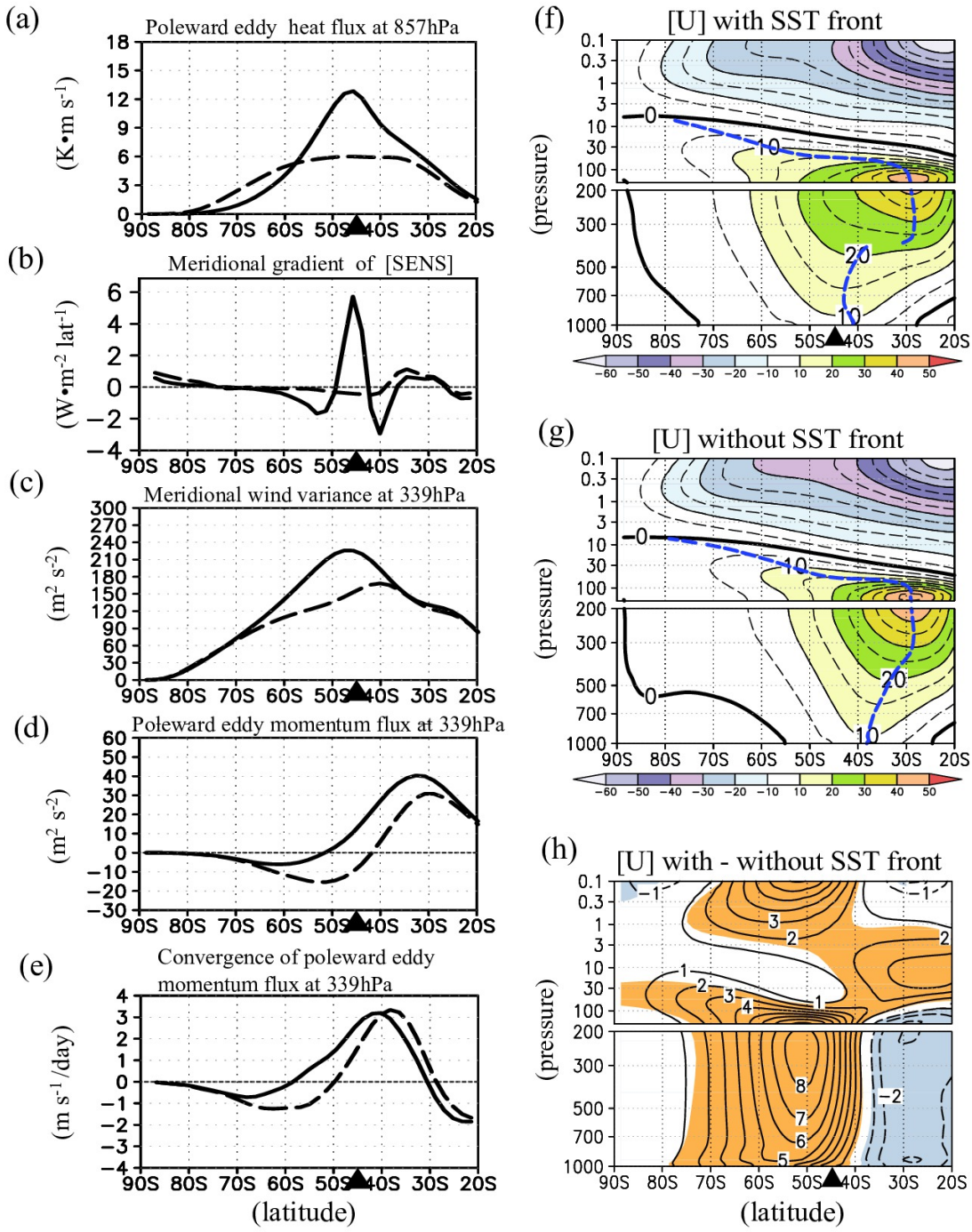

Figure 3.3. (a-e) Climatological latitudinal profiles of zonal-mean statistics averaged between 16th November and 16th December. (a) Poleward eddy heat flux at 857hPa associated with the wave components of zonal wavenumber 4 or more, for the experiments with (solid) and without (dashed) the front. (b) Meridional gradient of upward sensible heat flux. (c) Meridional wind variance at 339hPa. (d) poleward eddy momentum flux and (e) its meridional convergence, all associated with wave components of zonal wavenumber 4 or more. (f) Meridional section of climatological westerlies averaged over both the high- and low-ozone experiments with the oceanic front. Intervals are 10 and 5 (m s^{-1}) for thin-solid and thin-dashed lines, respectively. Thick solid lines indicate zero wind speed. Blue dashed lines denote the climatological westerly axes. Black triangle indicates the latitude of the oceanic front. (g) As in (f), but for the experiments without the front. (h) Difference between (f) and (g). Shading in (h) indicates the response exceeding the 95% confidence level based on the Student's t-test.

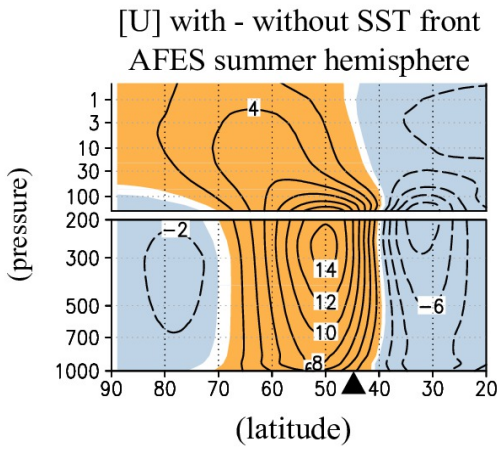

Figure 3.4. As Figure 3.3h, but for the summer hemisphere in the AFES experiment discussed in chapter 2.

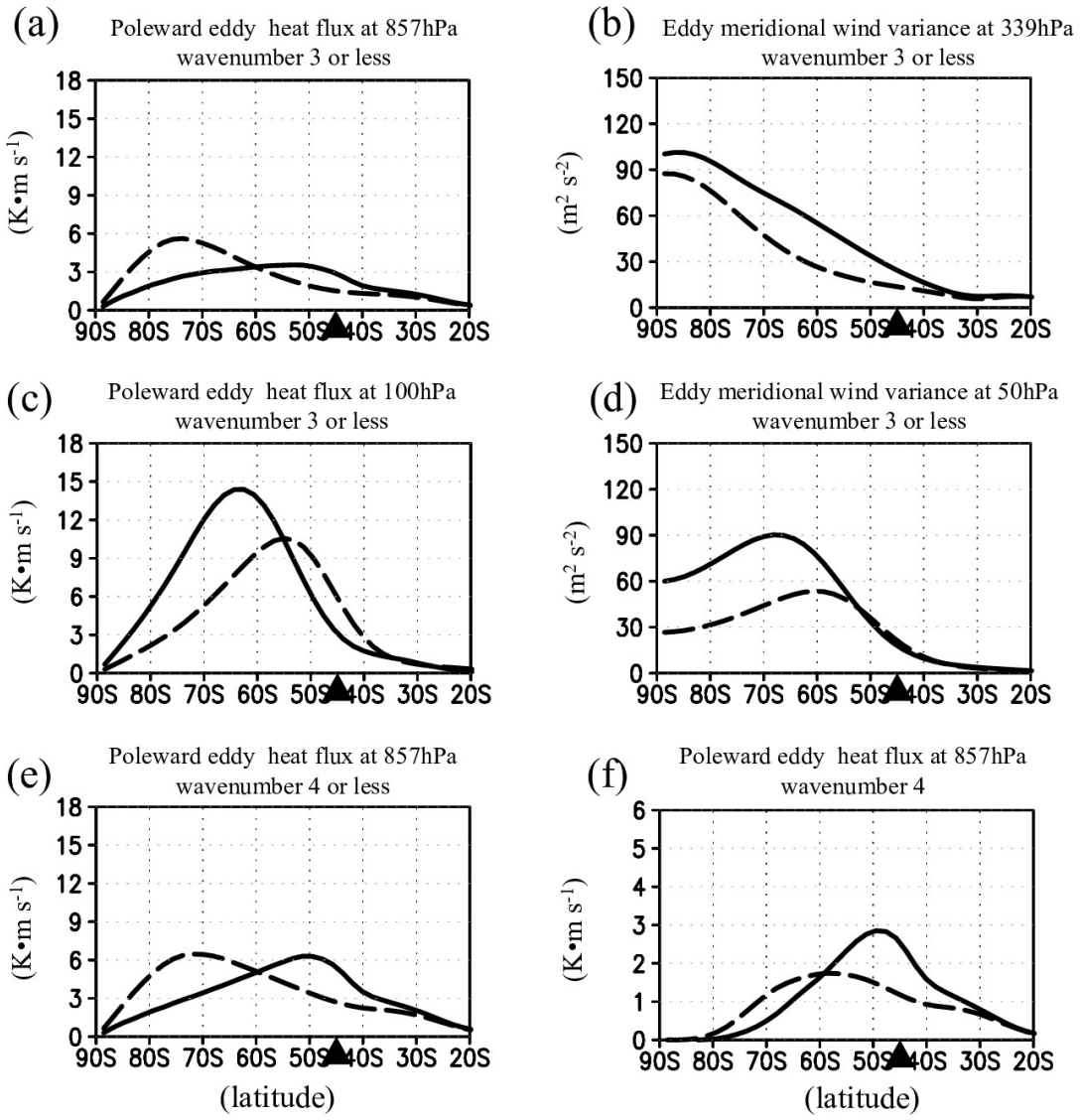

Figure 3.5. Climatological latitudinal profiles of zonal-mean statistics averaged between 16th November and 16th December. (a) As in Figure 3.3a, but for the wave components of zonal wavenumber 3 or less. (b) As in Figure 3.3c, but for the wave components of zonal wavenumber 3 or less. (c) As in (a), but for 100hPa. (d) As in (b), but for 50hPa. (e) As in (a), but for the wave components of zonal wavenumber 4 or less. (f) As in (a), but for only the wave component of zonal wavenumber 4.

3.3. Tropospheric circulation response to the prescribed ozone depletion

a) Response with the midlatitude oceanic frontal zone

For our investigation of the tropospheric westerly response to the prescribed ozone depletion in the stratosphere, we apply 31-day running-mean to [U] in order to remove daily fluctuations that are not related to the seasonal march. This procedure is roughly equivalent to the 90-day low-pass filtering applied in the previous investigations of the troposphere-stratosphere vertical coupling (Baldwin and Dunkerton 1999, 2001).

When the ozone depletion is assigned to the model, a poleward shift of the near-surface PFJ is simulated realistically in the presence of the midlatitude SST front. Figure 3.6a shows a time-height section of the zonal-mean westerly response simulated poleward of PFJ as a latitudinal average between 45°S and 60°S to the stratospheric ozone depletion in the presence of the midlatitude SST front. The ozone depletion results in the intensification of the stratospheric westerlies in spring through summer as observed. After the occurrence of the stratospheric response, the associated tropospheric response emerges in late November through mid-December as the intensification of the westerlies in the presence of the oceanic front (Figure 3.6a); the simulated response is consistent with the observed trends in zonal wind (Figure 3.9a) and geopotential height (Figure 1.5c; Thompson and Solomon 2002), although the simulated response emerges earlier by about a month. This midlatitude tropospheric westerly response in early summer (Figures 3.6a and 3.7a) corresponds well to the observed SAM trend toward its positive polarity (Figure 3.9b), which is manifested in the troposphere as the westerly acceleration poleward of the climatological PFJ axis (blue dashed line in Figures 3.3f and 3.7a; Limpasuvan and Hartmann 2000).

The westerly response is consistent with anomalous westerly acceleration driven by eddy forcing simulated in at the same latitudinal band just before the westerly response emerges in the troposphere (Figure 3.7c). The rate of the eddy-induced acceleration of the zonal-mean background westerly flow is estimated as 7-day running mean of the divergence of the Eliassen-Palm (EP) flux (Andrews et al. 1987) that represents the zonally averaged flux of easterly momentum carried by

atmospheric eddies. When the eddy component is defined as the instantaneous deviation of a given variable from its zonal mean, the meridional distribution of the response of the eddy westerly forcing corresponds well to that of the westerlies wind speed not only in the stratosphere but also in the troposphere (Figure 3.7c). The tropospheric eddy westerly acceleration in this period (on 11th through 16th November) is associated mainly with the reduction of the upward EP flux (Figures 3.7c and Figures 3.8a), to which modulated vertical structure of eddies (specifically, the weakened westward tilts of ridges and troughs) as a response to the ozone depletion mainly contributes while the decrease in eddy amplitude makes only a secondary contribution (Figure 3.8c). The simulated weakening of poleward eddy heat flux (equivalently, the upward EP flux) associated with modulations in vertical structure of eddies is in good agreement with the observed response in the midlatitude SH to the ozone depletion (Figures 3.9c-e), although the latter is more confined into the lower troposphere with a stronger response in the meridional component of the EP flux. Although the simulated westerly response in the presence of SST front (Figure 3.7a) shows somewhat different spatial structure from the observed westerly trend averaged throughout its mature period in January (Figure 3.9b), the model response is more similar to the observed change in its developing stage (late December through early January) with respect to its vertically coupled structure between the troposphere and stratosphere and a slight meridional tilting (Figure 3.9c).

Time-evolution of the response of the upper-tropospheric eddy westerly forcing is consistent with that of the westerlies (Figures 3.7a-b), which confirms the importance of tropospheric eddies for the westerly response. The strong response in the eddy westerly acceleration occurs around 11th November (Figure 3.10b), triggering the significant westerly response that matures in late November (Figure 3.10a). As mentioned earlier (Figure 3.8c), the eddy acceleration is due mainly to the weakened upward EP flux in the mid-troposphere (Figures 3.7c and 3.10c-e) contributed to by both synoptic-scale and planetary waves comparably (Figures 3.10f-g). It should be noted that planetary waves are climatologically intensified in the presence of SST front (Figure 3.5b). As discussed in section 2.3f and by Shiogama et al. (2005), their anomalous activity may also contribute to the phase shift of SAM to its positive polarity, although the in-depth investigation of this mechanism is beyond the scope of this study.

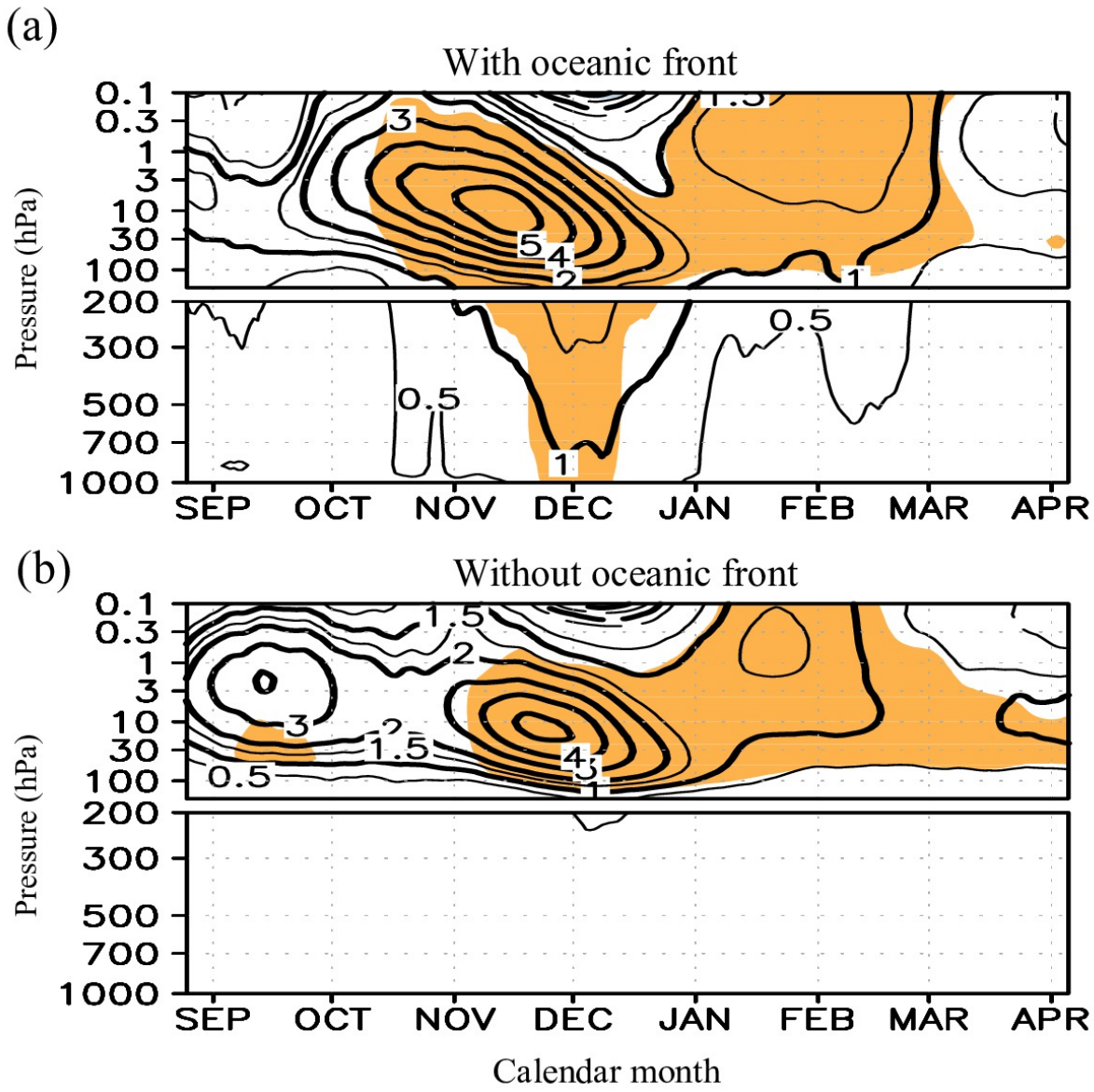

Figure 3.6. Time-height sections showing the seasonality of the 31-day running-mean zonally-averaged westerly response to the prescribed ozone depletion (m s^{-1}; contoured) averaged between 45°S and 60°S for the experiments (a) with and (b) without the oceanic front. Shading indicates the response exceeding the 95% confidence level based on the Student's t-test.

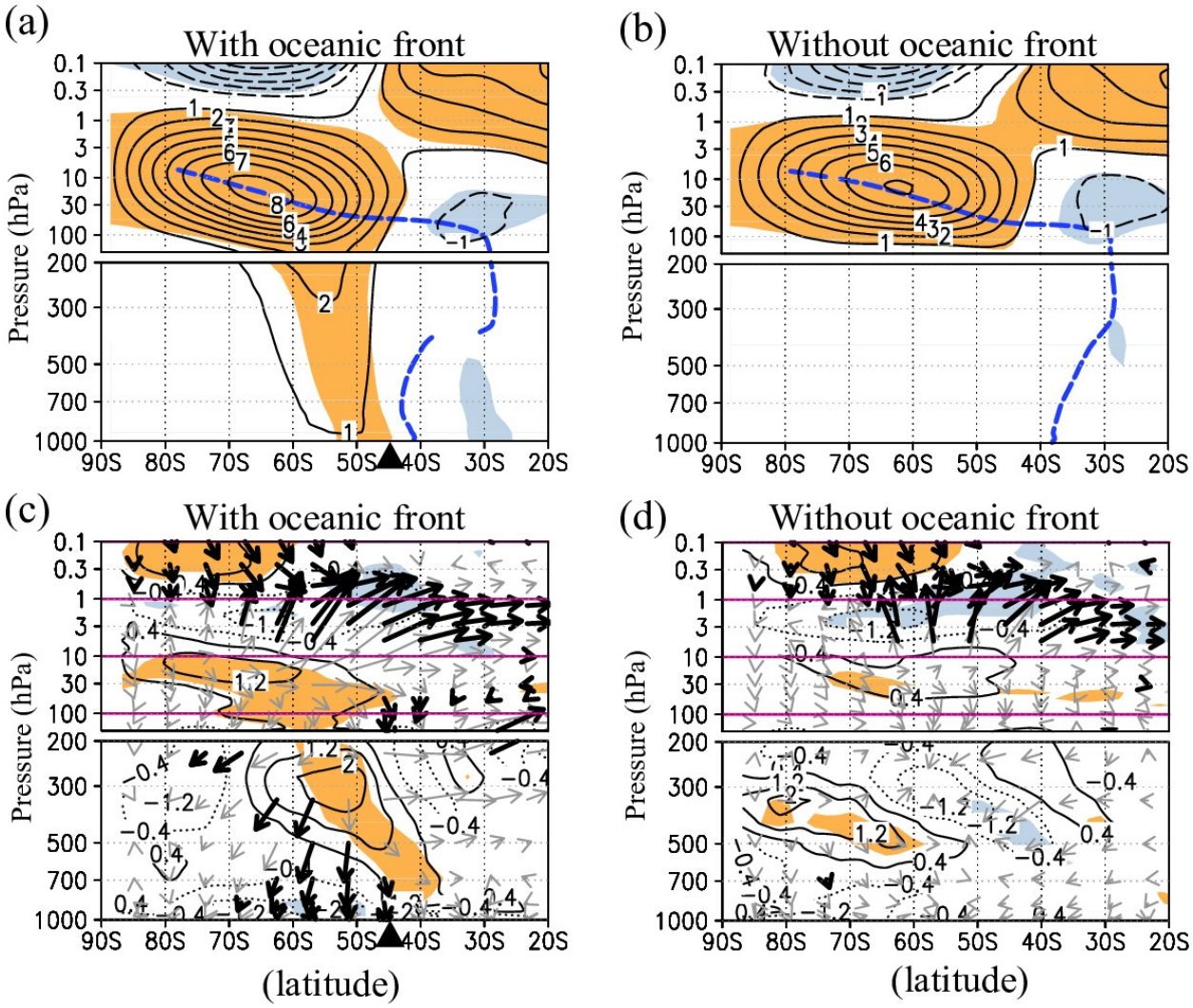

Figure 3.7. Meridional sections showing the structure of the early-summer atmospheric response simulated to the prescribed ozone depletion. (a)-(b). Zonal-mean zonal wind response in the 31-day average from 16th November to 16th December (contoured for every 1 m s^{-1}; sold and dashed lines for westerly and easterly responses, respectively) for experiments (a) with and (b) without the oceanic front. Shading indicates the response exceeding the 95% confidence level based on the Student's t-test. Blue-dashed lines denote the climatological axes of the westerlies. Black triangle indicates the latitude of the oceanic front. (c)-(d). As in (a)-(b), respectively, but for anomalous EP flux and westerly acceleration estimated by its divergence (m s^{-1}/day) as the 7-day average from 10th to 16th November. Thick black arrows mark the EP-flux response that exceeds the 95% confidence level.

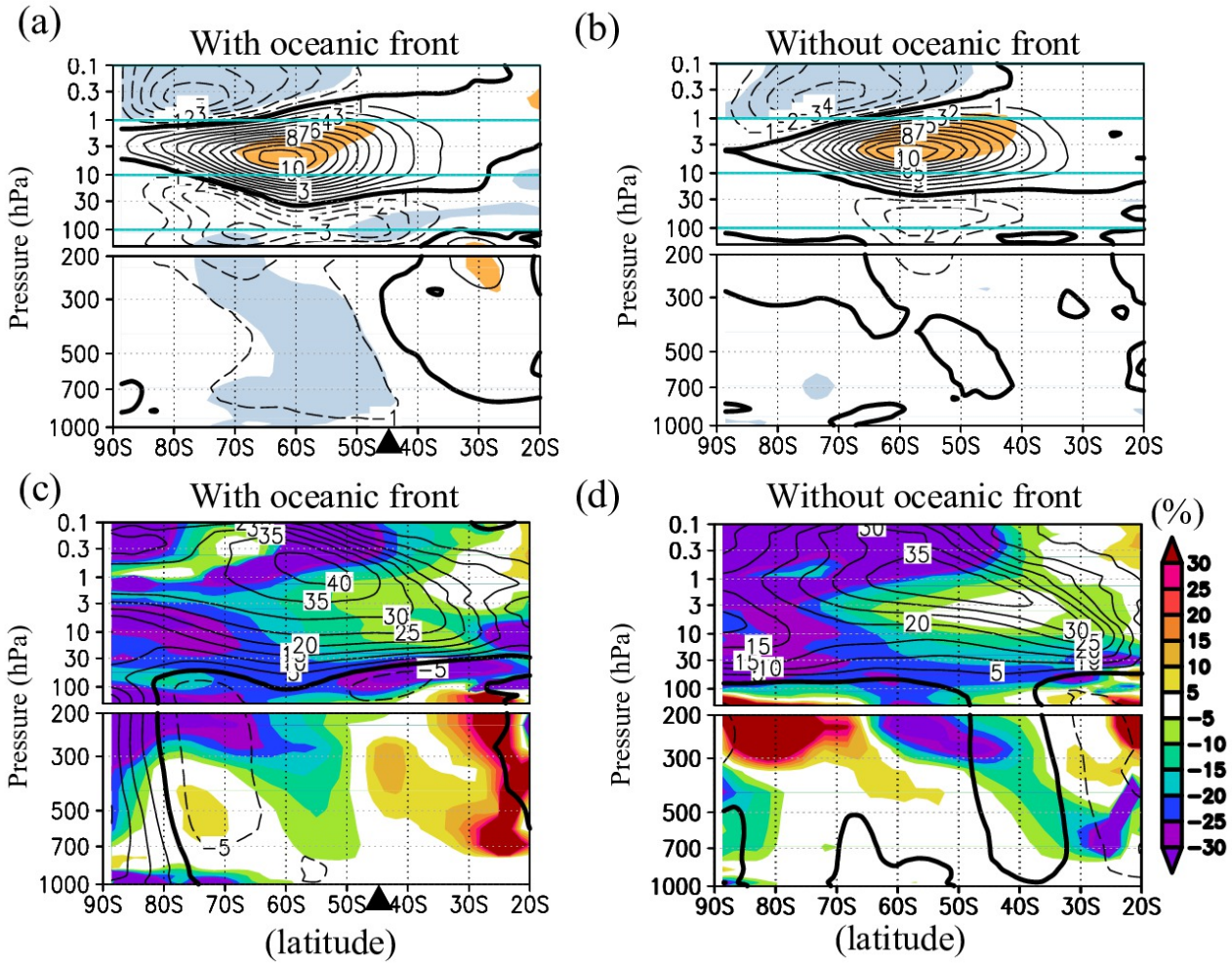

Figure 3.8. (a)-(b) As in Figure 3.7a-b, respectively, but for the response of poleward heat flux associated with eddies defined as instantaneous deviations from the zonal-mean state. Contour interval is 1 (K•m s^{-1}). Shading indicates the response exceeding the 90% confidence level based on the Student's t-test. Black triangle indicates the latitude of the oceanic front. (c)-(d). As in (a)-(b), respectively, but for the fractional change in the standard deviation of eddy meridional winds (contoured for every 5%) and the correlation coefficients between eddy meridional wind and temperature fluctuations (%, shaded).

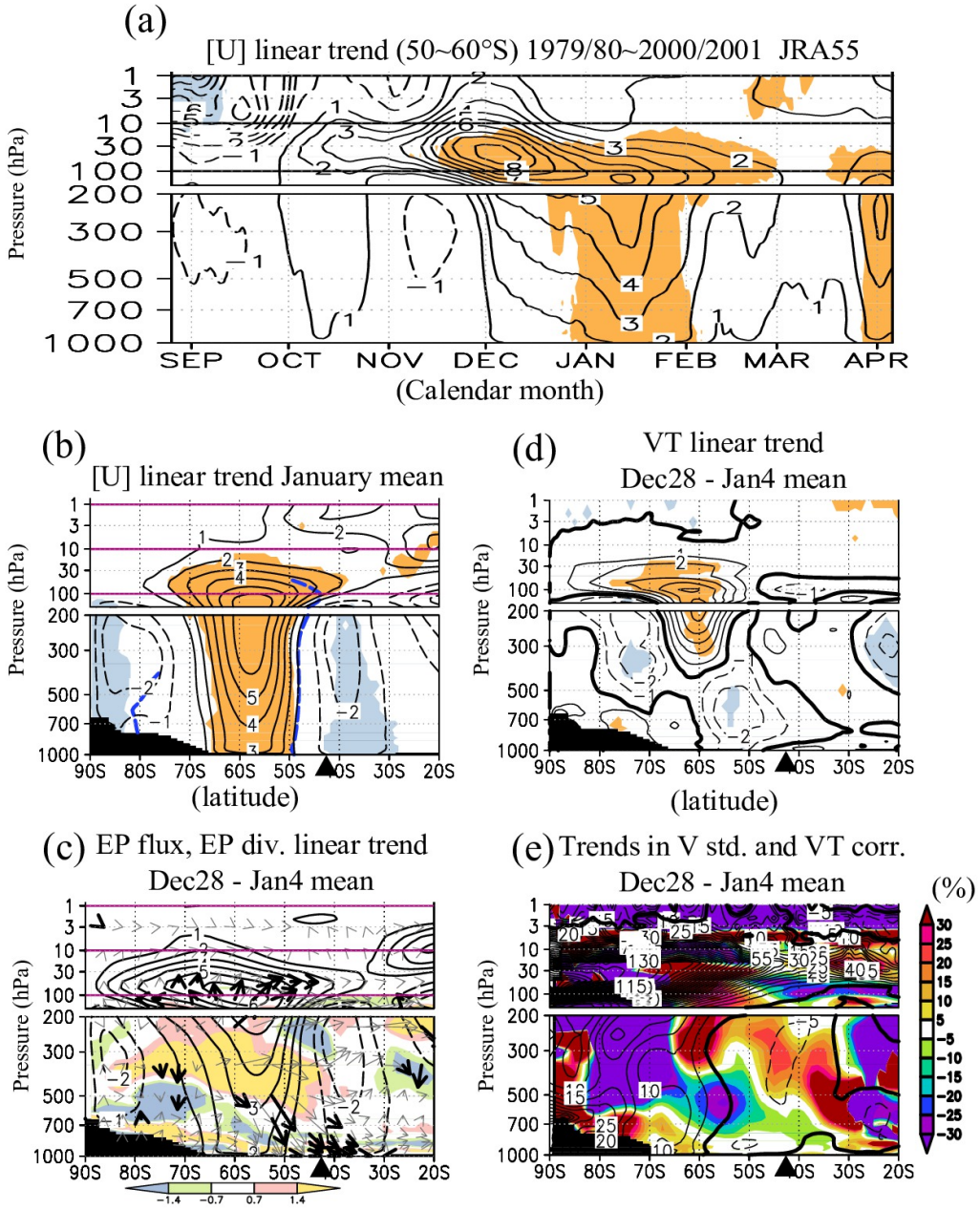

Figure 3.9. (a) Time-height section showing the seasonality of the zonally averaged 31-day running-mean 21-year linear trend of zonal-mean westerlies (m s^{-1}; contoured) averaged between 50°S and 60°S from 1979/80 to 2000/2001, on the basis of the JRA-55 reanalysis data. Shading indicates the trends exceeding the 90% confidence level based on the Mann-Kendall test. (b) As in (a), but for meridional section showing the linear trend in zonal mean westerlies averaged from 1st to 31st January (contoured for every 1 m s^{-1}; sold and dashed lines for anomalous westerlies and easterlies, respectively). Blue-dashed lines denote the climatological axes of the westerlies. Black triangle indicates the latitude of the oceanic front. (c) As in (b), but for the linear trend in EP flux (m^2 s^{-2}; vector) and eddy westerly acceleration estimated by the flux divergence (m s^{-1}/day; shading) as the 7-day average from 28th December to 3rd January. Thick black arrows indicate the trends in EP-flux exceeding the 90% confidence level. Contour indicates the westerly trend as the 31-day average from 16th December to 15th January. (d) As in (b), but for the linear trend in poleward heat flux associated with eddies defined as instantaneous deviations from the zonal-mean state. Contour interval is 1 (K•m s^{-1}). (e) As in (d), but for the fractional change in the standard deviation of eddy meridional winds (contoured for every 5%) and the correlation coefficients between eddy meridional wind and temperature fluctuations (%, shaded) estimated by their linear-trends divided by 5-year averages from 1979/80 to 1983/84.

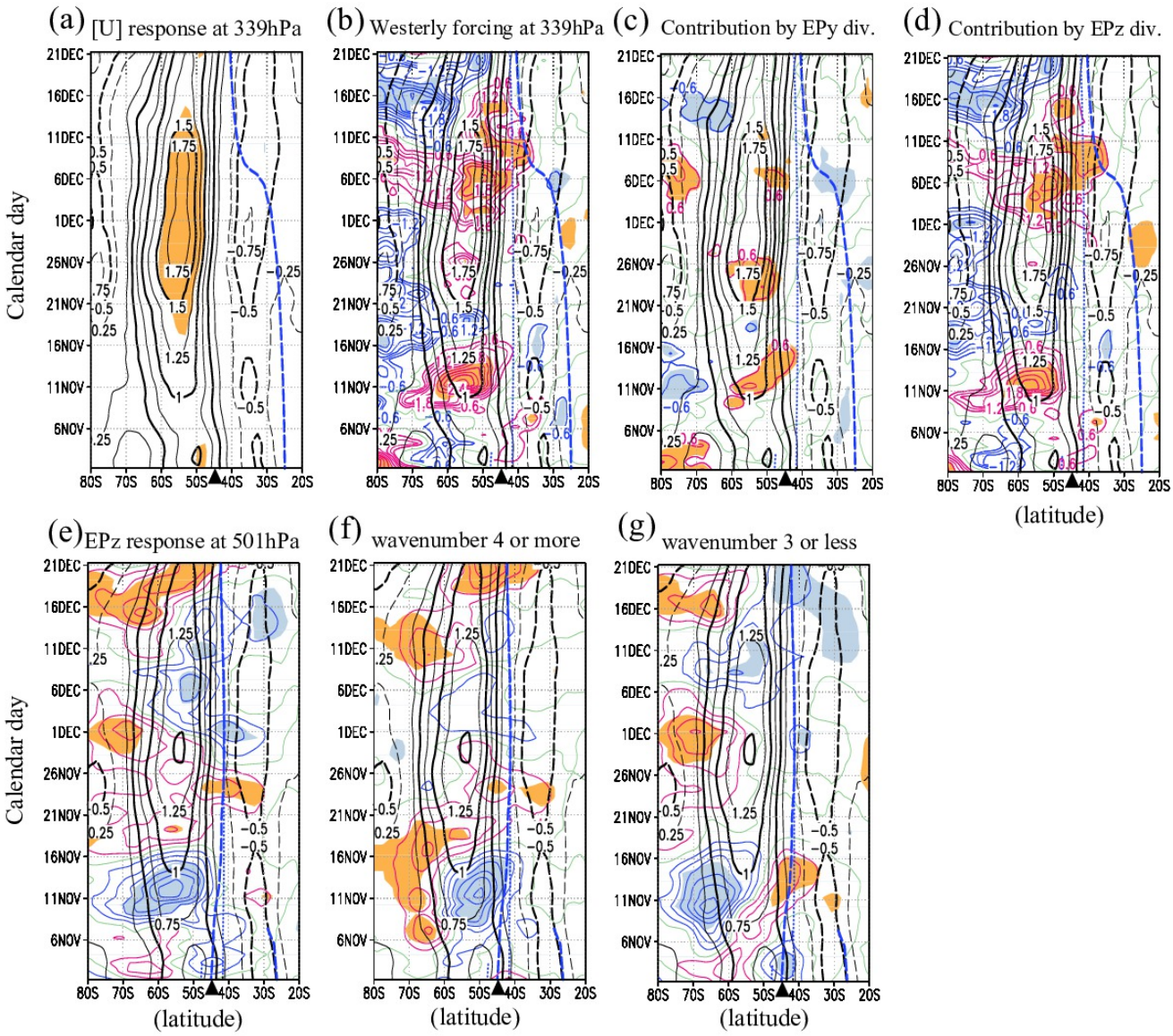

Figure 3.10. Latitude-time sections showing time evolutions of zonally averaged responses of the following variables to the prescribed ozone depletion in the presence of SST front. (a) [U], contoured for every 0.25 (m s^{-1}), and shaded if exceeding the 95% confidence level. (b) As in (a), but for the westerly forcing (m s^{-1}/day; color contours) estimated as the EP flux divergence associated with wave disturbances, superimposed on the [U] response itself (black contours). The disturbances are defined as local deviations from the zonal-mean state. (c) As in (b), but for the contribution to the eddy westerly acceleration (m s^{-1}/day; color contours) from the horizontal component of the EP flux. (d) As in (c), but for the contribution from the vertical component of the EP flux. (e) As in (b), but for the response of the vertical component of the EP flux at 501hPa (colored contours). (f) As in (e), but for the contribution from the disturbances with zonal wavenumber 4 or more. (g) As in (f), but for the contribution from planetary-scale disturbances with zonal wavenumber 3 or less. Shading in (b)-(e) indicates the response in excess of the 90% confidence level. Black triangle indicates the latitude of the oceanic front.

b) Response without the midlatitude oceanic frontal zone

In the absence of midlatitude oceanic front, the assigned ozone depletion results in the intensification of the stratospheric westerlies in spring through summer (Figures 3.6b and 3.7b), which is similar to the response in the presence of SST front (Figures 3.6a and 3.7a). Unlike what is observed and simulated in the presence of SST front, however, the associated westerly response in the troposphere is virtually lacking in the absence of SST front (Figures 3.6b and 3.7b). Nevertheless, the tropospheric PFJ response in connection to the stratosphere is hinted around the beginning of December, which is somewhat similar to the counterpart in the presence of SST front but not statistically significant at all throughout the season. If the latitudinal average of the westerly response is taken over slightly lower latitudes (40°~55°), in corresponding to the equatorward shift of the climatological PFJ axis in the lower troposphere, the tropospheric response to the ozone depletion is still insignificant in the absence of SST front (not shown). Neither the activity of tropospheric eddies nor the eddy-induced westerly acceleration exhibits any coherent significant changes in responding to the ozone depletion (Figures 3.7d and 3.8b), which is consistent with no significant westerly response in the troposphere in the response of SST front (Figure 3.7b).

In the absence of the SST front, the response of westerly wind is very weak even near the tropopause throughout the season (Figure 3.11a). The maximum amplitude of the response is decreased by about 70% and statistically much less significant compared to the counterpart in the presence of SST front (Figure 3.10a). Furthermore, the peak latitude of the westerly response (40°S~50°S) is unrealistically shifted equatorward from its counterpart with the SST front (50°S~60°S). Although some association among the responses in the westerly wind speed and eddy-induced westerly forcing is still found around 1st December (Figure 3.11b), the eddy forcing is much less organized than in the presence of SST front (Figure 3.10b). In this experiment, the significant response in the westerlies found only in a narrow latitudinal bands around 42°S around 11th December and it is confined into the upper troposphere (Figure 3.11c). Meanwhile, eddy easterly forcing found between 60° and 70°S is associated with the anomalous upward EP flux in the mid-troposphere (Figure 3.11c). The corresponding tropospheric easterly response is, however,

very weak and insignificant statistically (Figure 3.11a).

As discussed above, striking contrasts in the strength and peak latitude of the tropospheric westerly response and its association with the change in tropospheric wave activity are found between the AGCM experiments with and without the midlatitude SST front. The contrasts indicate that the midlatitude SST front can be crucially important for the transmission of the ozone-induced westerly trend from the stratosphere down to the surface through the climatological activation of wave disturbances in a near-surface baroclinic zones anchored along the SST front.

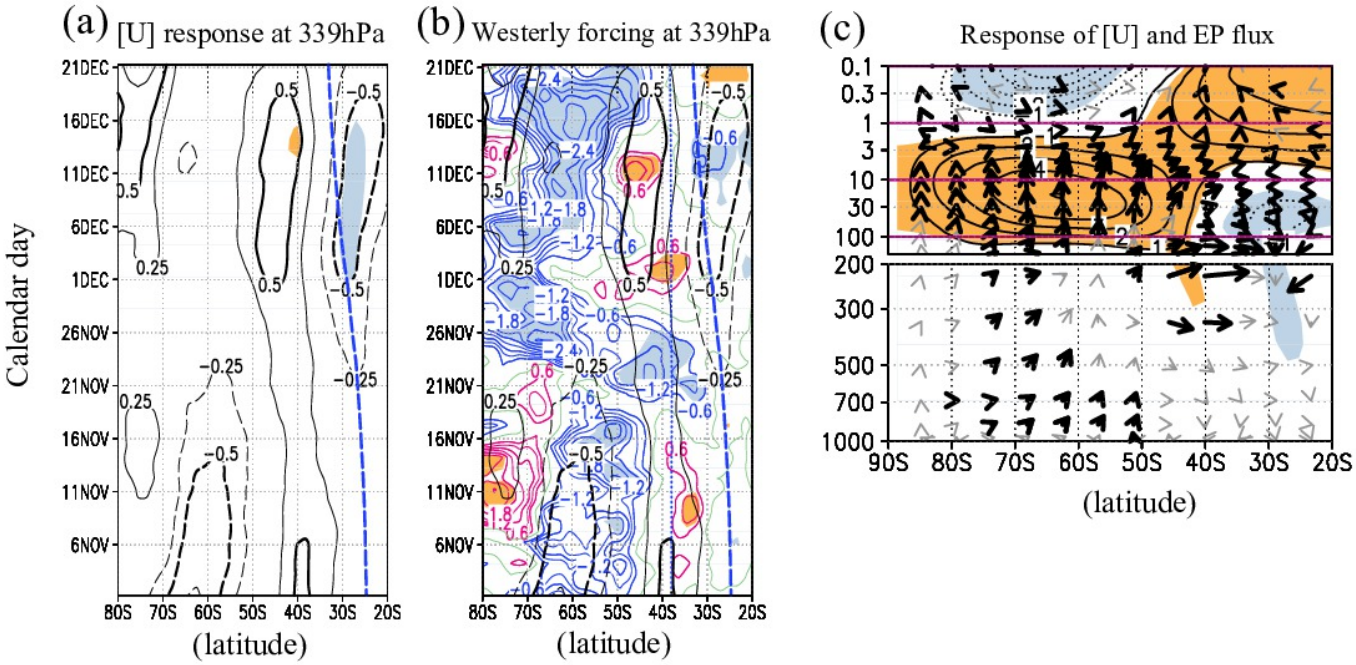

Figure 3.11. (a-b) Same as in Figure 3.10a-b, respectively, but for the experiments without the SST front. (c) Contours are as in Figure 3.7b, but for the response in the 31-day mean [U] averaged from 26th November to 27th December. Shading indicates the response exceeding the 95% confidence level. Vectors are as in Figure 3.7d, but for the 7-day mean EP flux averaged from 8th to 14th December. Black thick vector indicates the flux whose statistical significance exceeds the 90% confidence level.

3.4 Stratosphere-troposphere coupling of natural variability

a) Definition of the self-excited natural variability

The tropospheric SAM observed in connection with the stratospheric year-to-year variability is known to be pronounced from late spring to early summer (Thompson and Wallace 2000; Thompson et al. 2005). Since the observed tropospheric response to the stratospheric ozone depletion is manifested as the vertical coupling of the SAM, the pronounced dependence of the surface westerly response to the frontal SST gradient suggests that the oceanic front may have some significant impacts on the coupling of the SAM with the stratospheric year-to-year variability in that season. To confirm this, the troposphere-stratosphere coupling of the zonally symmetric self-excited natural variability is investigated in comparison of our AGCM experiments with and without the SST front.

To define the leading mode of the stratospheric year-to-year variability, an EOF analysis was applied to 13-hPa zonal-mean westerly profiles between 90°S and 20°S on 15th November in individual years after exposed to 31-day running mean. The particular date corresponds to the timing when the stratospheric westerly response simulated to the ozone depletion is most significant (Figure 3.6a). The contribution of the leading mode to the total variance of westerly variability at 13hPa is 80 (83) % when the oceanic front is present (absent). The meridional structure of the leading mode of the stratospheric year-to-year variability in our experiments is rather insensitive to the ozone profile (Figure 3.12). We therefore combined the outputs from the two experiments with and without the ozone depletion under the same SST profiles, which were used for our EOF analysis. The outcome of the analysis was utilized for constructing Figures 3.14-19.

As another approach to assess the vertical coupling, a similar EOF analysis was applied to 857-hPa zonal-mean westerly profiles within the same latitudinal bands on 1st December, when the tropospheric westerly response to the ozone depletion is most significant (Figure 3.6a). It should be noted that, unlike discussed for winter in Chapter 2, the annular mode extracted in those EOFs for summer exhibits “regime-like” characteristics to a lesser degree even in the presence of SST front.

Figure 3.13 shows plots of probability density of the peak latitude of 921hPa [U] separately for the experiments in the presence and absence of SST front. Regardless of the ozone concentration and presence of SST front, the probability density function based on all the time steps in early summer during a given experiment shows a dominant single peak, around which the westerly jetstream near the surface tends to fluctuate associated with the year-to-year variability (Figures 3.13a-f). The particular signature is in striking contrast with the corresponding diagram (Figure 3.13g) showing its counterpart for late winter (September) in the presence of SST front, which is characterized by distinct dual peaks that suggest regime-like characteristics of the variability. It is noteworthy that the [U] maximum in the positive phase in the presence of SST front tends to be located in higher latitudes when the ozone concentration is lower (Figures 3.13c and 3.13e), which is consistent with the westerly response to the ozone depletion (Figure 3.7a). In the absence of SST front, by contrast, the probability density is virtually identical between the high and low ozone concentrations (Figures 3.13d and 3.13f). In addition, the corresponding probability density distribution for September in the absence of SST front also shows a distinct climatological single peak (Figure 3.13h), in striking contrast to the regime-like behavior simulated in the presence of SST front (Figure 3.13g). These results confirm the importance of the midlatitude SST front for the regime-like behavior of SAM that is realized only in the winter season.

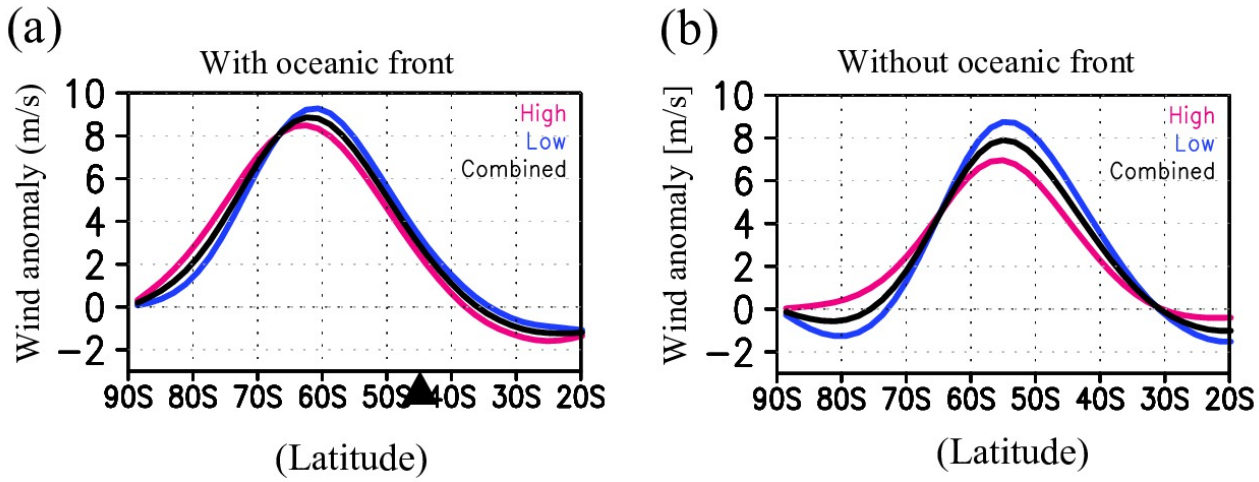

Figure 3.12. Latitudinal profiles showing the 31day-running mean anomalies of 13hPa zonal wind [U] on 15th November, in association with the dominant mode of stratospheric year-to-year variability. Red (blue) line indicates the profile for the experiments where the prescribed ozone concentration is higher (lower). Black color indicates the profile for the combined time series over both the high- and low-ozone experiments (a) with and (b) without the oceanic front.

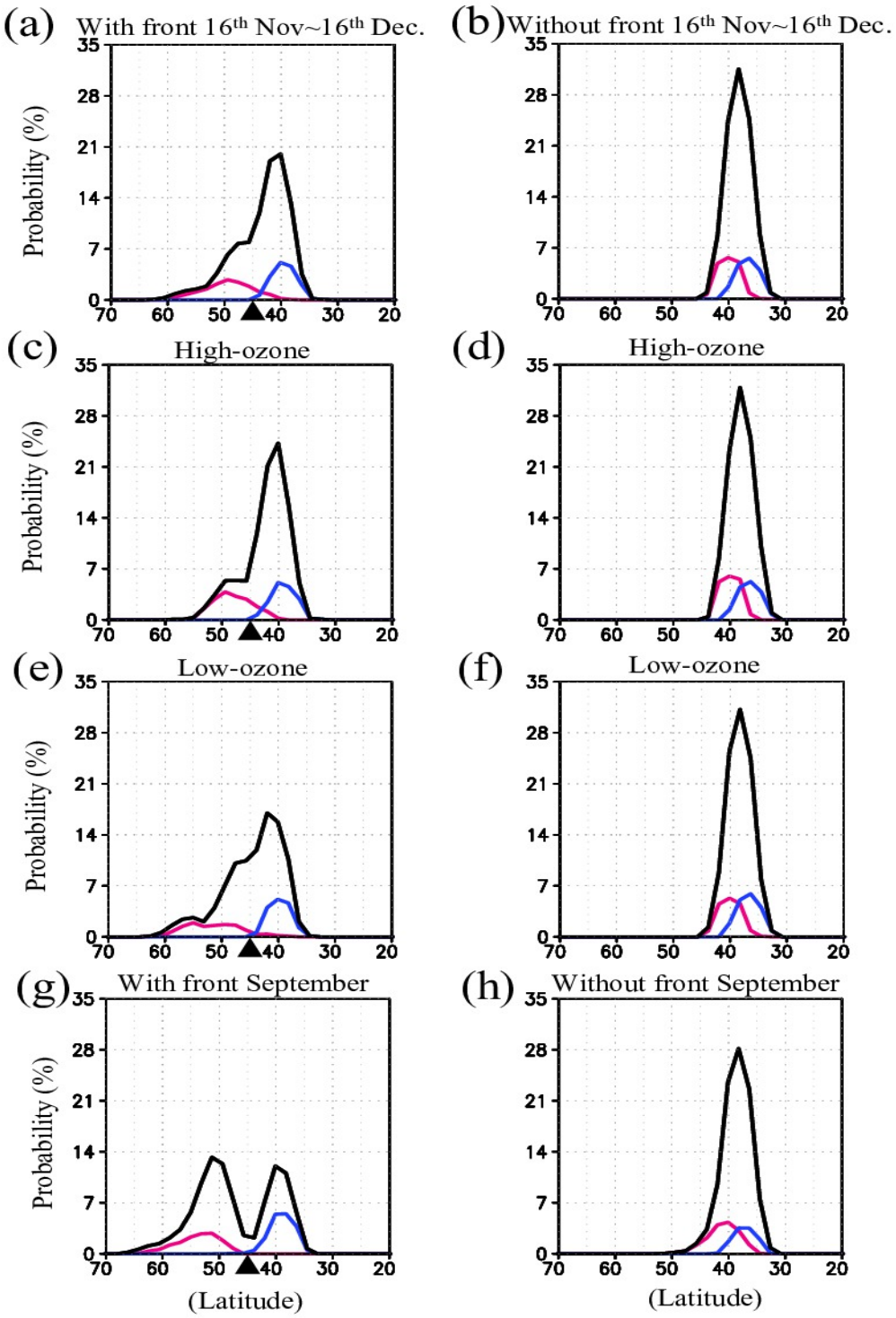

Figure 3.13. (a,c,e,g) Probability density of the peak latitude of 921hPa [U] based on all the daily time steps (black line) during a given experiment in the presence of SST front. Contributions only from the periods of strong positive and negative events are superimposed with red and blue lines, respectively. Those events are defined as the periods when the absolute value of the principal component time series exceeds a unit standard deviation. Black triangle indicates the latitude of the oceanic front. (a) Based on daily [U] profiles from 16th November to 16th December simulated in the high- and low-ozone experiments combined. (c) As in (a), but sampled only from the high-ozone experiment. (e) As in (b), but sampled only from the low-ozone experiment. (g) As in (a), but based on the period from 1st September to 30th September. (b,d,f,h) As in (a,c,e,g) respectively, but for the experiments in the absence of SST front.

b) Seasonality of the vertical coupling of natural variability and ozone-induced response in the presence of oceanic frontal zone

Figure 3.14a shows a time-height section of zonal-mean westerly anomalies averaged poleward of PFJ (45~60°S) that are correlated with the dominant year-to-year natural variability of the stratospheric polar vortex in the presence of SST front. Significant westerly anomalies are simulated in the troposphere from late spring to midsummer in the presence of SST front. Though its duration is slightly longer, this tropospheric signal (Figure 3.14a) shows a good correspondence with the one associated with the ozone-induced tropospheric climate change (Figure 3.6a). The similarity is consistent with the observations discussed in previous studies (Thompson et al. 2011; Sun et al. 2014). In fact, the meridional structure of the tropospheric westerly anomalies associated with the stratospheric natural variability is similar to that of the westerly response to the stratospheric ozone depletion (Figure 3.16a).

The vertical coupling of the year-to year natural variability is also evident even when the year-to-year [U] variability in the lower troposphere is taken as the reference time series (Figures 3.15a and 3.16c). As evident in Figure 3.16c, the meridional structure of the tropospheric year-to-year natural variability is in good correspondence with the tropospheric annular mode. In fact, the tropospheric annular mode is significantly coupled with the stratospheric westerlies (Figure 3.16c), consistently with the observations (Thompson and Wallace 2000). The latitude and height of the core of the stratospheric westerly anomalous (Figure 3.16c) also show a good correspondence with their counterpart associated with the stratospheric year-to-year variability (Figure 3.16a). Furthermore, the lower-tropospheric westerly anomalies in midlatitudes (45~60°) associated with the summertime annular mode are in significant positive correlation with the stratospheric westerly anomalies in late spring (Figure 3.15a).

As shown in Figure 3.17a, time-evolution of eddy-induced anomalous eddy westerly forcing in the upper troposphere associated with the stratospheric year-to-year variability is consistent with the evolution of upper-tropospheric westerly anomalies. As in the case of the response to the ozone depletion (Figure 3.10b), anomalous westerly acceleration by eddy-induced forcing diagnosed

through the divergence of the anomalous EP flux first emerges around 50°S around November 9th , to which the vertical component of the anomalous EP flux contributes more than its horizontal component (Figures 3.17b-c). Though not statistically significant, the weakening of the upward EP flux (i.e., its downward anomaly) in the mid-troposphere is hinted (Figure 3.17d), which is consistent with the response to the ozone depletion (Figure 3.10e). In contrast to its prominent response to the ozone depletion, virtually no contribution to this anomalous EP flux arises from synoptic-scale waves (Figure 3.17e), while the main contribution arises from planetary waves (Figure 3.17f). On the other hand, Figure 3.17a indicates that eddy westerly acceleration contributes positively to the maturing of the tropospheric westerly anomalies around 60°S in late November through early December. At this stage, the meridional and vertical components of the anomalous EP flux contribute comparably to the eddy forcing (Figures 3.17b-c), and most of the eddy forcing appears to arise from synoptic-scale eddies (Figures 3.17e-f).

The dynamics involved in the tropospheric westerly response to the stratospheric ozone depletion via vertical coupling of the annular mode is still highly controversial (e.g. Thompson et al. 2011; Garfinkel et al. 2013). Our results in the presence of the midlatitude SST front nonetheless confirms that the importance of troposphere-stratosphere coupling of annular variability in the generation of the tropospheric westerly response to the stratospheric ozone depletion, to which changes in the tropospheric wave activity contributes as induced by the stratospheric annular mode in spring. The vertical coupling of the year-to-year variability is robust against the shift of the reference date of the stratospheric variability to either of 1st November or 1st December (Figure 3.18a,c) in the presence of SST front.

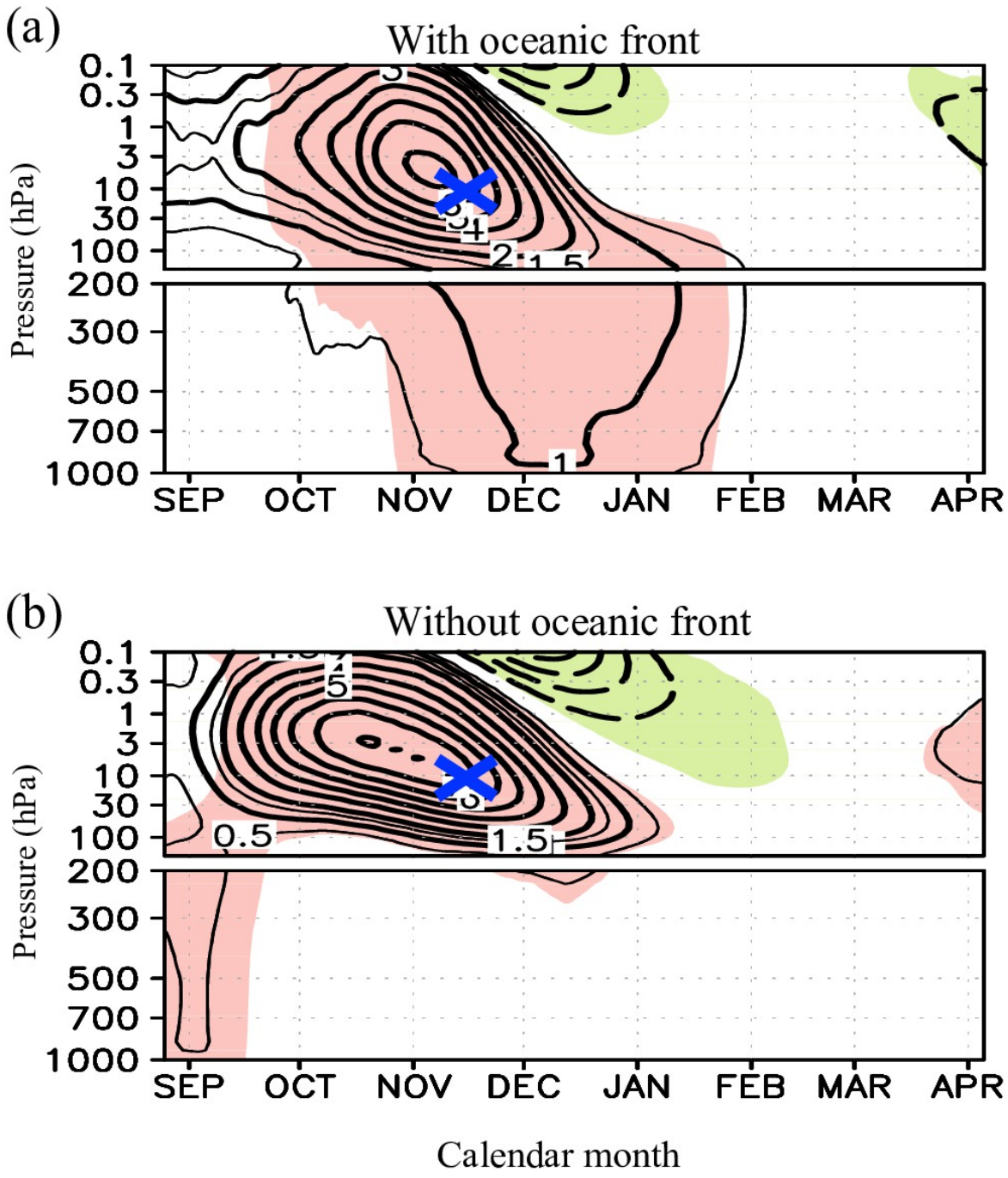

Figure 3.14. Time-height sections showing the seasonality of the 31-day running-mean westerly anomalies associated with the stratospheric year-to-year variability, regressed linearly on its PC1 time series based on 13hPa [U] variability (see text for details) in experiments (a) with the oceanic front and (b) without it. The reference pressure level (13hPa) and reference date (15th November) for the EOF analysis are marked by a cross in each of the panels. Shading indicates anomalies whose statistical significance exceeds the 95% confidence level based on the correlation.

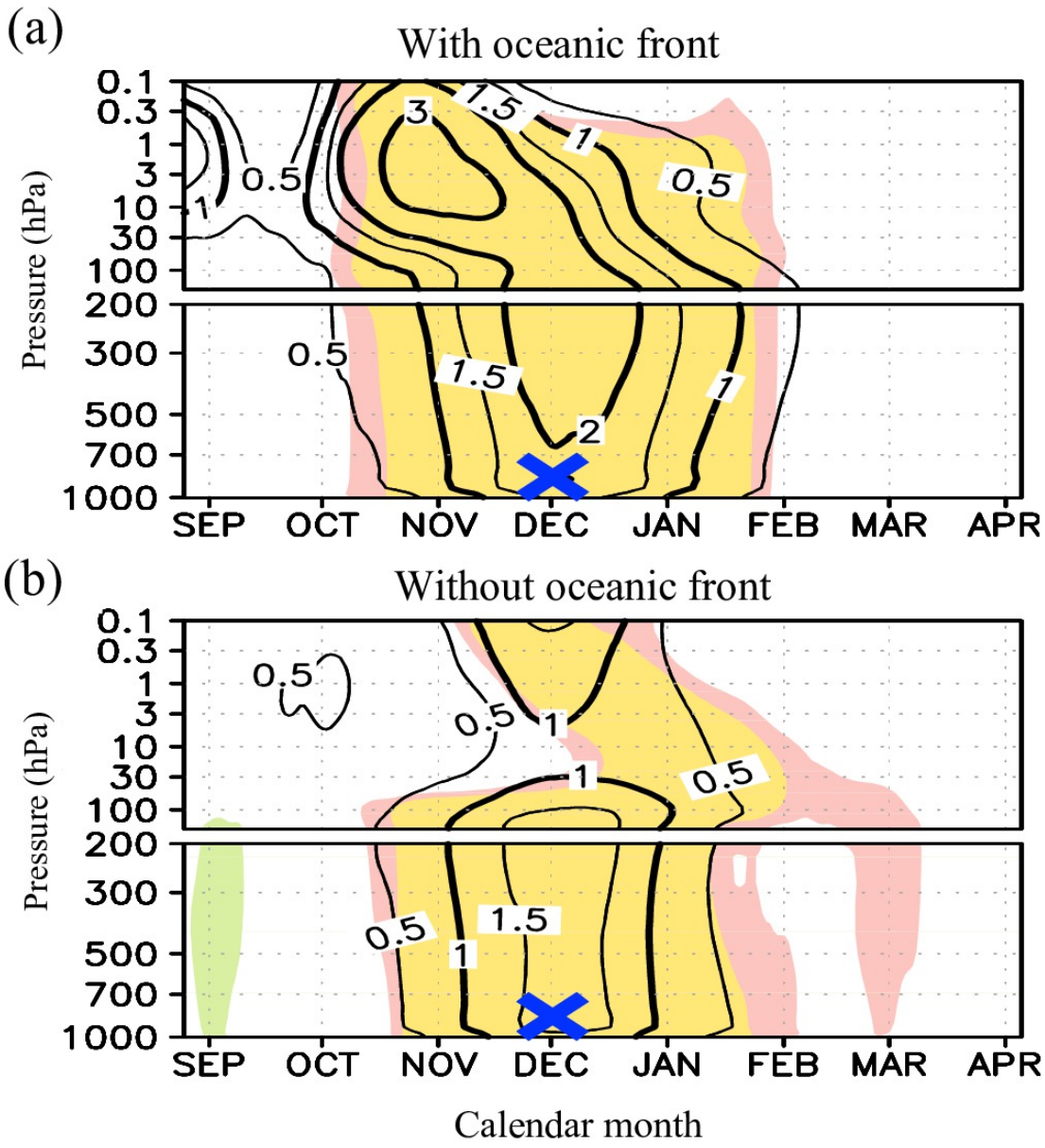

Figure 3.15. As in Figures 3.14, but for the reference pressure level at 857hPa and reference date of December 1st. Statistically significance exceeding the 95 (99)% confidence level based on the correlation is colored pink (yellow) for westerly anomalies and green (blue) for easterly anomalies.

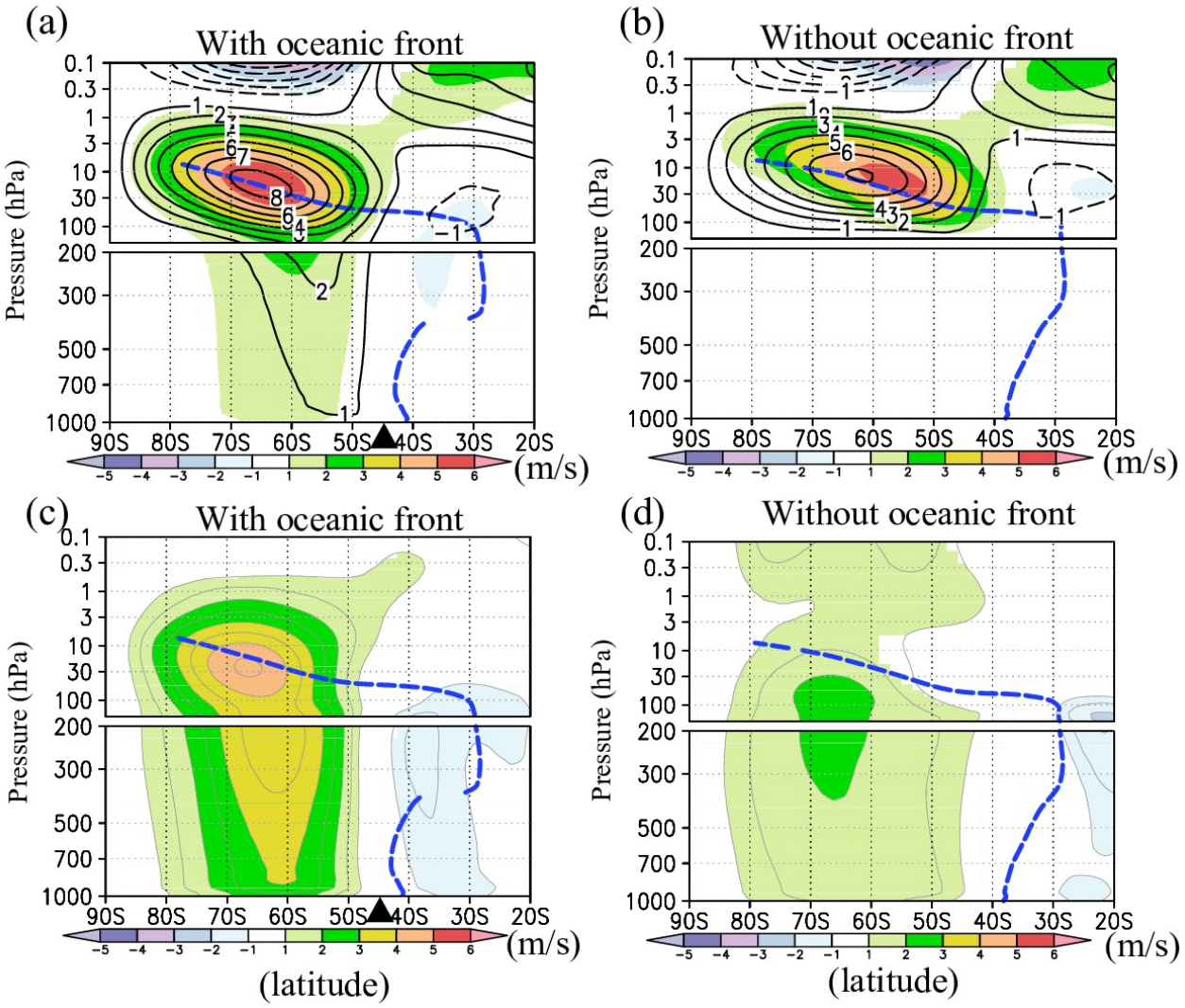

Figure 3.16. Meridional sections showing the westerly responses to the ozone depletion and anomalous westerlies associated with the year-to-year SAM variability. (a)-(b) Simulated ozone-induced westerly change (contoured as in Figure 3.7a), superimposed on the zonal-mean westerlies (color shaded) associated with the stratospheric year-to-year SAM variability, both averaged over 31 days between 16th November and 16th December in experiments (a) with and (b) without the midlatitude oceanic front. The shaded anomalies, obtained by regressing westerly anomalies linearly on the PC1 time series defined at 13hPa on 15th November, correspond to the year-to-year anomalies for the PC1 value of a unit standard deviation. Only the anomalies that are significant at the 95% confidence level are shaded. Dashed lines denote the climatological axes of the westerlies. (c)-(d). Tropospheric SAM signature as estimated by regressing the zonal-mean westerlies on PC1 time series for the 857hPa zonal-mean wind anomalies on 1st December (shading), both averaged over 31 days between 16th November and 16th December simulated in experiments (c) with and (d) without the oceanic front. The signature is also indicated by gray contours with the intervals of 0.5 (m s^{-1}).

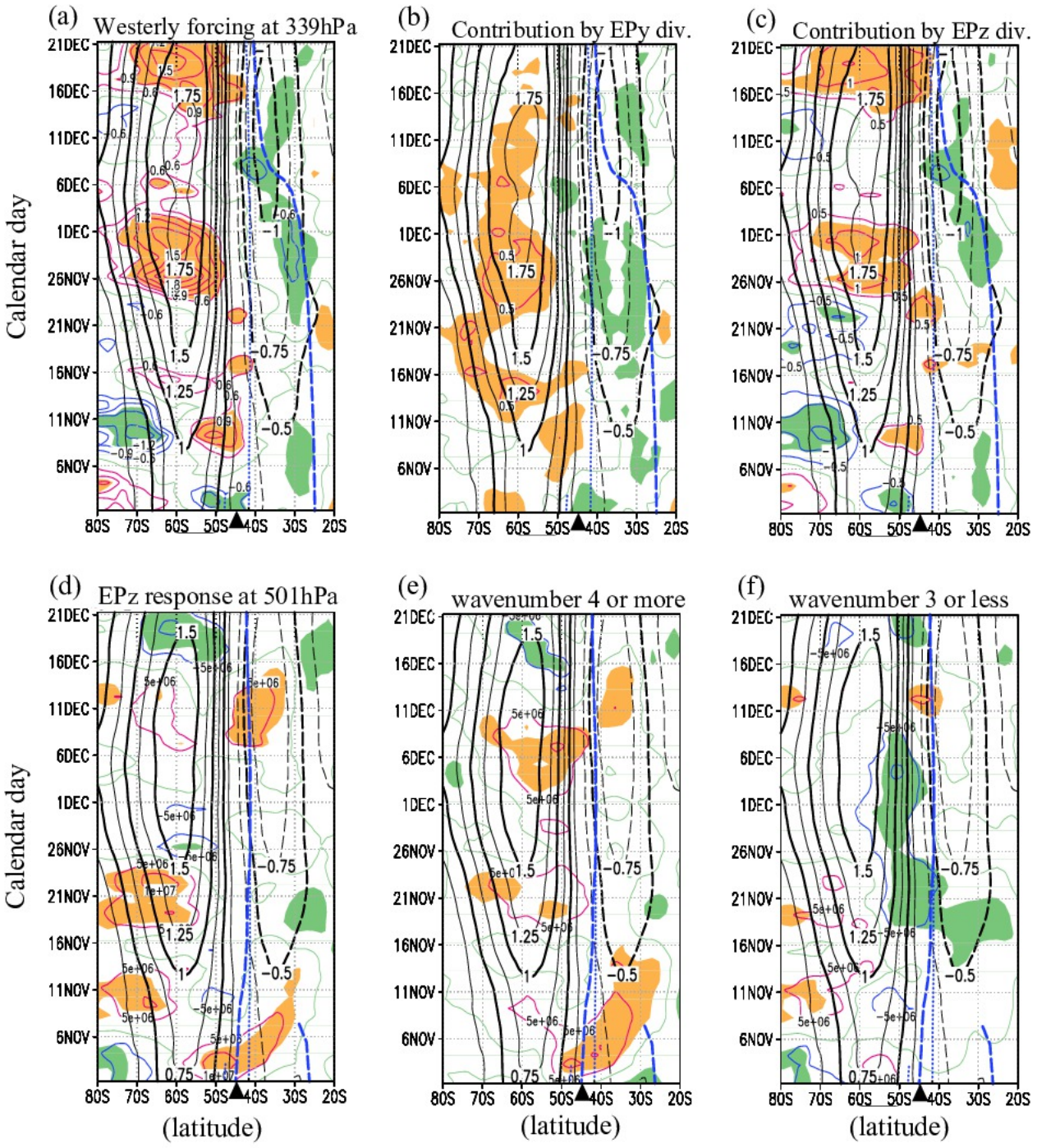

Figure 3.17. (a) Latitude-time section showing time evolutions of 339hPa anomalies in [U] (m $s^{-1;}$ black contours) and eddy westerly forcing (m s^{-1}/day; colored contours) as estimated as the anomalous EP flux divergence, both associated with the stratospheric year-to-year variability in the presence of SST front (black triangle). Shading is applied where the significance of the eddy forcing exceeds the 90% confidence level. Blue dashed lines denote the climatological westerly [U] axes at 339hPa. (b-c) As in (a), but for the anomalous eddy forcing associated only with the (b) horizontal and (c) vertical components of the EP flux. (d) As in (b), but for the vertical component of the anomalous EP flux at 501hPa (colored contours). (e-f) As in (d), but for the vertical component of the anomalous EP flux associated with disturbances only with (e) zonal wavenumber 4 or more and (f) zonal wavenumber 3 or less.

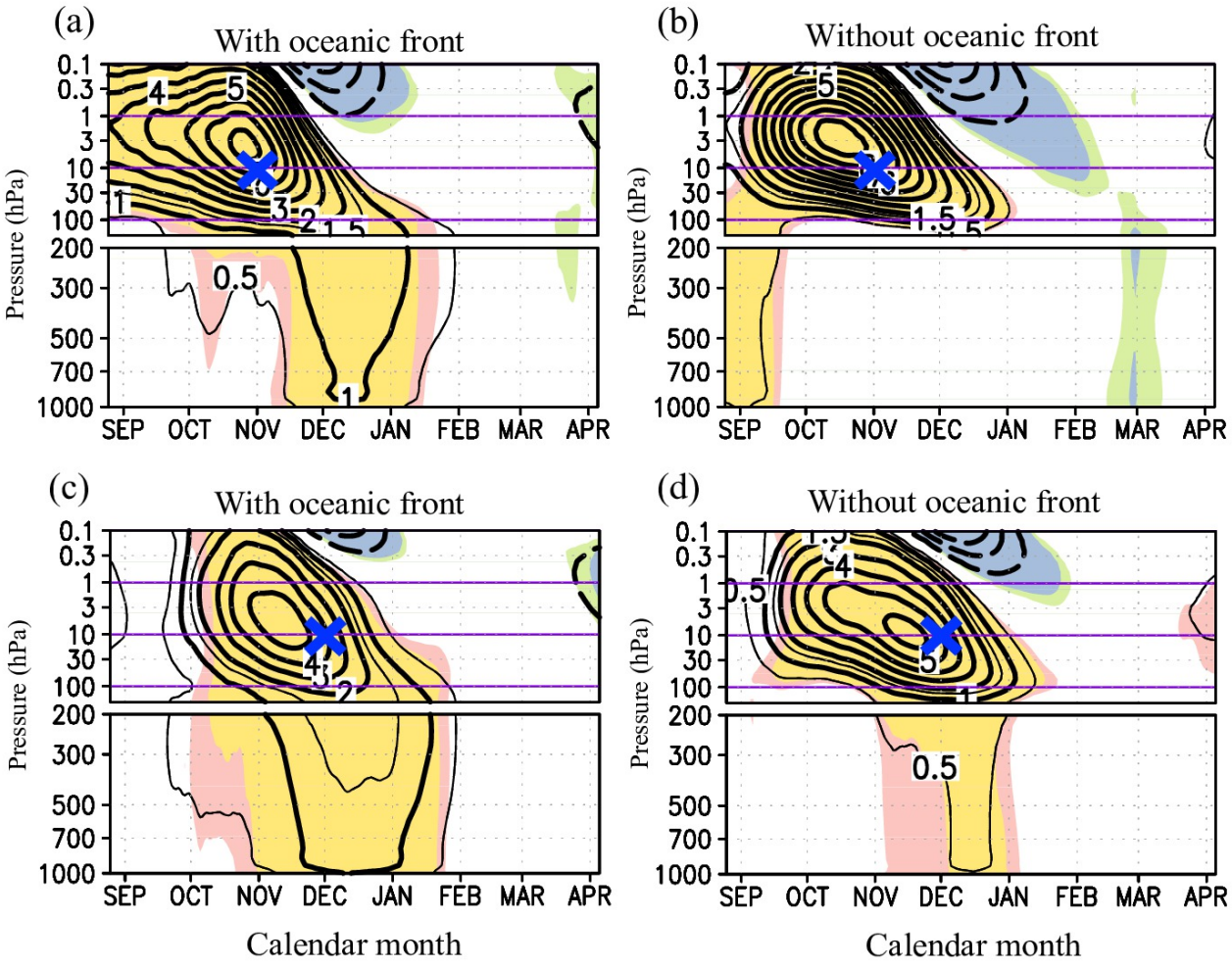

Figure 3.18. Same as in Figures 3.14 but for different reference dates for the stratospheric anomalies. (a)-(b). 1st November. (c)-(d). 1st December. Statistically significance exceeding the 95 (99)% confidence level based on correlation is colored pink (yellow) for westerly anomalies and green (blue) for easterly anomalies.

c) Vertical coupling without the midlatitude oceanic frontal zone

In the absence of midlatitude oceanic front, tropospheric year-to-year variability around the period of the maximum ozone depletion is not significant statistically (Figure 3.14b), which is consistent with the absence of the tropospheric westerly response to the ozone depletion (Figures 3.6b). Meridional structures of zonal wind anomalies associated with the stratospheric year-to-year variability and its response to the ozone depletion are mutually very similar, and both the anomalies and the response are confined in the stratosphere (Figure 3.16b). Nevertheless, time evolution of tropospheric westerly anomalies associated with the stratospheric year-to-year variability in the absence of SST front (black lines in Figure 3.19a) shows westerly anomalies in early through mid-November, which are much weaker and displaced equatorward by as much as 15° in latitude than the counterpart in the presence of SST front (Figure 3.17a). The associated eddy feedback forcing (Figure 3.19b-c) is, however, much less organized than their counterpart in the presence of SST front (Figure 3.17b-c), which is consistent with the weaker westerly anomalies by about 70% (Figures 3.17a and 3.19a). As pointed out by the previous studies (Nakamura et al. 2008; Sampe et al. 2013), the tropospheric annular mode signature is severely distorted in the absence of SST front (Figure 3.16d), which may affect its vertical coupling with the stratospheric variability and thereby the tropospheric response to the stratospheric ozone depletion.

It should be noted that changing the reference date for the stratospheric variability to 1st November does not qualitatively affect the results (Figure 3.18b). If the reference date is shifted to 1st December, however, significant tropospheric anomalies emerge even in the absence of the oceanic front (Figure 3.18d). Still, their amplitude is considerably smaller, reaching only half of that in the experiments with the SST front (compare Figures 3.18c and 3.18d). In fact, the early-summer tropospheric annular mode signature is not significantly coupled with the late-spring stratospheric variability in the absence of SST front (Figure 3.16d).

The above results indicate that the midlatitude oceanic front also plays a crucial role in triggering the downward coupling of the self-excited variability of the stratospheric polar vortex with the summertime tropospheric annular variability, by strengthening the eddy-driven westerlies in subpolar and mid-latitudes throughout the depth of the troposphere (Figures 3.3a and 3.3h; Nakamura et al. 2008; Sampe et al. 2013; Ogawa et al. 2012).

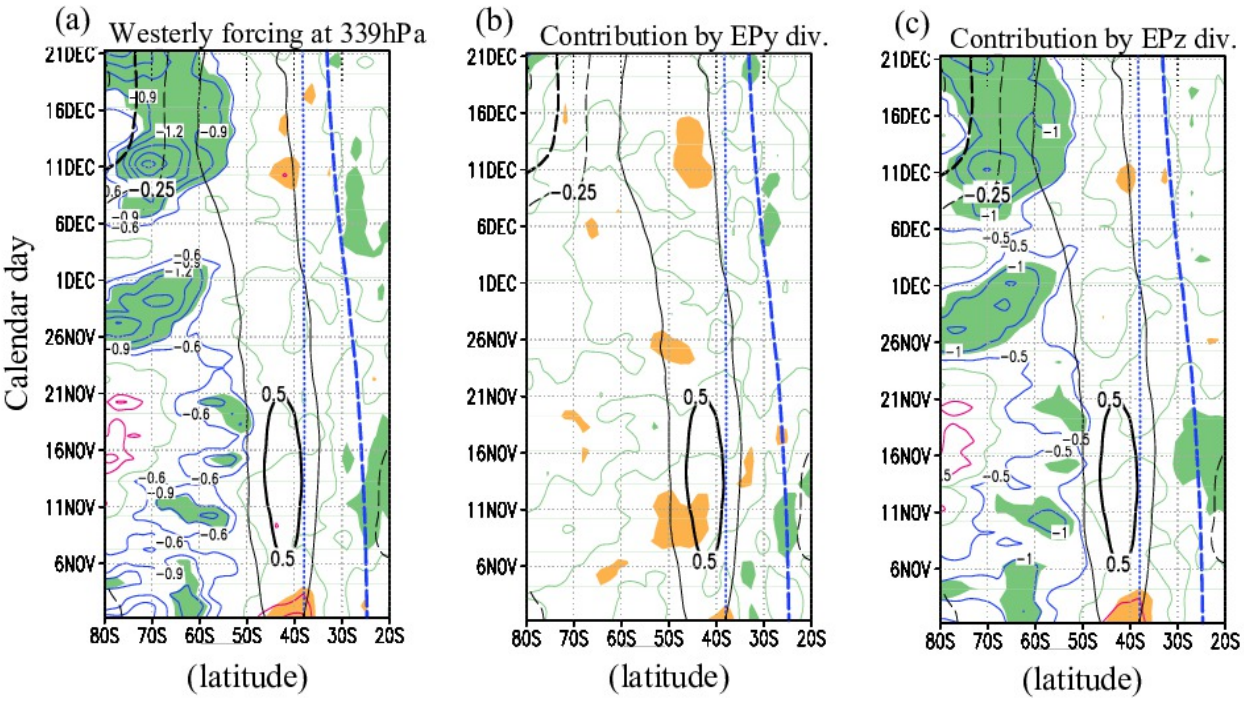

Figure 3.19. Same as in Figures 3.17a-c but for the experiments without SST front.

Chapter 4. Discussions and Conclusions

4.1. Importance of oceanic frontal zones for the wintertime annular variability

Since the recognition of the observed association among midlatitude oceanic front zones, stormtracks and PFJs in the climatological-mean state (Nakamura and Shimpo 2004; Nakamura et al. 2004), impacts of midlatitude oceanic frontal zones on the tropospheric general circulation have been investigated through aqua-planet AGCM experiments, including idealized experiments under the "aqua-planet" setting (Nakamura et al. 2008; Sampe et al. 2010; Ogawa et al. 2012). These studies demonstrated that a midlatitude oceanic frontal zones act to anchor stormtracks and thereby eddy-driven PFJs in the climatological-mean state through efficient restoration of surface baroclinicity by cross-frontal contrasts of a turbulent sensible heat flux. Recently, Sampe et al. (2013) showed that the removal of frontal SST gradient in their aqua-planet experiment impairs both amplitude and meridional structure of the annular mode especially in winter. The investigation in Chapter 2 is thus aimed to provide a comprehensive picture of how an oceanic frontal zone can influence the characteristics of the wintertime annular mode through aqua-planet AGCM experiments in which the latitude of the front is changed systematically. Through this well-thought-out set of aqua-planet experiments, the present study is successful in offering a comprehensive and in-depth view on the potential importance of midlatitude oceanic frontal zones for the wintertime annular mode.

First, the meridional structure of zonally symmetric low-frequency variability of the wintertime PFJ is found to exhibit strong sensitivity to the latitude of frontal SST gradient. In fact, the sensitivity is even stronger than those found for the climatological-mean state (Figure 2.2; Ogawa et al. 2012). The low-frequency variability is most active slightly poleward of the SST front, which tends to be in the vicinity of the axis of the near-surface westerlies in the climatological-mean state (Figure 2.3). Further investigations of the zonally symmetric variability were conducted through an EOF analysis to anomalous near-surface westerlies simulated in

individual experiments with a zonally symmetric oceanic frontal zone whose latitude varies from one experiment to another. In the presence of an extratropical SST front, the first EOF tends to reproduce realistic annular mode signature, which represents the latitudinal variability of PFJ (Lorentz and Hartmann 2001).

The most significant finding from the experiments is a regime-like behavior of the wintertime annular mode. The positive phase of the model annular mode represents a situation where the distinct PFJ axis forms with a lower-tropospheric stormtrack slightly poleward of the oceanic frontal zone, thus showing strong sensitivity to the latitude of the front (Figures 2.5a-b). In the negative phase, by contrast, the PFJ and storm track are situated around 38° regardless of the latitude of an oceanic frontal zone (Figures 2.6a-b), and they correspond well to their climatological-mean state in the non-front experiment. This insensitivity of the PFJ and stormtrack in the negative phase to the oceanic frontal zone can therefore be regarded as an indication that they are determined primarily through atmospheric internal dynamics with positive feedback between the eddy-driven PFJ and stormtrack that is unrelated to the lower-boundary condition (Robinson 2006). The wintertime annular mode as represented in our experiments with an extratropical oceanic front can be therefore interpreted as wobble between these two different quasi-equilibrium states or “regimes”.

The regime represented by the positive phase of the annular mode tends to be maintained through enhanced meridional gradient of upward sensible heat flux at the frontal latitude (Figures 2.9), which is crucially important for the recurrent development of baroclinic eddies to form a stormtrack and thereby the association among a stormtrack, PFJ and oceanic frontal zone (Nakamura et al. 2004, 2008). As suggested in the theory of baroclinic instability from a PV viewpoint (Hoskins et al. 1985) and indeed confirmed climatologically in aqua-planet experiments (e.g., Sampe et al. 2010, 2013), a surface baroclinic zone anchored along an oceanic frontal zone is crucially important for recurrent development of baroclinic eddies through the coupling of potential vorticity anomalies both at the surface and near the tropopause, rather than the mid-tropospheric baroclinicity associated with the vertical shear of STJ. Indeed, this thermodynamic influence of the

oceanic frontal zone is evident in the positive phase of the annular mode, which is characterized by the close association of a lower-tropospheric stormtrack and PFJ with an oceanic frontal zone (Figures 2.5a-b). Although the PFJ axis can indeed fluctuates purely as atmospheric self-excited variability (Limpasuvan and Hartmann 2000), the eddy development can be activated once the PFJ axis approaches in the vicinity of an oceanic frontal zone at a middle or subpolar latitude. In this situation, the eddy momentum and heat flux acts to anchor PFJ over the cool ocean surface slightly poleward of the frontal latitude. The residence time of the PFJ axis around the frontal zone can thus be prolonged to constitute a dynamical regime represented as the positive phase of the annular mode.

During the negative phase of the annular mode, by contrast, the PFJ axis tends to stay far away from the frontal zone. Although active development of baroclinic eddies is hinted in the vicinity of the front (Figure 2.6c), but eddy activity cannot be organized into a stormtrack (Figure 2.6b). In this regime, the joint axes of the PFJ and stormtrack seem to be determined by atmospheric internal dynamics, as indicated by the distinct peak of their residence time around 38° regardless of the latitude of the oceanic front (Figure 2.8). The longer residence time reflected by this regime-like signature is consistent with a hint of dual latitudinal peaks in the zonal wind variance (Figure 2.3) and the regime-like behavior of the first EOF of zonal wind anomalies. The regime-like behavior tends to be most apparent for a subpolar oceanic front, which acts to anchor the stormtrack in the positive phase of the annular mode far away from its latitude in the negative phase. A schematic describing the regime-like behavior of the wintertime annular mode is shown in Figure 4.1a.

The aforementioned regime-like behavior of the annular mode simulated in aqua-planet experiments in the presence of a midlatitude or subpolar oceanic frontal zone is also applicable to the observed SAM to some extent. The analysis described in Chapter 2 has revealed that inter-basin differences in the zonal wind variability associate with SAM that are superimposed on the dominant zonally uniform anomalies are closely related to the latitudinal differences in the midlatitude oceanic frontal zones among the basins (Figures 2.27-29). The zonal wind variability shows regime-like behavior especially over the South Pacific (Figure 2.31a), where the oceanic frontal

zone is located around 55°S. The positive phase of the annular mode is associated with the enhanced gradient in upward sensible heat flux across the subpolar oceanic frontal zone (Figure 2.30), which is similar to the findings in the aqua-planet experiments of this study. It is therefore suggested that the observed SAM also represents the regime-like characteristics especially over the South Pacific.

The notion of "regime-like" behavior of the wintertime SAM has already been pointed out in previous studies but from a rather phenomenological viewpoint (Yoden et al. 1987, Itoh et al. 1999). They argued that the positive phase of SAM represents the double jet structure with distinct separation between PFJ and STJ while the negative phase represents the merged single jet structure. The findings of the present study add further significance to their interpretations from a dynamical viewpoint. In fact, the present study emphasizes that the regime-like behavior of the wintertime SAM discussed in these previous studies can be understood in depth from a consideration of the influence of an oceanic front. Our aqua-planet experiments suggest that the particular regime represented by distinct double jet structure associated with the positive phase of SAM corresponds to the regime when the extratropical tropospheric circulation is under the enhanced influence of the oceanic front. It is thus inferred that one of the two attractors (or attractor-ruins) in phase space found in Itoh et al. (1999) based on the reanalysis data may be strongly related to the surface temperature gradient determined by the lower-boundary condition, whereas the other is formed by atmospheric internal dynamics unrelated to the lower-boundary condition. Therefore, the regime-like behavior of the annular mode as revealed in the bimodality of the probability density function in the zonal wind axis (Figures 2.11a-c) may become clearer when the SST front is located farther away from the particular latitude determined by the atmospheric internal dynamics. In fact, the regime-like character is ambiguous in the South Indian Ocean even in winter (Figure 2.31b), where the SST front is located at 45°, only ~3° poleward of the particular latitude (42°) that is considered to be determined by the atmospheric internal dynamics (Figure 2.32e). This observed situation is consistent with the ambiguous regime-like behavior simulated in a particular aqua-planet experiment with the SST front located at 40°, which is only ~2° poleward of the

particular latitude (38°) determined by the atmospheric internal dynamics in the model. It is therefore suggested that the annular-mode behavior is almost absent when the SST front is too close to the particular latitude determined by the atmospheric internal dynamics, which is somewhat similar condition as in the NF condition (Figure 4.1b). On the contrary, the marked "split-flow regime" over the wintertime Southern Pacific Ocean as discussed in Bals-Elsholz et al. (2001), is owing probably to the location of the oceanic frontal zone at 55°, as much as 13° poleward of the particular latitude (42°) determined by atmospheric internal dynamics. Although their "split-flow index (SFI)" is different from the conventional SAM index in representation of the STJ variability, the PFJ variability represented by the SFI and SAM index is essentially the same. As shown in Figure 2.5d, the PFJ axis at the tropopause level tends to be situated at higher latitudes when the SST front is located at subpolar latitudes in the positive polarity of the model annular mode, showing a distinct split-jet structure.

In our aqua-planet experiments, phase-transition of the annular mode is found to be triggered by low-frequency wave disturbances (section 2.3f), which is consistent with the wintertime transition events of the observed SAM (Shiogama et al. 2005). It is shown that the two prominent transition events are triggered associated with injection of wave packets rather than zonally symmetric westerly forcing. Migratory synoptic-scale eddies act to maintain the polarity of the annular mode rather than change it. Shiogama et al. (2005) showed that low-frequency wave anomalies triggering the observed phase transition of SAM are rather localized in the South Pacific. They pointed out that zonal asymmetries in wave-guide structure for quasi-stationary Rossby waves due to the zonally varying PFJ axis may lead to the localization of the wave anomalies. In fact, the PFJ axis tends to follow the local axis of SST front (Nakamura et al. 2004) especially in winter. It can thus be speculated that the zonal asymmetries in the latitude of SST front influence the localization of the westerly forcing in the observed phase transition of SAM.

It has also been demonstrated in the present study that the wintertime climatological-mean state can be understood as a superposition of the two distinct regimes that correspond to the two phases of the annular mode both in the observations and aqua-planet experiments (Figure 2.32). The

latitudinal sensitivity of the climatological-mean PFJ to the latitudes of oceanic frontal zones over the individual ocean basins as discussed in Nakamura et al. (2004) can be understood as the manifestation of the one regime representing the closer association among the oceanic frontal zone, stormtrack and PFJ. Furthermore, the counterintuitively weak sensitivity of the climatological-mean PFJ axis simulated in aqua-planet experiments by Ogawa et al. (2012) to the latitude of frontal SST gradient, especially if located at subpolar latitude, can also be understood as the large influence of the other regime where atmospheric internal dynamics are dominant (Robinson 2006), in contrast to the observation (Nakamura et al. 2004). It should be noted that the regime-like behavior of the annular mode is limited to the winter season in both the observations and the aqua-planet experiments with oceanic frontal zones at middle and subpolar latitudes. Further investigation of what determines the seasonality of the dynamical characteristics of the annular mode is required in future study.

When a prominent oceanic front is located in the subtropics, by contrast, the regime-like behavior of the model annular mode is virtually absent (Figure 2.21). The annular mode represents small wobble of the near-surface PFJ axis around its climatological-mean position (Figures 2.21a-b), which is similar to the case in the absence of an oceanic front (Figure 2.11e). The differences in the annular mode characteristics in the presence of a subtropical SST front from those in the presence of an SST front at higher latitude are attributable to multiple factors. Interestingly, the PFJ and associated stormtrack in the negative phase of the annular mode, by definition, must be closer to the SST front if located at 30° or 35°, but they form poleward of the front around the particular latitude (38°) at which the PFJ and stormtrack tend to be situated in the absence of SST front (Figure 2.6a). In the positive phase, they form poleward of the particular latitude (38°) farther away from the SST front (Figure 2.5a). It is thus suggested that the ability of the subtropical SST front to anchor the stormtrack and eddy-driven PFJ may be somehow suppressed and thereby the separation between the particular latitudes determined by the SST front and atmospheric internal dynamics is diminished (Figure 4.1b). A possible factor can be the influence of downward motion associated with the Hadley Cell below the STJ core (Figure 2.23), which acts to hamper the baroclinic development of eddies along the subtropical SST front.

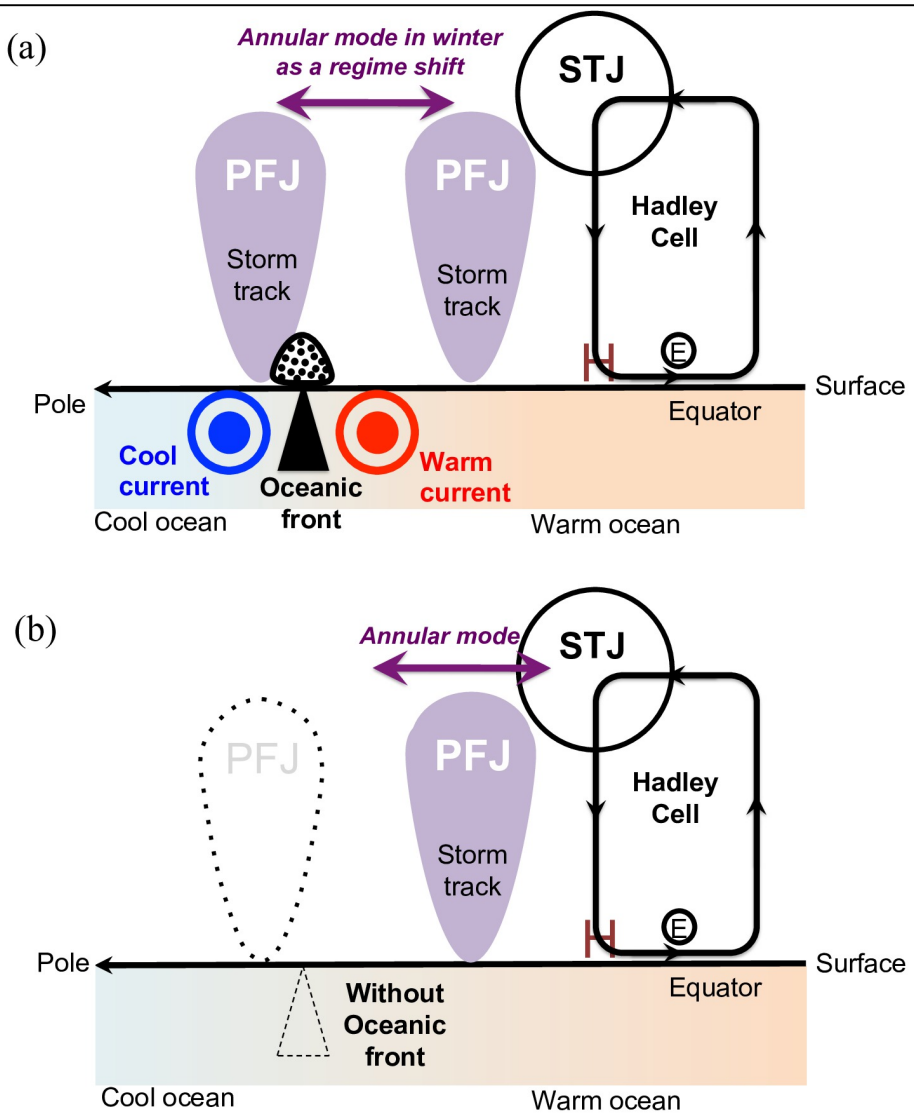

Figure 4.1. (a) A schematic diagram of the tropospheric wintertime annular mode signature in the presence of an oceanic front at a middle or subpolar latitude as observed in the Southern Hemisphere, as a modification of Nakamura et al. (2004). A midlatitude oceanic front (black triangle) is formed where warm and cool eastward ocean currents (blue and red circles) are confluent. In the wintertime subtropics, strong STJ forms in the upper-troposphere associated with the surface high-pressure belt underneath (denoted as "H"). Its westerly momentum is supplied through the surface momentum exchange between the ocean and the easterly trades equatorward of the high-pressure belt (denoted as "E"). PFJ is driven through the eddy momentum transport from STJ. In the positive phase of the annular mode, the stormtrack tends to form along the surface baroclinic zone (stippling) anchored by the midlatitude oceanic frontal zone (dark triangle), and PFJ (purple shading) is driven slightly poleward of the frontal latitude and distinct from STJ to form a double-jet regime. In the negative phase, in contrast, their joint axes of storm track and eddy-driven PFJ tend to form at the latitudinal position determined by atmospheric internal dynamics (Robinson 2006), and PFJ is merged with STJ to form a single-jet regime. The wintertime annular mode represents a transition between these two regimes in case the SST front is located poleward from the particular latitude related to atmospheric internal dynamics farther than a particular latitudinal distance. (b) As in (a), but the circulation that would be realized in the absence of SST front. Without the anchoring effect by the SST front, the positions of the stormtrack and PFJ are solely determined by the atmospheric internal dynamics. The annular mode represents small wobble from their climatological-mean positions but not regime-like behavior. When the SST front is too close to the latitude determined by atmospheric internal dynamics or located in the subtropics, the anchoring effect by SST front cannot effectively act to form the stormtrack and PFJ poleward from the particular latitude shown in (b) and regime-like behavior of the annular mode is lost.

4.2. Importance of oceanic front for the ozone-induced climate trend over the summertime Southern Hemisphere

While the summertime climatic trend observed during the late 20th century over the extratropical Southern Hemisphere has been understood as a shift of SAM toward its positive phase as a response to the stratospheric ozone depletion, the mechanisms for the translation of the stratospheric response to the ozone depletion down to the tropospheric SAM are still highly controversial (Thompson et al. 2011). Recent studies (Nakamura et al; 2008, Sampe et al. 2013), demonstrated that a removal of midlatitude frontal gradient in SST can significantly affect tropospheric annular mode characteristics. The set of aqua-planet AGCM experiments conducted in Chapter 3 was thus aimed to investigate the potential importance of an oceanic frontal zone for the tropospheric climatic response to the stratospheric ozone depletion over Antarctica, which is a viewpoint that was completely overlooked in previous studies.

The aqua-planet experiments in this study are the first to demonstrate that the oceanic front is crucial for translating the influence of the springtime stratospheric cooling by the ozone depletion down into the stratosphere in triggering the shift of the tropospheric annular mode to its positive phase. While the springtime cooling and associated intensification of the subpolar westerlies in the stratosphere due to the ozone depletion can be reproduced regardless of the presence of the midlatitude SST front, the surface westerly response can be reproduced with realistic frontal structure only in the presence of SST front. Virtually no response with statistical significance was simulated in the absence of the SST front even though the same ozone depletion as in the presence of SST front was prescribed. It is further revealed that midlatitude oceanic frontal zones are crucial for the stratosphere-troposphere connectivity of zonally symmetric year-to-year natural variability in early summer associated with the tropospheric annular mode. In the presence of a midlatitude oceanic frontal zone, the natural variability associated with the tropospheric annular mode shows realistic meridional structure and amplitude, which is accompanied by the vertical coupling between the troposphere and the stratosphere. In the absence of SST front, by contrast, the meridional

structure of the tropospheric annular mode is distorted and its amplitude is reduced, in association with its markedly weaker connectivity with the stratospheric natural variability. The weakened vertical connectivity of the year-to-year variability via the tropospheric annular mode is consistent with the reduced tropospheric climatic response to the stratospheric forcing in the absence of oceanic frontal zone. The schematic (Figure 4.2) shows the impact of a midlatitude oceanic frontal zone to excite the vertical coupling and thereby induce the climate change responding to the stratospheric ozone depletion.

It should be noted that the summertime annular mode signature simulated in none of the AGCMs used in Chapters 2 and 3 (Figures 2.33b and 3.13a, respectively) is regime-like. Indeed, observed horizontal asymmetry of the wintertime SAM, presumably because of its regime-like behavior as discussed in Chapter 2, becomes virtually absent in summer (Codron 2005). Meanwhile, the presence of the midlatitude SST front in each of the AGCMs leads to the substantial strengthening of the stormtrack activity and eddy-driven westerlies in summer at the middle and subpolar latitudes throughout the depth of the troposphere and even in the lower stratosphere (Figures 3.3h and 3.4). The midlatitude SST front also leads to the stronger upper-tropospheric planetary waves in the polar and subpolar regions, which can enhance their upward propagation into the stratosphere.

This study not only demonstrates the crucial importance of a midlatitude oceanic frontal zone for the tropospheric climate response to the stratospheric ozone depletion, but also provides implications for previous controversy on how the stratospheric ozone depletion can influence the tropospheric climate. Grise et al. (2009), for example, argued that a reduction of downward longwave radiation to the troposphere is a key to translate the ozone-induced stratospheric climatic response to the troposphere. The present study suggests that such radiative process may not be the main driver for the tropospheric response, since the downward longwave radiation from the stratosphere should not be sensitive to the intensity of SST gradient. The present study also raises a question on the importance of the downward control from the stratospheric wave forcing onto the tropospheric westerly response as suggested by Song and Robinson (2004). As indicated in Figure

4.3a, the anomalous residual circulation as a response to the stratospheric ozone depletion is confined mostly into the troposphere even in the presence of SST front, and the downward control from the stratosphere to the surface westerly, if any, appears to be too weak to act as a main driving mechanism for the tropospheric response. Rather, the near-surface westerly forcing associated with the response in the residual circulation is associated mostly with the organized wave response in the upper troposphere (Figure 3.7c). It should be noted that no significant surface westerly forcing associated with residual circulation is simulated in the absence of the SST front (Figure 4.3b), consistent with the absence of organized wave response in the upper troposphere (Figure 3.7d). It is therefore the modulated tropospheric wave activity that is most important for the tropospheric westerly response to the ozone depletion, which supports the arguments by Kushner and Polvani (2004) and Garfinkel et al. (2013).

Nevertheless, understanding the dynamical processes through which the stratospheric ozone depletion induces the response in the tropospheric wave activity is not straightforward, as discussed in section 3.4b. In fact, the anomalous wave activity induced by the stratospheric ozone depletion is not necessarily consistent with the anomalous wave activity associated with the stratospheric year-to-year variability (Figure 4.4). The tropospheric response in wave activity may not be fully understood from a viewpoint of a simple vertical coupling associated with the annular mode, and future studies are required for better understanding. Furthermore, one may argue that the latitudinal position of the mean PFJ may be important for the downward translation of the ozone-induced circulation anomaly regardless of what determines the PFJ latitude, and the SST front might not necessary be the sole factor to form PFJ poleward of 40° as observed in the SH. Nevertheless, it is suggested that the midlatitude SST fronts in the real SH substantially contribute to the maintenance of the mean PFJ poleward of 40° as discussed in Nakamura et al. (2004, 2008; red lines in Figure 1.12c). Therefore, the importance of the SST front cannot be overlooked in understanding the downward translation of the ozone-induced circulation anomaly as discussed in this study.

Meanwhile, several studies (Son et al. 2008; Thompson et al. 2011) pointed out that the stratospheric ozone concentration will recover in future and the recovery will act to change the

tropospheric westerlies wind in the opposing to the trend observed in the 20th century. The possible future trend in early summer induced by the ozone recovery must be toward the negative polarity of SAM counteracting the climatic trend induced by increasing greenhouse gases (Thompson et al. 2011). Therefore, the present study suggests that the realistic representation of the midlatitude frontal zone over the Southern Ocean in a global climate model is required for the reliable future climate prediction in the extratropical SH. In fact, it has been suggested through an inter-comparison of CMIP3 and CMIP5 climate models that an accurate reproduction of the ozone-induced surface climate trend observed in the late 20th century requires an appropriate representation of a sharp midlatitude SST front in those state-of-the-art climate models (Ogawa et al. 2014, in preparation).

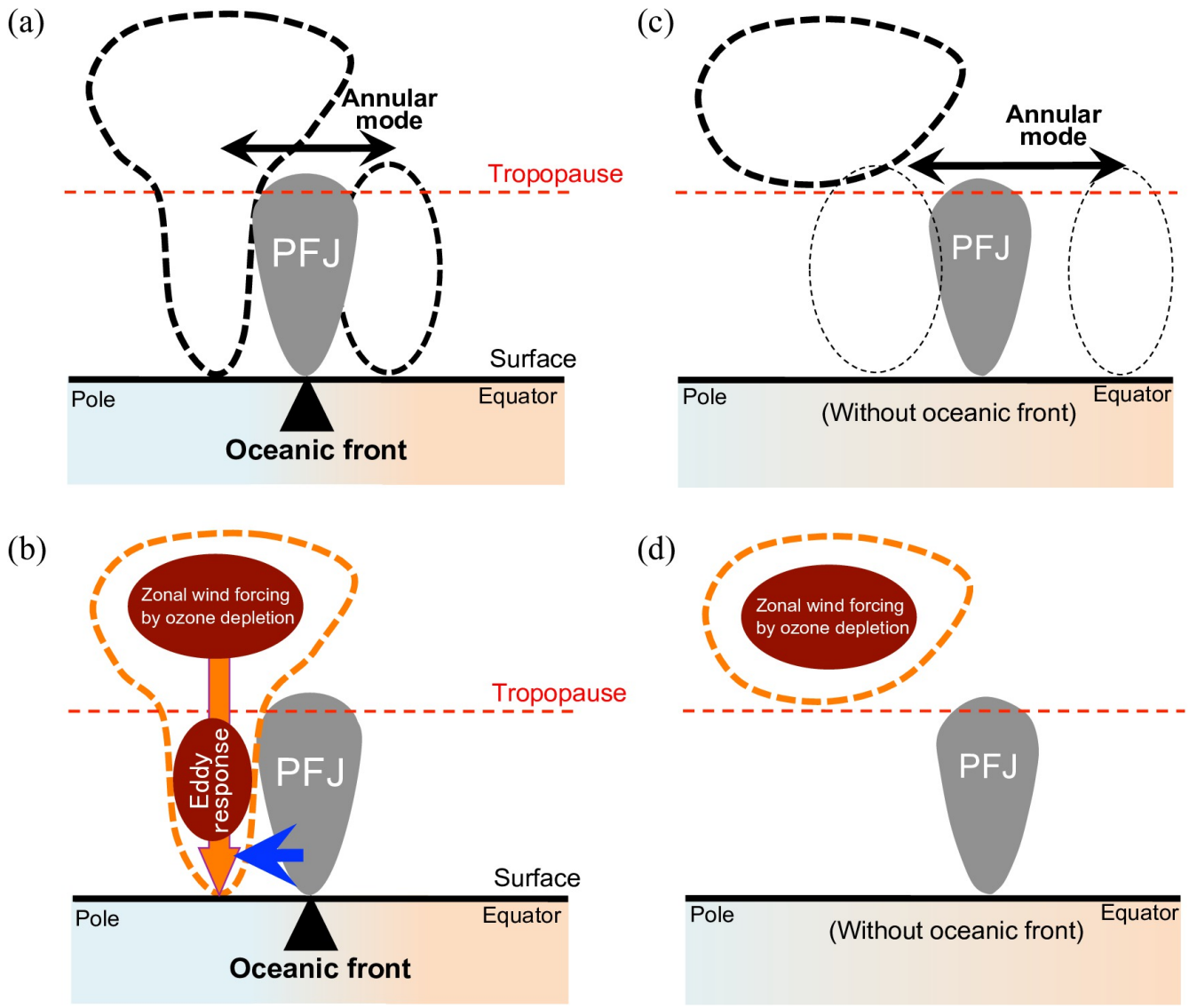

Figure 4.2. A schematic showing the importance of a midlatitude oceanic frontal zone for inducing the lower-tropospheric westerly response as the positive polarity of the annular mode to the stratospheric westerly forcing induced by the ozone depletion. In the presence of the midlatitude oceanic frontal zone (a), the tropospheric annular mode structure in the spring-summer season represents wobble of the PFJ axis as observed (with associated wind anomalies indicated with thick dashed lines). The anomalous westerly poleward of the mean PFJ axis near the oceanic frontal zone (triangle) is connected with the self-excited stratospheric natural variability (dashed line in the stratosphere), through which (b) a stratospheric westerly anomaly forced by the ozone depletion can be translated all the way down to the surface as the positive phase of the annular mode concomitant with a tropospheric response in eddy activity. In the absence of oceanic front (c), by contrast, the tropospheric annular mode structure is distorted with reduced amplitude (thin dashed lines) associated with the equatorward shift of the mean westerly axis and weakened stormtrack activity, (d) which impairs the vertical connectivity of the year-to-year variability across the tropopause. Thus, the stratospheric westerly anomaly forced by ozone depletion can hardly be translated down to the troposphere.

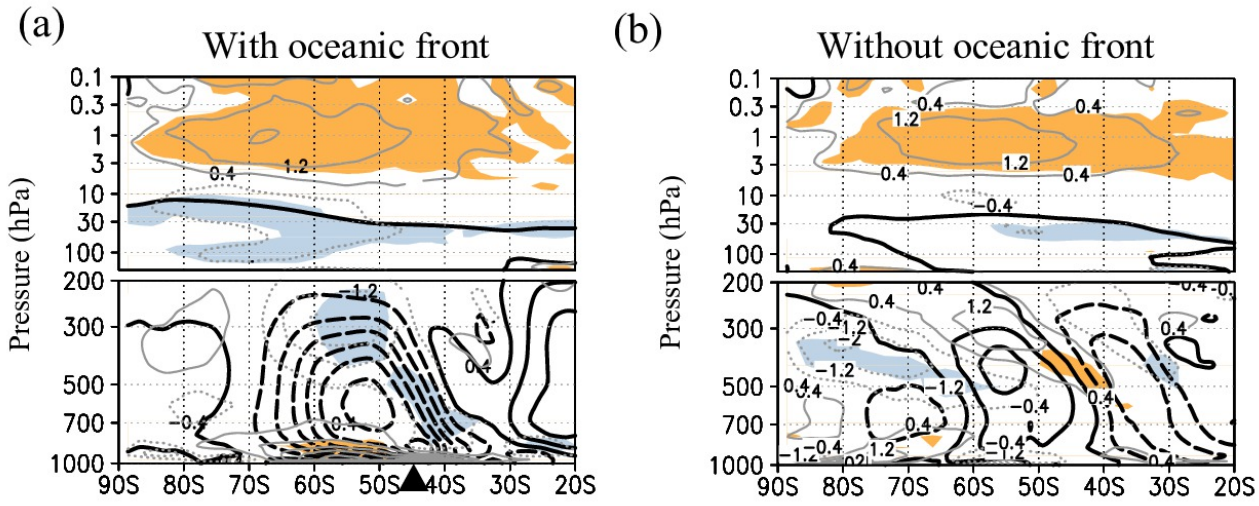

Figure 4.3. Meridional sections showing the response of residual mass-streamfunction (thick black contours, solid lines for counterclockwise circulation) and associated westerly acceleration (thin gray contour, every 1m s^{-1}/day) estimated as the 7-day average from 10th to 16th November, in the experiments (a) with and (b) without the oceanic front. Shading indicates the statistically significant response exceeding the 95% confidence level based on the Student's t-test. Black triangle indicates the latitude of the oceanic front.

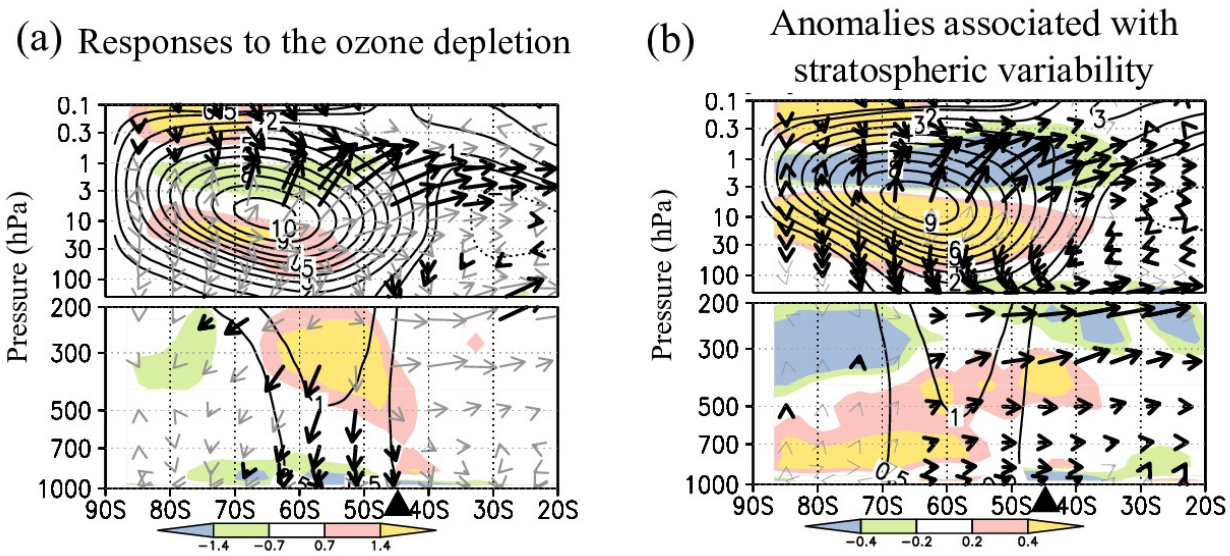

Figure 4.4. (a) Meridional sections showing the structure of the early-summer atmospheric response simulated to the prescribed ozone depletion in the presence of oceanic frontal zone. Zonal-mean zonal wind response in the 31-day average from 28th October to 28th November is indicated by contours (for every 1 m s^{-1}; sold and dashed lines for anomalous westerlies and easterlies, respectively), while the response in EP flux is indicated as the 7-day average from 10th to 16th November. Thick black arrows indicate the statistically significant anomalous flux exceeding the 95% confidence level. Shading indicates the westerly forcing estimated as the EP-flux divergence. (b) As in (a), but for the anomalous westerlies (contour) and anomalous EP flux (vector) averaged over the same periods in association with the zonally symmetric year-to-year variability (see text).

4.3. Conclusions

The present study has contributed to substantial advance in our understanding of the impacts of midlatitude oceanic frontal zones on the formation and variability of the extratropical general circulation in the troposphere. In contrast to many previous studies on the climatological-mean impacts of a midlatitude oceanic frontal zone on a stormtrack and eddy-driven PFJ, the present study has demonstrated that the importance of an oceanic frontal zone is not limited to the climatological-mean state but can strongly influence the characteristics of the tropospheric annular variability as well as its vertical coupling with the stratospheric variability and thereby enables to translate the impact of stratospheric ozone depletion into the tropospheric climatic change. These new findings in the present study can indeed explain observed inter-basin differences in the tropospheric SAM signature, urging the necessity for realistic reproduction of the midlatitude SST gradients for reproducing the observed summertime climate trend and projecting future climatic changes in the extratropical SH. It is therefore concluded that the extratropical tropospheric circulation and its dominant variability (annular mode) and long-term trends can no longer be interpreted purely as atmospheric internal processes but should be interpreted from a viewpoint of their coupling with the underlying ocean. Although the direct thermal influence by a midlatitude oceanic front is limited to a narrow latitudinal band with a certain longitudinal extent, its influence can be extended farther downstream through stormtrack activity and also meridionally through eddy propagation and associated momentum transport. It is thus suggested that an appropriate representation of midlatitude oceanic frontal zones in global climate models is required for the realistic reproduction of the annular mode variability, and thereby the climate reproduction and future projection.

Despite its substantial contribution to our better understanding of the impacts of midlatitude oceanic frontal zones on the formation and variability of the tropospheric general circulation, the present study cannot fully cover all the aspects of the tropospheric general circulation. For example, it is left for future examination why the summertime annular mode exhibits regime-like behavior to a lesser degree that its wintertime counterpart. In addition, the potential importance of midlatitude

oceanic frontal zones for the presence of the tropospheric circulation over the extratropical SH to the increasing greenhouse effect is also left for future investigation. Furthermore, the present study highlights the impacts of an oceanic frontal zone on the atmosphere, but the driving of oceanic currents by the surface westerlies and their role in the maintenance of oceanic fronts are neglected. In reality, however, ocean currents and associated frontal zones must constitute an interacting system with the atmospheric circulation, as argued in Nakamura et al. (2004). Impacts of anomalous surface westerlies associated with SAM on midlatitude SST have also been pointed out (Ciasto and Thompson 2008). Furthermore, a possibility of the latitudinal shift of oceanic frontal zones associated with the future trends in the surface westerlies induced by the global warming is also suggested in several recent studies (e.g., Beal et al. 2011). Therefore, deeper understanding of the impacts of midlatitude oceanic frontal zones on the observed extratropical circulation should be made from a viewpoint of fully coupled ocean-atmosphere interactions.

Acknowledgments

I thank Prof. Hisashi Nakamura for his guidance and encouragement throughout the course of this study. I also greatly appreciate the referees of this thesis, Prof. M. Watanabe, Prof. M. Takahashi, Prof. Y. Masumoto, and Prof. H. Miura, whose useful comments and suggestions have led to many improvements in this study. I used the AFES in support of Japan Agency for Marine-Earth Science and Technology (JAMSTEC) and the ECHAM5 in support of Deutsche Klimarechenzentrum (DKRZ). In my daily academic life, I thank Dr. K. Nishii, Dr. T. Miyasaka and Dr. Y. Kosaka in University of Tokyo and Dr. A. Kuwano-Yoshida in JAMSTEC to guide and encourage me from the beginning of my master-course study. I also appreciate Dr. L. Wang, Dr. A. Laîné, Dr. N. Shi and all the students of our research group to give fruitful comments to my results in weekly meetings. I cannot forget many supports and encouragements by Dr. N.-E. Omrani, Prof. N. Keenlyside and Prof. R. Greatbatch in my research visit to GEOMAR in Germany and Geophysical Institute in Norway. Finally, I eternally thank my family to support my academic life.

References

Andrews, D, J. R. Holton, and C. B. Leovy, 1987: *Middle Atmosphere Dynamics*, 489pp, Academic Press.

Baldwin, M. P., and T. J. Dunkerton, 1999: Propagation of the Arctic Oscillation from the stratosphere to the troposphere. *J. Geophys. Res.*, **104**, 30937–30946.

Baldwin, M. P., and T. J. Dunkerton, 2001: Stratospheric harbingers of anomalous weather regimes. *Science*, **294**, 581–584.

Bals-Elsholz, T. M., E. H. Atallah, L. F. Bosart, T. A. Wasula, M. J. Cempa, and A. R. Lupo, 2001: The wintertime Southern Hemisphere split jet: Structure variability and evolution. *J. Climate*, **14**, 4191–4215.

Beal, L. M., and coauthors, 2011: On the role of the Agulhas system in ocean circulation and climate. *Nature*, **472**, 429–436.

Brayshaw, D. J., B. J. Hoskins, and M. Blackburn, 2008: The storm- track response to idealized SST perturbations in an aqua-planet GCM. *J. Atmos. Sci.*, **65**, 2842–2860.

Charney, J. G., 1947: The dynamics of long waves in a baroclinic westerly current. *J. Meteor.*, **4**, 135-162.

Charney, J. G., and P. G. Drazin, 1961: Propagation of planetary- scale disturbances from the lower into the upper atmosphere. *J. Geophys. Res.*, **66**, 83–109.

Chen, G., R. A. Plumb, and J. Lu, 2010: Sensitivities of zonal mean atmospheric circulation to SST warming in an aqua-planet model. *Geophys. Res. Lett.*, **37**, L12701.

Ciasto, L. M., and D. W. J. Thompson, 2008: Observations of large-scale ocean-atmosphere interaction in the Southern Hemisphere. *J. Climate*, **21**, 1244–1259.

Codron, F., 2005: Relation between annular modes and the mean state: Southern Hemisphere summer. *J. Climate,* **18**, 320–330.

Codron, F., 2007: Relations between annular modes and the mean state: Southern Hemisphere winter. *J. Atmos. Sci.*, **64**, 3328–3339.

Deremble, B., G. Lapeyre and M. Ghil, 2012: Atmospheric Dynamics Triggered by an Oceanic SST Front in a Moist Quasigeostrophic Model. *J. Atmos. Sci.*, **69**, 1617–1632.

Eady, E. T., 1949: Long waves and cyclone waves. *Tellus*, **1**, 33-52.

Ebita, A., and coauthors, 2011: The Japanese 55-year Reanalysis "JRA-55": an interim report, *SOLA*, **7**, 149-152.

Eichelberger, S. J., and D. L. Hartmann, 2007: Zonal jet structure and the leading mode of variability. *J. Climate,* **20**, 5149–5163.

Exner, F. M., 1913: Über monatliche Witterungsanomalien auf der nördlichen Erdhälfte im Winter. *Sitzb. Mathem .-Naturw , Kl., Acad. der Wissenshaften*, **CXXII, Bd. Abd, IIa**, 1165-1240.

Garfinkel, C. I., D. W. Waugh, and E. P. Gerber 2013: The Effect of tropospheric jet latitude on coupling between the stratospheric polar vortex and the troposphere. *J. Climate,* 26, 2077–2095.

Gillett, N. P. and D. W. J. Thompson, 2003: Simulation of recent Southern Hemisphere climate change. *Science,* **302**, 273–275.

Gillett, N. P., T. D. Dell and P. D. Jones, 2006: Regional climate impacts of the Southern Annular Mode. *Geophys. Res. Lett.*, **33**, L23704.

Grise, K. M., D. W. J. Thompson, and P. M. Forster, 2009: On the Role of Radiative Processes in Stratosphere-Troposphere Coupling. *J. Climate*, **22**, 4154-4161.

Haynes, P. 2005: Stratospheric dynamics. *Ann. Rev. Fluid Mech.*, **37**, 263-293.

Hartmann, D. L., and F. Lo, 1998: Wave-driven zonal flow vacillation in the Southern Hemisphere. *J. Atmos. Sci.*, **55**, 1303-1315.

Held, I. M., and A. Y. Hou, 1980: Nonlinear axially symmetric circulations in a nearly inviscid atmosphere. *J. Atmos. Sci.*, **37**, 515-533.

Hoskins, B. J., M. E. McIntyre, and A. W. Robertson, 1985: On the use and significance of isentropic potential vorticity maps. *Quart. J. Roy. Meteor. Soc*., **111**, 877-946.

Hoskins, B. J., and P. J. Valdes, 1990: On the existence of storm tracks. *J. Atmos. Sci.*, **47**, 1854–1864.

Hoskins, B. J., 1991: Towards a PV-θ view of the general circulation. 1991: *Tellus*, **43A**, 27-35.

Hotta, D., and H. Nakamura, 2011: On the significance of sensible heat supply from the ocean in the maintenance of mean baroclinicity along storm tracks. *J. Climate*, **24**, 3377–3401.

Itoh, H., M. Kimoto, and H. Aoki, 1999: Alternation between the Single and Double Jet Structures in the Southern Hemisphere. Part I: Chaotic Wandering. *J. Meteor. Soc. Japan,* **77**, 399-412.

Kidson, J. W., 1988: Indices of the Southern Hemisphere zonal wind. *J. Climate*, **1**, 183-194.

Kimoto, M., F. -F., Jin, M. Watanabe, and N. Yasutomi, 2001: Zonal-eddy coupling and a neutral mode theory for the Arctic Oscillation. *Geophys. Res. Lett.,* **28**, 737-740.

Kuroda Y. and K. Kodera, 1998: Interannual variability in the troposphere and stratosphere of the southern hemisphere winter. *J. Geophys. Res.*, **103**, 13787-13799.

Kushner, P. J. and L. M. Polvani, 2004: Stratosphere-troposphere coupling in a relatively simple AGCM: The role of eddies. *J. Climate,* **17**, 629–639.

Kushnir, Y., W. A. Robinson, I. Bladé, N. M. J. Hall, S. Peng, and R. Sutton, 2002: Atmospheric GCM response to extratropical SST anomalies: Synthesis and evaluation. *J. Climate*, **15**, 2233– 2256.

Lau, N.-C., and E. O. Holopainen, 1984: Transient eddy forcing of the time-mean flow as identified by geopotential tendencies. *J. Atmos. Sci.*, **41**, 313-328.

Lee, S., and H.-K. Kim, 2003: The dynamical relationship between subtropical and eddy-driven jets. *J. Atmos. Sci.*, **60**, 1490-1503.

Limpasuvan, V. and D. L. Hartmann, 1999: Eddies and annular modes of climate variability. *Geophys. Res. Lett.*, **26**, 3133–3136.

Limpasuvan, V., and D. L. Hartmann, 2000: Wave-maintained annular modes of climate variability. *J. Climate*, **13**, 4414-4429.

Lorenz, D. J., and D. L. Hartmann, 2001: Eddy-zonal flow feedback in the Southern Hemisphere. *J. Atmos. Sci.*, **58**, 3312-3327.

Lorenz, D. J., and D. L. Hartmann, 2003: Eddy–zonal flow feedback in the Northern Hemisphere

winter. *J. Climate*, **16**, 1212–1227.

Nakamura, H., and T. Sampe, 2002: Trapping of synoptic-scale disturbances into the North-Pacific subtropical jet core in midwinter. *Geophys. Res. Lett*., **29**, doi:1029/2002GL015335.

Nakamura, H., T. Sampe, Y. Tanimoto, and A. Shimpo, 2004: Observed associations among storm tracks, jet streams and midlatitude oceanic fronts. Earth's Climate: *The Ocean-Atmosphere Interaction*, C. Wang, S.-P. Xie and J. A. Carton, Eds., Geophys. Monogr., **147**, American Geophysical Union, pp.329-345.

Nakamura, H., and A. Shimpo, 2004: Seasonal variations in the Southern Hemisphere storm tracks and jet streams as revealed in a reanalysis dataset. *J. Climate*, **17**, 1828-1844.

Nakamura, H., T. Sampe, A. Goto, W. Ohfuchi, and S.-P. Xie, 2008: On the importance of midlatitude oceanic frontal zones for the mean state and dominant variability in the tropospheric circulation. *Geophys. Res. Lett.*, **35**, L15709.

Nonaka, M., H. Nakamura, B. Taguchi, N. Komori, A. Yoshida-Kuwano, and K. Takaya, 2009: Air-sea heat exchanges characteristic to a prominent midlatitude oceanic front in the South Indian Ocean as simulated in a high-resolution coupled GCM. *J. Climate*, **22**, 6515–6535.

Ogawa, F., H. Nakamura, K. Nishii, T. Miyasaka, and A. Kuwano-Yoshida, 2012: Dependence of the climatological axial latitudes of the tropospheric westerlies and storm tracks on the latitude of an extratropical oceanic front. *Geophys. Res. Lett.*, **39**, L05804.

Ogawa, F., N.-E. Omrani, K. Nishii, H. Nakamura, and N. Keenlyside, 2014: Ozone-induced climate changes propped up by the Southern Hemisphere oceanic front. To be submitted to *Science*.

Ohfuchi, W., H. Nakamura, M. Yoshioka, T. Enomoto, K. Takaya, X. Peng, S. Yamane, T. Nishimura, Y. Kurihara, and K. Ninomiya, 2004: 10-km mesh meso-scale resolving global simulations of the atmosphere on the Earth Simulator - Preliminary outcomes of AFES (AGCM for the Earth Simulator), *J. Earth Simulator*, **1**, 8-34.

Onogi, K. and coauthors, 2007: The JRA-25 reanalysis. *J. Meteor. Soc. Japan*, **85**, 369-432.

Palmén, E., and C. W. Newton, 1969: Atmospheric Circulation Systems: *Their Structure and*

Physical Interpretation, Academic Press, New York, 603 pp.

Polvani L. M., D. W. Waugh, G. J. P. Correa and S. -W. Son, 2011: Stratospheric ozone depletion: The main driver of twentieth-century atmospheric circulation changes in the Southern Hemisphere. *J. Climate,* **24**, 795–812.

Reynolds, R. W., T. M. Smith, C. Liu, D. B. Chelton, K. S. Casey and M. G. Schlax 2007: Daily high-resolution-blended analyses for sea surface temperature. *J. Climate,* **20**, 5473–5496.

Ring, M. J., and R. A. Plumb, 2007: Forced annular mode patterns in a simple atmospheric general circulation model. *J. Atmos. Sci.*, **64**, 3611–3626.

Ring, M. J., and R. A. Plumb, 2008: The response of a simplified GCM to axisymmetric forcings: Applicability of the fluctuation–dissipation theorem. *J. Atmos. Sci.*, **65**, 3880–3898.

Robinson, W. A., 2006: On the self-maintenance of midlatitude jets. *J. Atmos. Sci.*, **63**, 2109–2122.

Roeckner and coauthors, 2003: The atmospheric general circulation model ECHAM5. Part I: Model description. *Max Planck Institute for Meteorology Rep.* **349**, 127 pp.

Rossby, C.-G., 1939: Relation between variations in the intensity of the zonal circulation of the atmosphere and the displacements of the semi-permanent centers of action. *J. Mar. Res*., **2**, 38-55.

Sampe, T., H. Nakamura, A. Goto, and W. Ohfuchi, 2010: Significance of a midlatitude SST frontal zone in the formation of a storm track and an eddy-driven westerly jet. *J. Climate*, **23**, 1793–1814.

Sampe, T., H. Nakamura, A. Goto, 2013: Potential Influence of a Midlatitude Oceanic Frontal Zone on the Annular Variability in the Extratropical Atmosphere as Revealed by Aqua-Planet Experiments. *J. Meteor. Soc. Japan,* **91A**, 243-267.

Sanders, F., and J. R. Gyakum, 1980: Synoptic-dynamic climatology of the “bomb”. *Mon. Wea. Rev*., **108**, 1589-1606.

Shiogama, H., T. Terao, and H. Kida, 2004: The role of high-frequency eddy forcing in the maintenance and transition of the Southern Hemisphere annular mode. *J. Meteor. Soc. Japan*, **82**, 101–113.

Shiogama, H., T. Terao, H. Kida, and T. Iwashima, 2005: Roles of low- and high-frequency eddies in the transitional process of the Southern Hemisphere annular mode. *J. Climate*, **18**, 782–794.

Sinclair, M. R., 1995: A climatology of cyclogenesis for the Southern Hemisphere. *Mon. Wea. Rev*., **123**, 1601-1619.

Son, S.-W., and S. Lee, 2005: The response of westerly jets to thermal driving in a primitive equation model. *J. Atmos. Sci.*, **62**, 3741–3757.

Son, S.-W. and coauthors, 2008: The impact of stratospheric ozone recovery on the Southern Hemisphere westerly jet. *Science*, **320**, 1486–1489.

Song, Y., and W. A. Robinson, 2004: Dynamical mechanisms for stratospheric influences on the troposphere. *J. Atmos. Sci.*, **61**, 1711–1725.

Sun, L., G. Chen, and W. A. Robinson, 2014: The role of stratospheric polar vortex breakdown in Southern Hemisphere climate trends. *J. Atmos. Sci.*, **71**, 2335-2353.

Taguchi, B., H. Nakamura, M. Nonaka, and S. -P. Xie, 2009: Influences of the Kuroshio/Oyashio Extensions on air-sea heat exchanges and storm track activity as revealed in regional atmospheric model simulations for the 2003/4 cold season. *J. Climate,* **22**, 6536–6560.

Takaya, K., and H. Nakamura, 2001: A formulation of a phase-independent wave-activity flux for stationary and migratory quasi-geostrophic eddies on a zonally varying basic flow. *J. Atmos. Sci.*, **58**, 608-627.

Thompson, D. W. J, and J. M. Wallace, 1998: The Arctic Oscillation signature in the wintertime geopotential height and temperature fields. *Geophys. Res. Lett*., **25**, 1297-1300.

Thompson, D. W. J., and J. M. Wallace, 2000: Annular modes in the extratropical circulation. Part I: Month-to-month variability. *J. Climate*, **13**, 1000-1016.

Thompson, D. W. J., J. M. Wallace, and G. C. Hegerl, 2000: Annular modes in the extratropical circulation: Part II: Trends. *J. Climate*, **13**, 1018-1036.

Thompson D. W. J. and S. Solomon 2002 Interpretation of recent Southern Hemisphere climate change. Science, **296**, 895–899.

Thompson, D. W. J., M. P. Baldwin, and S. Solomon, 2005: Stratosphere-troposphere coupling in the Southern Hemisphere. *J. Atmos. Sci.*, **62(3)**, 708-715.

Thompson, D. W. J., S. Solomon, P. J. Kushner, M. H. England, K. M. Grise and D. J. Karoly, 2011: Signatures of the Antarctic ozone hole in Southern Hemisphere surface climate change. *Nature Geoscience,* **4**, 741-749.

Wallace, J. M., 2000: North Atlantic Oscillation/Annular Mode: Two paradigms—One phenomenon. *Quart. J. Roy. Meteor. Soc.*, **126**, 791–805.

Watanabe, M., and F.-F. Jin, 2004: Dynamical prototype of the Arctic Oscillation as revealed by a neutral singular vector. *J. Climate,* **17**, 2119-2138.

White, G. H., 1980: Skewness, Kurtosis and Extreme Values of Northern Hemisphere Geopotential Heights. *Mon. Wea. Rev.*, **108**, 1446-1454.

Yoden, S., M. Shiotani, and I. Hirota, 1987: Multiple planetary flow regimes in the Southern Hemisphere. *J. Meteor. Soc. Japan,* **65**, 571–586.

Yu, J.-Y., and D. L. Hartmann, 1993: Zonal flow vacillation and eddy forcing in a simple GCM of the atmosphere. *J. Atmos. Sci.*, **50**, 3244-3259.

Yu, L., X. Jin, and R. A. Weller, 2008: Multidecade Global Flux Datasets from the Objectively Analyzed Air-sea Fluxes (OAFlux) Project: Latent and sensible heat fluxes, ocean evaporation, and related surface meteorological variables. *Woods Hole Oceanographic Institution, OAFlux Project Technical Report.* OA-2008-01, 64pp. Woods Hole. Massachusetts.